A comparison of three surface flux datasets for use with standalone ocean climate models

Hadley Centre technical note 64

Ian Culverwell , Helene Banks

13 March 2006

A comparison of three surface flux datasets for use with standalone ocean climate models

Ian Culverwell and Helene Banks

Hadley Centre for Climate Prediction and Research, -
Met Office, FitzRoy Road, Exeter EX1 3PB -

13th March 2006

Abstract

This report reviews the literature on the specification of surface forcing in standalone ocean GCMs, describes how the problem has been treated in some past projects with Met Office involvement, and compares and contrasts three new flux forcing datasets, one based on station observations, one based on NWP reanalyses and one based on the HadGAM1 AGCM.

1. Introduction

This report concerns surface fluxes in standalone ocean general circulation models (OGCMs) – that is, OGCMs not coupled to atmosphere GCMs. Standalone OGCMs allow the rapid and "clean" development of ocean models without the complication of feedbacks from an AGCM. Although the absence of such feedbacks limits the use of standalone OGCMs in climate modelling, it does allow preliminary investigation of the response of the ocean to surface forcings. Furthermore, in a complex multi-system coupled environment like FLUME (Mullerworth, 2006) in which the systems are coupled to each other "anonymously" (ie without the need for one submodel to know the internal details of the other), it's important that each component can be run independently, at least for testing and development. In addition, precise control of the surface fluxes is useful when developing parameterisation schemes in ocean models. Finally, of course, standalone OGCMs are quicker to run than fully coupled GCMs, which allows faster turnaround of development work and sensitivity tests.

For all these reasons, it is desirable to run standalone ocean models. One drawback is that the fluxes of heat, momentum and freshwater across the ocean surface need to be specified as boundary conditions. The specification of these fluxes is the subject of this report. We begin by briefly reviewing the literature, and follow this by describing some previous experiences in

projects with Met Office involvement. We then compare and contrast three relatively new surface flux datasets. We do not report the results of using these fluxes in standalone ocean models: these will be the subject of a later report. Nor do we discuss fluxes between the ocean and sea-ice, as these are subtle questions which deserve special attention.

2. Review of surface forcings

2.1 Heat

2.1.1 Haney Forcing

Modern approaches to the problem of specifying surface fluxes in OGCMs began with Haney (1971), who pointed out that early attempts to model heat flux from the surface to the first ocean model layer in terms of the temperature difference between the surface and the first model level were undermined by the fact that the vertical eddy diffusion/conduction coefficient is largely unknown. Haney instead looked at the problem from above, reasoning that the heat lost from the atmosphere must equal the heat gained by the ocean. On this basis he derived expressions for the shortwave heating (SW), longwave heating (LW), latent heating (LH) and sensible heating (SH) in terms of the sea surface temperature (SST) and various atmospheric near-surface parameters such as air temperature T_A and relative humidity RH_A, cloud cover and wind speed. He also assumed that T_A and SST were close enough to allow a one term Taylor's series expansion, thus:

$$Q(SST) = Q(T_A) + \lambda\,(SST - T_A) \qquad (1)$$

where Q is the sum of the component heat fluxes. (Throughout this report Q > 0 means that the heat flux is *into* the ocean.) Haney derived expressions for λ (formally equal to dQ/dT at T_A) from climatological atmospheric data (even though he clearly realised the limitations of removing synoptic variability, especially for latent and sensible heating). He did this by means of "bulk formulae" – see Appendix A for more details. λ is generally negative, which expresses the negative feedback of SST on ocean heat uptake, and rather flat, with a mean value (see Haney's figures 8 and 9) of around -40 $W/m^2/K$. Assuming a mixed layer depth of 100 m, this equates to an e^{-1} time for the damping of SST anomalies of about 4 months. $Q(T_A)$ contains contributions from the radiation and the latent heating. The latter depends on $q_{sat}(SST)$-$q(T_A)$, which has a non-zero contribution to Q, proportional to (1- RH_A), even if SST= T_A. It is important to note that, despite the use of a one term Taylor expansion in (1), the relaxation term $\lambda\,(SST - T_A)$ is not necessarily a small

correction to $Q(T_A)$: for typical air-sea temperature differences of a few K, both terms could be comparable size (of order 100 W/m^2).

Haney went on to rewrite (1) as

$$Q(SST) = \lambda\,(SST - T_A^{eff}) \qquad (2)$$

where $T_A^{eff} = T_A - Q(T_A)/\lambda$ is an "effective" air temperature, which is much more strongly peaked on the equator (by perhaps 5K) than the real air temperature (see Haney's figure 11). Locally (eg around Western Boundary Currents) it can differ from T_A by up to 10K (Oberhuber, 1988).

Although Haney was quite specific about the calculation of λ and $Q(T_A)$, later authors have often described any relation like (1), which implies a relaxation of SST to a specified value, as "Haney relaxation" or "Haney forcing". Usually, the specified field is taken to be observations or climatology. Sometimes, an equation like (2), in which T_A^{eff} is replaced with T_{obs} is used, but this is wrong (unless λ is very large) as it ignores the zeroth order term $Q(T_{obs})$ in the Taylor expansion. On other occasions, T_A^{eff} is replaced with SST_{clim}, which is better, as they follow each other closely, but there can still be large differences (Oberhuber, 1988). Relaxation via eqn (2) to SST_{clim} also leads to the contradiction that an ocean model with realistic non-zero heat fluxes must have "incorrect" SSTs (Killworth et al, 2000). Often, though, "Haney relaxation" is simply an additional term in the surface forcing, included to prevent the model SSTs from drifting too far from more-or-less well-known and realistic values. (This is certainly the spirit behind "3D Haney forcing", in which Newtonian relaxation like (1) is applied to the temperature throughout the body of the ocean.) In such applications, λ is often a global constant.

2.1.2 Beyond Haney

Haney's 1971 paper defined a means of calculating the heat flux into the ocean, in terms of observable atmospheric variables, which has been applied many times since. There are, however, limitations. Haney's paper said nothing about fluxes of freshwater or momentum. Nor did it include any feedbacks between the ocean and the atmosphere. For example, T_A is prescribed, no matter how the modelled SST develops. In reality, T_A is closely tied to SST. And clouds can provide a positive feedback between SST and LW emission. (Increasing SST implies increasing evaporation implies more cloud cover implies less net LW cooling of the ocean surface implies increasing SST.) As a result of these and other feedbacks, Foreman calculated λ defined by (1) from values of the equation's other variables generated in a coupled model, and found values as large as $\pm$100 W/m^2/K (Gordon 1993). This wide range throws doubt on the whole idea of simple Haney forcing. It is natural to ask whether anything better can be done.

Several authors have tried to account for the impact of varying SST on the atmospheric feedbacks without going to the expense of a fully coupled GCM. Bretherton (1982) stressed that the *spatial size* of the SST anomaly is crucial: small scale atmospheric temperature anomalies can be advected away quickly by atmospheric winds, leading to a rapid relaxation to the specified SST, while larger scale air-sea temperature differences can only dissipate by LW radiative equilibration between air and sea, which is a much slower process. Both limits are contained within his general Green's function formulation of (2), which displays such non-local teleconnections explicitly:

$$Q(\mathbf{x}) = \int \lambda(\mathbf{x}, \mathbf{x'}) \, [T_A^{eff}(\mathbf{x'}) - SST(\mathbf{x'})] \, d\mathbf{x'}. \qquad (2')$$

(Haney forcing obviously corresponds to $\lambda(\mathbf{x},\mathbf{x'}) \sim -\delta(\mathbf{x}-\mathbf{x'})$.) Rahmstorf and Willebrand (1995) applied this idea by assuming a specific (Laplacian) form of the advective dispersal of heat anomalies by atmospheric winds, and derived the expression

$$Q(SST) = \gamma \, (T^{rest} - SST) \; - \; \mu \, \nabla^2 (T^{rest} - SST) \qquad (2'')$$

for the heat flow into the ocean surface. Here, γ (<< Haney's λ) represents relaxation by loss or gain of LW heat, while the diffusion coefficient μ depends on the grid resolution. T^{rest} is a prescribed restoring temperature which cannot be identified with T_A or Haney's T_A^{eff}, as the atmosphere's temperature T_A is now free to evolve. Rahmstorf and Willebrand obtained encouraging predictions of SST by using (2') in a simple two-basin model.

Equation (2') can be thought of as a kind of energy balance model (EBM) (see North, 1988, for a review). In such models, the vertically integrated atmospheric temperature evolves according to the flux difference between the top (specified) and bottom (modelled) of the atmosphere. One-dimensional (ie zonally meaned) EBMs can account for the horizontal heat (and moisture) flux divergence in a less prescriptive manner than (2'). EBMs are often coupled to mixed layer ocean models for paleoclimate modelling (eg Stocker et al, 1992). Lohmann et al (1996) were some of the first to use EBMs coupled to a full 3D ocean GCM; their results will be touched on in Section 2.2.

For small scale temperature anomalies, (2'') reverts to Haney forcing (with a different coefficient, and replacing ∇^2 with $-k^2$). For larger scale anomalies, it reverts to Schopf's (1983) "zero heat capacity" (or, better, "fixed heat transport") model in which SST anomalies relax slowly (e^{-1} time ~ 500 days) by parameterised LW cooling from the atmosphere. Schopf found that the rapid and intense (ie only slowly damped) dynamically induced SST anomalies were needed for a successful simulation of El Nino. This mirrors

Philander and Seigel's (1985) successful tropical modelling where they used a version of (1) in which (SST-T_A), rather than T_A, is held constant.

Bentsen and Drange (2000) advocate specifying fluxes *and* using bulk formulae (Appendix A) by (iteratively) inverting the latter to determine the atmospheric conditions (T_A etc) that would have produced the *given* fluxes with the *given* SSTs. The resulting transfer coefficients in the bulk formulae are then applied to these derived T_As and the *modelled* SSTs. If the given SST matches the modelled SST this procedure returns the original heat fluxes; if not, the fluxes are modified appropriately (ie reduced if the SST is too high). Bentsen and Drange's ideas were used successfully in the PREDICATE project, a multi-model comparison of decadal predictions of European climate (eg Frankignoul et al 2004).

Seager at al (1995) tried to include more feedbacks on the atmosphere (eg in the dry layer beneath marine Sc cloud) by means of a single mixed layer model. They had some success in calculating the distributions of SH and LH over the open ocean, but found difficulties near cold winter continents.

Despite the realism and success of all these "atmospheric slab models" (ie single-level atmosphere coupled to a multi-level ocean) they do not seem to have been taken up enthusiastically by ocean modellers. This may be due to the extra complexity involved, or perhaps modellers are still deterred by the wide range of λ values which appear in coupled GCMs. For whatever reason, many modellers are happy to apply "Haney relaxation" to a specified temperature, with a constant coefficient λ, and to simply account for the implied extra heat flow in their heat budget calculations. Those particularly interested in atmosphere-ocean interactions have latterly preferred to use fully coupled models, especially as they can now be run without flux-adjustment (eg Gordon et al, 2000).

2.2 Freshwater

The surface freshwater flux determines the salinity and therefore (partially) the surface density, and thus deserves attention in any coupled climate model. The change in sea surface salinity (SSS) caused by a freshwater flux F in a rigid lid model is simply given by (eg Foreman 1990):

$$dSSS/dt = - F\ SSS / \rho\ \Delta z_1 \qquad (3)$$

(In OGCMs with a free surface, equation (3) needs careful modification to account for the change in volume of the top layer. See Roullet and Madec, 2000, for details.) Unfortunately, the correlation of F and SSS in (3) then implies a global mean salinity drift, even if the global average freshwater flux is zero. For this reason, SSS in equation (3) is often (eg in the UM (Foreman, 1990)) replaced with a constant reference sea surface salinity. But non-

drifting globally averaged salinities still require globally zero freshwater fluxes, which is easier said than done, as will be shown in Section 3.4.

To prevent any resulting drift of the sea surface salinity, many modellers have simply applied a "Haney relaxation" of SSS to a climatological value:

$$dSSS/dt = -\lambda_s (SSS - SSS_{clim}) \qquad (4)$$

(where λ_s^{-1} ~ 4 months ~ the same timescale as implied by (1)), with the open admission that there is no real physical justification for such a relation.

The freshwater flux boundary condition has received more attention, however, since Bryan (1986) discovered that under "mixed boundary conditions", in which SST obeys Haney relaxation while the freshwater flux is prescribed, GCMs can develop a *variety* of steady states. He first ran a stable GCM with SSS relaxation given by (4). When he applied this diagnosed forcing to the same GCM, the polar halocline collapsed. By increasing the salinity at high latitudes he was able to produce a meridionally symmetrical THC. By further perturbing the SSS asymmetrically he was able to generate N-S or S-N circulations. This sensitivity has since been reproduced by many modellers (eg Moore and Reason 1993; Power and Kleeman 1993). Zhang et al (1993) showed that Bryan's polar halocline collapse (PHC) could be prevented by the use of flux boundary conditions on temperature as well as salinity. This is true whether the fluxes are specified directly or generated from Schopf's (1983) zero heat capacity model. Their conclusion was echoed by Mikolajewicz and Maier-Reimer (1994), who found some PHC stabilisation by modelling the surface heat flux as the sum of a specified flux and a weak Haney relaxation to climatological SSTs. (The freshwater flux was again prescribed.) And Rahmstorf and Willebrand (1995) found that their two lengthscale model of surface heat flux (eqn (2'')) deters Bryan's polar halocline collapse. Finally, Lohmann et al (1996) found that coupling their ocean model to an energy balance model (Section 2.1) led to a PHC sensitivity somewhere between Shopf's model and one with mixed BCs.

2.3 Momentum

The boundary condition on momentum is more straightforward than that of heat or salinity: the windstress τ at the sea surface is specified directly or calculated from atmospheric winds by means of a bulk formula (see equation (A.3) in Appendix A for more details). Most examinations of the subject have therefore concentrated on the quality of the source data. Josey et al (2002) compared 5 wind stress datasets: the SOC COADS-derived dataset, 2 other "observational" datasets, and 2 "reanalysis" datasets. They were all in reasonable agreement, except for the commonly used Hellerman and Rosenstein (HR) (1993) climatology, whose stresses were too high in low

latitudes. Bryan et al compared observational (HR again), reanalysis and NCAR GCM-derived wind stresses in the tropical (1995b) and the extratropical (1995a) North Atlantic. They likewise found the HR stresses to be too high in the tropics. The meridional stress (τ_ϕ) from the (ECMWF) reanalyses was too weak and too broad in the convergence zone, which they put down to problems analysing divergent flow in the AGCM. This didn't prevent it from being able to model the flow in the tropical Atlantic satisfactorily, however. The weakest dataset in the tropics was that derived from the AGCM (CCM2). Generally, the predicted currents agree with each other and with observations reasonably well. In the extratropics there was similarly little sensitivity to the wind stress climatology (despite large differences in the implied Sverdrup transports). At 25N the HR and ECMWF wind stresses generate currents that were close to observational estimates – again, CCM2 was the odd one out.

3 Data sources

Until now, most of the discussion has centred on the relaxing, negative feedback terms like $\lambda(SST - T_A)$ in (1). But the basic driving terms like $Q(T_A)$ also need specifying (unless, for example in an idealised case study, λ is unrealistically large). There are three main sources of these: ship or station observations, NWP model reanalyses, and climate model integrations. We now examine each of these briefly.

3.1 Ship or station observations

Direct observations of turbulent heat and momentum fluxes (<w'T'>, <w'q'> and <w'**u**'>) across the ocean surface are exceedingly rare. Instead, more accessible measurements of SST and atmospheric wind, humidity and temperature are combined to produce estimates of the heat flux into the ocean. This is done using bulk formulae, as described in Appendix A.

In Section 5.1 we examine some fluxes derived from ship and buoy data.

3.2 Operational reanalyses

Reanalysis projects (eg Kalnay et al 1996 for the NCEP/NCAR datasets) are designed to give the best possible estimate of the state of the atmosphere over a long period (~40 years), by recalculating atmospheric analyses based on all historically available observations and a fixed, up-to-date data assimilation system and forecast model. There are two ways of using the data to generate surface fluxes. The modelled fluxes of heat, momentum and

freshwater can be suitably averaged to provide climatological fluxes directly. Alternatively, these fluxes can be inferred from the difference between the TOA radiation fields and the divergence of the atmospheric heat fluxes derived from the reanalyses. Trenberth et al (2001a) favour the second approach, as they find direct model surface fluxes are biased, principally through errors in model clouds. They also find (2001b) good agreement between ocean heat transports derived as above, those from direct measurements in the ocean (eg Hall and Bryden 1982) and those from coupled models run without flux adjustment (eg Gordon et al 2000).

In Section 5.2 we examine some fluxes derived (mostly) from operational reanalyses.

3.3 GCM output

A third source of flux data is a spun-up climate model. AGCMS calculate surface fluxes in their boundary layer schemes – bulk formulae, in effect, but designed to provide the best fluxes of T, q and **v** to the free atmosphere rather than the ocean. These models are run with specified SSTs. The difference between these SSTs and the SSTs predicted by an OGCM driven by the AGCM fluxes says something about the fidelity of the ocean or the atmosphere model's thermal response. Realistically, one would probably run the model with Haney relaxation to the climatological SSTs and use the size of the relaxation terms to measure the drift of the OGCM.

Alternatively, the fluxes could be taken from a coupled GCM. In this case, a direct comparison of the behaviour of the two ocean models would appear – except that the ocean-to-atmosphere feedbacks present in the original coupled run would be absent in the standalone OGCM run. This is of course the principal disadvantage of standalone ocean models. But if the *same* ocean model is run coupled and decoupled, then a comparison of the runs says something about the magnitude of these A-O feedbacks, and this is of use to coupled climate modellers.

In Section 5.3 we examine some fluxes derived from an AGCM.

3.4 Adjustment of fluxes

Whatever the source of the data, it is unlikely that the net (global, annual average) fluxes into the ocean are small enough for them to be used directly in climate integrations without inducing large artificial drifts in T and S. For instance, a net heat flux imbalance of only $3W/m^2$ (and Section 5 describes fluxes much more out of balance) equates to an integrated northward ocean heat transport of around 1PW. Given that the latest estimates of this quantity are less than 2PW (Trenberth et al 2001b, and references therein), this is unacceptably large. The heat flux fields therefore have to be adjusted. This

can be done by a formal least-squares minimisation of the net heat input, subject to observational constraints on the basic fields (eg Grist and Josey, 2003), or by more-or-less ad-hoc modification of the fields based on expert judgement of the integrity of the various sources of data (eg Large and Yeager, 2004). Similarly for the net freshwater forcing. Here a net PMEPR imbalance of 3mg/m^2/s (and again, much larger figures appear in Section 5) equates to an integrated northward ocean freshwater transport of around 1Sv, which is of the same order as the estimated total flow (eg Gnanachaud and Wunsch, 2000). The remedy is less clear in this case, and seems to have received less attention in the literature. Even less interest seems to have been paid to the problem of net torque on the ocean arising from incompletely balanced windstresses, even though the resulting effects may be no less significant.

Appendix B gives more details of the changes in the heat fields brought about by the adjustments applied to two of the datasets described in this report.

4. Some examples of surface forcings in OGCMs

The following is a brief discussion of how and where the above ideas have been used in projects involving the Met Office.

The PREDICATE (1999) project has been mentioned already; it looked at atmosphere-ocean couplings in the North Atlantic and at decadal predictions of European climate. It used Bentsen and Drange's (2000) "inverse bulk formulae" approach to derive turbulent fluxes of heat and momentum. Precipitation and runoff are prescribed, and then the SSS is restored by equation (4) (Pardaens, 2004, pers. comm.).

FOAM, the Met Office's deep ocean forecasting system (FOAM, 2006) takes air-sea heat fluxes every 6 hours from operational NWP models. SST and SSS are relaxed to Levitus climatology.

GloSea (2002) is the ensemble seasonal forecasting ocean model, based on HadCM3 with a stretched grid. To initialise the ocean state, air-sea fluxes derived from ERA-40 reanalyses are applied daily, as is Haney relaxation to the ERA-40 SSTs and SSSs, and long timescale relaxation of ocean body temperatures and salinities to Levitus climatology.

The standalone UM ocean model (Foreman, 1990) can be driven by specified air-sea fluxes, together with relaxation of SST, SSS and sea-ice depth.

NEMO (Madec et al, 1998), the European ocean model which the Met Office is adopting as its next ocean model, can be driven by fluxes of heat and moisture or by specifying atmospheric variables and applying bulk formulae. At present, wind stresses have to be specified directly. SST and SSS can be

relaxed to specified values with constant Haney relaxation coefficients λ and λ_s, and interior temperatures and salinities to background fields.

In its default global climate configuration, NEMO is coupled to the LIM ice model, which requires the use of bulk formulae. However, the model can be run without sea-ice, which allows fluxes to be directly specified. This is the way we intend to use it in our evaluation of three new surface flux datasets – to an examination of which we now turn.

5. Evaluation of three surface flux datasets

5.1 Adjusted SOC fluxes

The original SOC dataset (Josey et al 1998) comprises monthly mean air-sea fluxes of heat, momentum and freshwater. These are derived from COADS ship reports from 1980-1993, corrected for known observational biases. Smith's (1988) bulk formulae are used to calculate LH, SH and τ, while LW and SW are calculated by Clark et al's (1974) and Reed's (1977) formulae, respectively. Corrected present weather reports give the precipitation. Global monthly means are produced on a 1° X 1° grid by iteratively correcting the background field.

The resulting global, annual mean total heat flux into the ocean is 30 W/m^2. As described above, this is unacceptably large for ocean climate modelling, as it implies global heat transports of order 10 PW. The heat fields (only) were therefore adjusted objectively (Grist and Josey 2003) by multiplying each heat field by an adjustable parameter. These parameters' values were adjusted until the resulting implied heat transports gave the best match (in a least-squares sense) to hydrographically estimates of the heat transports (Gnanachaud and Wunsch 2000). The first attempt reduced the global heat imbalance from 30 W/m^2 to -5 W/m^2. This was mainly brought about by an increase in latent heat cooling and a decrease in shortwave heating. This is still too large, so they repeated the analysis with the additional constraint that the net imbalance was less than 2 W/m^2 in magnitude, which is consistent with the observed decadal temperature variation. (Constraining the overall heat imbalance to be exactly zero required an unrealistically large change in LH cooling.) Their final best estimate had a net heat imbalance of -2 W/m^2, and it is these adjusted fields which we discuss below.

Figures 1a-1i show the LH, SH, LW, SW, total heat, precipitation, total freshwater, zonal windstress and meridional windstress for the adjusted SOC datasets.

The upper panels show the annual means, with zonal means for individual months and for the whole year alongside. The lower panels show the standard deviation of the field in time, with the standard deviation in longitude for each month alongside, together with the zonal mean of the standard deviation in time (ie the data on the map). (This last curve, labelled "ANN" on the figures, is not equal to the mean of the monthly longitudinal standard deviations (coloured curves), because the operations of taking the standard deviation and taking the mean do not commute. Fig 1c should clarify this.)

5.1.1 **Heat**

It is clear, as expected, that the largest two components of the heat budget are the LH cooling (Fig 1a) and the SW heating (Fig 1c). The shortwave heating is of course concentrated in the Tropics, with large variations in the extratropics. The Mediterranean and the South-West Atlantic show the strongest variability, although the SOC authors caution against putting too much faith in fields south of 40°S because of the paucity of source ship and buoy data in the Southern Ocean. The latent cooling is greatest (and has the greatest variability) over the Gulf Stream and the Kuroshio Current. It's smallest at high latitudes and in the Equatorial East Pacific, over the upwelling region associated with the Peruvian Eastern Boundary current – a relatively steady signal. The sensible heat loss is largest over the Gulf Stream and Kuroshio Currents in DJF; otherwise it's fairly steady in space and time, as is the longwave heating.

The total heat into the ocean (LH+SH+LW+SW), Fig 1e, is of course positive in the tropics and negative outside them, with a local maximum on the Equatorial E Pacific (least LH cooling) and local minima over the strong Western boundary currents (most LH cooling in DJF). The variability is smallest over the equator and largest over the WBCs. The global, annual mean heat input to the ocean is -2.5 W/m^2, which is close to SOC's reported value of -2W/m^2.

5.1.2 **Freshwater**

The precipitation rate (Fig 1f) is noisier than the other fields. It is largest (and most variable) in the ITCZ and SPCZ. The maximum over the Gulf Stream peaks in DJF; that over the Kuroshio Current peaks in MJJ and SON (App C, Fig C.1f). There is more variability in the Southern hemisphere than in the Northern.

The net freshwater flux (PMEPR=precipitation-evaporation+runoff[1])), Fig 1g, inherits the noisiness of the precipitation field. It has a characteristic +–+–+ signal in the zonal mean. The global, annual average freshwater flux is -6.7 mg/m^2/s, which equates to a very large freshwater transport of -2.6 Sv. This is a consequence of the adjustment process: increasing the LH cooling necessarily increases the evaporation rate, which destroys the freshwater balance. (The unadjusted fields had a net PMEPR of -0.7 mg/m^2/s = -0.2 Sv, which is much more tolerable.) To get around this unacceptably large freshwater transport we intend to simply rescale the precipitation fluxes to restore the balance, until a revised set of fluxes in which heat and freshwater fields are simultaneously adjusted is available (Josey, 2004, pers. comm.).

5.1.3 **Momentum**

The zonal windstress τ_λ (Fig 1h) is largest in high latitudes, particularly over the Southern Ocean. The greatest variability is over the Arabian Sea. Monthly fields (App C, Fig C.1h) attribute this to the Indian Monsoon: τ_λ is much larger in JJA. The mean eastwards stress on the ocean is 5.4e-3 N/m^2. The meridional windstress τ_ϕ (Fig 1i) shows the Equatorial convergence of the winds, and the Eastern boundary currents off Austrialia and S America, as well as the Indian Monsoon variability again.

5.2 GFDL Corrected Normal Year Forcing

The GFDL dataset (Large and Yeager 2004) is derived from a variety of sources. NCAR reanalyses provide the atmospheric fields every 6 hours for 53 years on a T62 (~200km) grid. ISCCP satellite products provide the SW and LW fields every day or month from 1983 to 2000. Monthly precipitation fields are a patchwork of data from 3 different sources, each containing satellite and gauge data. Runoff (as used in SOC) is derived from Baumgartner and Reichel's (1975) climatology, split into localised river runoff where estimates of this exist, with the remainder distributed evenly along the coast of each basin. The supplied SSTs, needed to calculate turbulent fluxes via bulk formulae, come from analyses based on in situ and satellite observations.

Large and Yeager combined all these products over the 17 years when all the data sources are available. They found a net heat input of 31 W/m^2 and a net freshwater input of 3.4 mg/m^2/s. As noted before, these are unacceptably

[1] The runoff is not provided in the SOC dataset, so we have borrowed the runoff field from the GFDL dataset (Section 5.2). This is at the same 1° resolution as the SOC datasets, but it has a slightly different land-sea mask, and so we have bilinearly interpolated to the SOC grid. The highly localised nature of this field makes it sensitive to interpolation, so we have globally rescaled the interpolated runoff to match the global average of the original data.

large. By increasing the wind speed and reducing the humidity of the air, which increase the LH cooling, and by reducing the SW forcing over the tropics and subtropics, they were able to reduce the net heat imbalance to 1.0W/m^2. (There are also minor changes to the temperature poleward of 60S, which affects SH, and to LW poleward of 60N. These have small effects on the heat budgets.) The precipitation is then scaled and shifted, so that the resulting mean freshwater forcing is -0.1 mg/m^2/s.

Large and Yeager have produced fluxes over the 43 year period 1958-2000, by assuming periodicity in those source datasets that don't extend that far in time. This allows some interannual variability in the forcing. They have also produced a "Normal Year Forcing" climatology, by averaging over corresponding dates and times in the 43 years, carefully wrapping fields around from the end of the year to its beginning, giving low weightings to anomalous years, and so on. This Corrected Normal Year Forcing (CNYF) is what we will discuss in detail below.

The atmospheric fields and SSTs have been downloaded and passed through bulk formulae (see Appendix A) to derive turbulent fluxes every 6 hours for the Normal Year. Similarly for the SW, LW, PPN and runoff. These are then averaged into monthly means. (Passing time-averaged fields through bulk formulae is quicker but produces very weak fluxes, because of the non-linearities in the bulk formulae which make LH(<q>) much less than <LH(q)>. Fissell et al (1977) highlight the importance of not averaging source data too long before calculating fluxes: they find a 70% reduction in windstress by averaging 3 hourly source data over 3 months.)

Figs 2a-2i show the same fields as figs 1a-1i on the same colour scales. Many of the plots show noise arising from Gibbs oscillations on the Gaussian grid of the NCAR spectral model which generated the atmospheric variables (Winton, 2004, pers. comm.). To get a fair comparison with the SOC dataset, all fields are masked over a sea-ice field defined by the given SST field. As all the plots show the same general features as the SOC fields, we concentrate here on the differences.

5.2.1 **Heat**

The global mean LH is similar to that of SOC, though there's rather more cooling in the tropics and perhaps a little less over the Gulf Stream and Kuroshio. There's less variation in time over the latter, too. There are large local signals in SH at the edge of the sea ice; otherwise, SH looks similar to LH. The SW has a similar pattern to SOC's, but is about 10 W/m^2 larger almost everywhere. The LW cooling is stronger over the middle of the ocean basins, but its local minima off Newfoundland, Peru and Angola are not apparent in the SOC LW data. The mean total heat input looks similar to that of SOC, though with less heat input to the tropics and more in the extratropics. The GFDL total heat input has less variability over the Western Boundary Currents.

The global average heat input is 1.3 W/m^2, close to the reported (Large & Yeager, 2004) figure of 1.0 W/m^2.

5.2.2 **Freshwater**

The GFDL mean PPN rate is very similar to SOC's in outline, the only clear difference being that the GFDL field is smoother. This is probably because it is derived from satellite (and gauge) data rather than ship weather reports. The precipitation rate over the Gulf and Kuroshio, and over the ITCZ and SPCZ, is a little higher in the GFDL dataset. The annual mean precipitation rates agree to within about 10%. The runoff field is the same as SOC's, as discussed above. The total freshwater flux is much smoother (in space and time) than SOC's, and has a net input of -2.7 mg/m^2/s. This is better than SOC's -6.7 mg/m^2/s, but still a long way from GFDL's reported figure of -0.1 mg/m^2/s. Since the 6% reduction in evaporation rate needed to restore freshwater balance would increase the net heat input to 8W/m^2, we intend instead to increase the precipitation rate (everywhere) by 7% before forcing an ocean model with these fluxes.

5.2.3 **Momentum**

The annual mean zonal momentum τ_λ is a bit stronger than SOC's everywhere (excepet the tropical west Pacific), especially over the ACC. It's more variable in time almost everywhere, except for the Monsoon, which appears a bit weaker in the monthly means (App C, Fig C.2h). The mean eastwards stress on the ocean is 6.0e-3 N/m^2, similar to the SOC figure. Meridional stresses τ_ϕ are similar to SOC's in the mean, but have slightly more variability in the far North.

5.3 HadGAM1 AMIP2 Forcing

HadGAM1 has been run between 1978 and 2003 with recent ("ensemble member 2") AMIP2 SST and sea-ice fields (Martin et al 2004). Monthly mean modelled heat, momentum and freshwater fluxes have been averaged over all 24 years to produce a HadGAM1 "Normal Year Forcing" dataset, which will be described below. Since these fields are less strongly constrained by observations than the other datasets (apart from the SSTs and sea-ice), a comparison with the others should say something about the integrity of the fluxes from the HadGAM1 model.

Figs 3a-i show the usual fluxes in the standard format. Since the fields show the same general structure as the other two datasets, we concentrate on the differences between them here.

5.3.1 **Heat**

HadGAM1's latent heat loss is 10% greater than SOC's or GFDL's; it also has the greatest variability over the WBCs. The sensible cooling is larger and more variable over the Gulf and Kuroshio; otherwise it's similar to the other two datasets. The SW heating in HadGAM1 is larger everywhere, but of comparable variability, except in the Mediterranean where SOC is much more variable. The HadGAM1 LW cooling is stronger in the tropics and weaker in the extratropics than in either of the other two datasets. The stronger latent cooling and SW heating complement each other partially, so that the net heat input looks fairly similar to the other two, but is overall rather better balanced. The large temporal variability of the total heat field over the Gulf and Kuroshio is closer to SOC than to GFDL. The overall annual average net heat input to the ocean is just 0.2 W/m^2.

5.3.2 **Freshwater**

The HadGAM1 precipitation field is larger than that of the other two datasets, by around 20% in the mean. Rainfall over the Indian Ocean and the warm pool is much stronger, particularly in summer. The higher precipitation is balanced by the increased evaporation/latent cooling, so that the net freshwater[2] is better balanced than in either SOC or GFDL: a net flux of -0.6 $mg/m^2/s$ before applying the land sea mask. Doing this masks the Arctic river runoff so that this figure rises to -2.3 $mg/m^2/s$ (which gives an indication of its sensitivity to such details). The4 HadGAM1 freshwater flux is much more variable in the tropics, however, although (like GFDL) it has none of the variability over the SH storm tracks seen in the SOC dataset. As for the other two datasets, the precipitation will be rescaled to ensure zero net freshwater input before being used to force a standalone ocean model.

5.3.3 **Momentum**

The HadGAM1 zonal stress τ_λ is stronger in the (NH and SH) storm tracks than it is in the other two datasets. It's more variable in the N Pacific and S Indian oceans. A stronger Indian Monsoon shows up in the monthly means (App C, Fig C.3h). The mean eastwards wind stress on the ocean is 11.3e-3 N/m^2, twice as large as in SOC or GFDL. (Bear in mind, however, that this is a small residual average of a field that varies between ±0.2 N/m^2. And when weighted by $\cos(\phi)$, to give an estimate of the net *torque* on the ocean, HadGAM1 has a *smaller* residual (-0.33 mN/m^2) than SOC (-2.77 mN/m^2) or GFDL (-2.64 mN/m^2).) The meridional stress τ_ϕ is fairly similar in mean and variance in all three datasets. (Note that its contour range is half that of τ_λ.)

[2] The HadGAM1 runoff fields have been obtained by conservatively redistributing runoff on (atmosphere model) land points onto adjacent (ocean model) sea points. The resulting global mean of 3.1 $mg/m^2/s$ is reassuringly close to the GFDL figure of 3.2 $mg/m^2/s$.

6 Comparison of the 3 datasets

6.1 **Annual means**

The differences between the datasets are further examined in Figs 4a-i. These show difference plots, for the annual mean of each field, for each of the datasets, taken in pairs. These should help to reinforce and to make quantitative the conclusions discussed above.

6.1.1 Heat

Fig 4a shows that HadGAM1 has more latent heat cooling than SOC over most of the ocean, and more than GFDL over the subtropics (especially the Sc regions). SOC has the least latent cooling in the tropics.

The sensible heating differences (Fig 4b, on the same contour range as Fig4a), are clearly smaller generally. The most significant signal is SOC's approximately uniform 5 W/m^2 SH deficit and HadGAM1's excess SH loss over the Gulf Stream and Kuroshio.

The SW heating comparisons in Fig 4c show a nearly uniform 10 W/m^2 excess of GFDL over SOC, and the ~25 W/m^2 excess of HadGAM1 over SOC in the tropics.

Fig 4d suggests that HadGAM1 has an excess LW cooling in the tropics and a deficit in the extratropics.

The resulting differences in total heating are shown in Fig 4e. They are clearly largely dominated by the latent cooling and SW heating differences.

6.1.2 Freshwater

The excess tropical precipitation in HadGAM1 is clear from Fig 4f. It's hard to see any other signal.

The net freshwater (Fig 4g) shows this and HadGAM1's higher evaporation in the Sc regions, as is evident in Fig 4a.

6.1.3 Windstress

HadGAM1's excessive zonal windstress over the Southern Ocean is clear from Fig 4h, as is its stronger tropical easterlies. GFDL is stronger than SOC in these respects too.

There's a stronger southerly component of the windstress (Fig 4i) over the Southern Ocean in GFDL than in HadGAM1, and in HadGAM1 than in SOC.

6.2 **Zonal, annual means**

Fig 5 shows the zonal means of total heat, net freshwater and zonal windstress over the global ocean. It highlights the following features from Figs 4c, 4g and 4h.

6.2.1 Total heat

The equatorial peak is clearly strongest in HadGAM1. The GFDL peak has a broader limb in the Southern Hemisphere; the SOC peak is broader in the Northern. Poleward of the Gulf Stream and Kuroshio minima, GFDL is more positive and SOC and HadGAM1 are similar.

6.2.2 Net freshwater

HadGAM1 is again largest at the equator, with a strong twin peak that is not apparent in the other datasets. HadGAM1 is also largest in the extratropics.

6.2.3 Zonal windstress

SOC and GFDL are broadly similar throughout. HadGAM1 has stronger westerlies in the Southern Ocean and Northern hemisphere extratropics. Its subtropical easterlies are also generally the strongest.

6.3 **Seasonal variation**

We approximate the time-dependence of any climatological field *f* as:

$$f(t) \approx c_0 + \sum_{n=1}^{N} c_n \cos(2\pi n t / T - \varphi_n)$$

where T=1 year (the periodicity of *f*), $c_n \geq 0$ and $-\pi < \varphi_n \leq \pi$. With only 12 monthly fields, we truncate the series at N=2 (ie we look at annual and binannual cycles only). Note that c_0, the annual mean of *f*, has already been plotted in the top panels of Figs1-3.

In Figs 6 we plot the normalised amplitude of mode *n*, $\gamma_n := c_n / \sqrt{2}s$, where *s*, the standard deviation of *f*, has already been plotted in the bottom panels of Figs1-3. Note that $\sum_n \gamma_n^2 = 1$, so that γ_n^2 is the fraction of the variance of *f* explained by the nth mode. We also plot, as a vector of magnitude γ_n, the peak time of the nth mode, $t_n := \varphi_n T / 2\pi n$. (Note that for negative fields, this is actually the time at which *f* is *weakest*, ie least negative.)

6.3.1 Total heat

Figs 6.1 plot the amplitude and phase of the n=1 and n=2 modes of the total heat input for the three datasets. The annual solstitial cycle in the extratropics and biannual equinoctial cycle in the tropics are clear in all three. The biannual cycle in the tropics appears a little more widespread in the SOC dataset. HadGAM1 has the strongest annual cycle on the equator, particularly in the Indian Ocean, Indonesia and the west Pacific.

6.3.2 Net freshwater

The n=1 and n=2 cycles of this are shown in Figs 6.2. SOC shows little coherent signal in the Southern hemisphere, but is probably closest to HadGAM1 in the Northern. In particular, both show a strong annual cycle in the NW Atlantic, which is missing in the GFDL dataset. This has been traced to the evaporation rather than the precipitation (not shown). Timeseries of net freshwater at (60W, 40N) (Fig 7, top panel) show that the GFDL climatology is much noisier (arguably having an n=3 component) which reduces the amplitude of the n=1 annual cycle which is apparent in SOC and HadGAM1.

6.3.3 Zonal momentum

The n=1 and n=2 cycles of this are shown in Figs 6.3. Again, GFDL is the odd one out in the extratropical Northern hemisphere (the n=1 component is smaller). It peaks in winter as expected. (Bear in mind that $\tau_\lambda < 0$ in the subtropics (see eg Fig 1h), so that $|\tau_\lambda|$ peaks in winter too.) The ribbon of binannual variability across the Southern N Atlantic is striking. There's some evidence of it in HadGAM1, but very little in GFDL. Timeseries of τ_λ at (30W, 25N) (Fig 7, bottom panel) confirm the strong n=2 cycle in SOC (and the noise in GFDL). It is also clear that if the January SOC figure matched the January HadGAM1 figure, there would be little difference between the two datasets at this point, so we should be careful not to read too much into this.

HadGAM1 also has a pronounced biannual cycle in τ_λ in the Southern hemisphere over the ACC, particularly upstream of Drake Passage and the Tasman Sea. There's weaker evidence for this in the GFDL fluxes. It may be a result of normalising with respect to a smaller standard deviation in HadGAM1 (cf Figs 1h, 2h and 3h).

In general, HadGAM1 is the smoothest (in time) of the datasets (largest percentage of variance explained by n=1 and n=2 modes) and GFDL the noisiest. The exception is the net freshwater flux, where, due to the noise in the precipitation rate (based on ship weather reports), SOC is the noisiest.

6.4 **Global, annual means**

Table 1 lists the global, annual averages of the components of the heat, freshwater and momentum fluxes for all three datasets.

Table 1: Summary of surface flux datasets

.

	LH (Wm^{-2})	SH (Wm^{-2})	SW (Wm^{-2})	LW (Wm^{-2})	Total heat (Wm^{-2})	PPN ($mg/m^2/s$)	EVAP ($mg/m^2/s$)	RUN ($mg/m^2/s$)	Total fresh water ($mg/m^2/s$)	TAUX (mN/m^2)	TAUY (mN/m^2)
SOC (adjusted)	-	-		-54.2	-2.5			3.1	-6.7	5.4	2.2
GFDL (CNYF)	-	-		-55.1	1.3			3.2	-2.7	6.0	-1.5
HadGAM1 (AMIP2)	-	-		-55.2	0.2			3.1	-2.3	11.3	0.4

It is clear that the HadGAM1 dataset has the highest latent cooling, SW heating and precipitation. This is interesting because the adjustments applied to the original SOC and GFDL datasets to improve their overall heat balance involved an increase in the LH cooling and a reduction in the SW heating. The results would have been closer to the HadGAM1 figures if they'd increased the LH even more and left the SW alone. (The unadjusted SOC and GFDL mean SW fluxes were 180 and 185W/m^2 respectively.) SOC's small SW heating rate is partially offset by its small sensible heat loss.

The freshwater budget, however, suggests that the adjusted latent heat fluxes may already be too high. This is because the best available observational estimates of precipitation (CMAP (Xie and Arkin, 1997), GPCP (Adler et al, 2003)) suggest an annual mean over the ocean of between 33 and 35 mg/m^2/s, which is close to the SOC figure. The evaporation rate needed to balance this precipitation (assuming a runoff flux of 3 mg/m^2/s) implies a latent heat flux of about 90 W/m^2 – similar to the *unadjusted* SOC and GFDL fluxes (92 and 82 W/m^2 respectively)! A higher latent heating rate than this would destroy the freshwater budget (as it has for SOC) unless the precipitation rate were too high (as it appears to be for GFDL or HadGAM1).

The precipitation rate in HadGAM1 is significantly higher than in the SOC or GFDL datasets, or the observations, which provides further evidence that the tropical convection is too strong in HadGAM1 (Martin et al, 2004).

HadGAM1 has a significantly larger average net eastwards windstress on the ocean than SOC or GFDL, although these are small residuals. The HadGAM1 windstress magnitudes are larger than in GFDL or SOC.

7. Summary, conclusions and future work

This report has looked at the specification of air-sea fluxes in standalone ocean General Circulation Models. A brief literature review has discussed the origins of "Haney Forcing", and highlighted its strengths and weaknesses. Particular problems with "mixed" boundary conditions in climate integrations have been described. Some examples of surface forcings in recent ocean modelling projects have been listed. Finally, three flux datasets have been compared and contrasted. The results of using these datasets in a standalone OGCM will be the subject of a later report.

The SOC surface flux dataset was originally derived from COADS ship reports. The resulting fluxes were then adjusted to achieve better overall heat balance. The resulting SW heating and sensible cooling are the smallest of all the datasets. One consequence of the increased latent heat loss coming from the adjustment process is that the freshwater balance between precipitation and evaporation is destroyed. This will be corrected before the fluxes are used to drive climate models.

The GFDL dataset was derived from a variety of sources: NCAR reanalyses, ISCCP satellite observations, rain gauges etc. The resulting heat fluxes were out of balance by some 30 W/m^2, which, coincidentally, is about the same as in the original SOC dataset. By increasing the latent heating and reducing the SW heating, GFDL were able to balance the heat budget quite closely. Unlike SOC, the precipitation rate was adjusted, so that this dataset has a better freshwater balance.

The HadGAM1 dataset was produced by averaging monthly fluxes from a 24 year AMIP2 run. It has the closest heat and freshwater balance of any of the datasets, but the strongest wind stresses. Tropical precipitation is stronger (and has a larger variance) than in the other two datasets, which is indicative of the overactive Hadley circulation in HadGAM1. This increased freshwater input is balanced by a larger evaporation rate. The higher latent heat loss associated with this is balanced (globally) by higher SW heating.

Table 1 lists the global means of various fields in the three datasets, and shows differences in heat or freshwater input of a few W/m^2 or $mg/m^2/s$. However, these figures mask large local differences between the three datasets (eg ± 50 W/m^2 (Fig 4e) and ± 20 $mg/m^2/s$ (Fig 4g)).

We propose to use each of the datasets described in this report to force the NEMO ocean model. This model is formulated in general orthogonal curvilinear coordinates, which allows the North Pole singularity to be removed by means of a tripolar grid (Madec et al, 1998). The resulting grids are far from regular, and mapping fluxes conservatively to such grids needs special attention. However, methods for doing this are available (eg Jones, 1999), and these should allow the fluxes described here to be applied to an ocean model directly.

We have in fact already run a low resolution (2°) version of the NEMO model, forced by the all three flux datasets, for 100 years. It appears to be reasonably stable, and to respond predictably to the forcings. We expect that all three datasets can be run through a high resolution (1°) version of NEMO for a similar period, to examine the model's sensitivity to surface forcings.

8. Acknowledgements

We would like to thank Chris Gordon for his encouragement and advice. Anne Pardaens was very helpful with many aspects of freshwater forcing. Simon Josey at SOC, Michael Winton at GFDL and Gill Martin at Met Office (HadGAM1) gave very useful advice on their respective datasets. Jonathan Gregory kindly amended his PV-WAVE procedures to allow irregularly gridded netcdf data to be converted to pp-format.

9. References

Adler R F, Huffman G J, Chang A, Ferraro R, Xie P P, Janowiak J, Rudolf B, Schneider U, Curtis S, Bolvin D, Gruber A, Susskind J, Arkin P and Nelkin E, 2003: The Version-2 Global Precipitation Climatology Project (GPCP) Monthly Precipitation Analysis (1979-Present), *Journal of Hydrometeorology*, **4**, pp 1147-1167.

Baumgartner A and Reichel E, 1975: The world water balance, Elsevier, New York, 180pp.

Bentsen M and Drange H, 2000: Parametrizing surface fluxes in ocean models using the NCEP/NCAR reanalysis data. *RegClim General Technical Report No. 4*, Norwegian Institute for Air Research, Kjeller, Norway, pp 149-158.

Blanc T V, 1985: Variation of Bulk-Derived Surface Flux, Stability, and Roughness Results Due to the Use of Different Transfer Coefficient Schemes, *Journal of Physical Oceanography*, **15**, No. 6, pp. 650-669.

Bretherton F P, 1982: Ocean Climate Modelling, *Prog Oceanography*, **11**, pp 93-129.

Bryan F, 1986: High latitude salinity effects and hemispheric thermohaline circulations, *Nature*, **323**, pp 301-304.

Bryan F O, Boning C W and Holland W R, 1995a: On the midlatitude circulation in a high-resolution model of the North Atlantic, *Journal of Physical Oceanography*, **25**, pp 289-305.

Bryan F O, Wainer I and Holland W R, 1995b: Sensitivity of the tropical Atlantic circulation to specification of wind stress climatology, *Journal of Geophysical Research*, **100**, No C12, pp 24729-24744.

Bryden H and Imawaki S, 2001: Ocean Heat Transport, Chapter 6.1 of *Ocean Circulation and Climate*, eds Siedler G, Church J and Gould J, International Geophysical Series, Academic Press, **77**, pp 455-474.

Clark N E L, Eber L, Laurs R M, Renner J A and Saur J F T, 1974: Heat exchange between ocean and atmosphere in the eastern North Pacific for 1961-71. *NOAA Tech Rep NMFS SSRF-682*, US Dep of Com, Washington DC, 108pp.

Fairall C W, Bradley E F, Rogers D P, Edson J B and Young G S, 1996: Bulk parameterization of air-sea fluxes for Tropical Ocean-Global Atmosphere Coupled-Ocean Atmosphere Response Experiment, *Journal of Geophysical Research*, **101**, No C2, pp 3747-3764.

Fissel D B, Pond S and Miyake M, 1977: Computation of Surface Fluxes from Climatological and Synoptic Data, *Mon Wea Rev*, **105**, pp 26-36.

FOAM, 2006: http://www.metoffice.gov.uk/research/ncof/foam/index.html

Foreman S, 1990: Application of surface heat and fresh water fluxes, *Met Office UMDP 50.*

Frankignoul C, Ketsenare E, Botzet M, Carril A F, Drange H, Pardaens A, Terray L and Sutton R, 2004: An intercomparison between the surface heat flux feedback in five coupled models, COADS and the NCEP reanalysis, *Climate Dynamics*, **22**, pp 373-388.

GloSea, description from DEMETER background 2002: http://www.ecmwf.int/research/demeter/general/docmodel/meto.html

Gnanachaud A and Wunsch C, 2000: Improved estimates of global heat circulation, heat transport and mixing from hydrographic data, *Nature*, **408**, No 6811, pp 453-457.

Gordon C, 1993: Parameters for Haney forcing, http://www-nwp/~frmb/parameters/haney.html

Gordon C, Cooper C, Senior C A, Banks H, Gregory J M, Johns T C, Mitchell J F B and Wood R A, 2000: The simulation of SST sea ice extents and ocean heat transports in a version of the Hadley Centre coupled model without flux adjustments, *Climate Dynamics*, **16**, pp 147-168.

Grist J P and Josey S A, 2003: Inverse analysis adjustment of the SOC air-sea flux climatology using ocean heat transport constraints, *Journal of Climate*, **16**, No 20, pp 3274-3295.

Hall M H and Bryden H L, 1982: Direct estimates and mechanisms of ocean heat transport, *Deep-Sea Res*, **29**, No 3A, pp 339-359.

Haney R L, 1971: Surface Thermal Boundary Condition for Ocean Circulation Models, *Journal of Physical Oceanography*, **1**, No. 4, pp. 241-248.

Hellerman S and Rosenstein M, 1983: Normal Monthly Wind Stress Over the World Ocean with Error Estimates, *Journal of Physical Oceanography*, **13**, pp 1093-1104.

Jones P W, 1999: First- and second-order conservative remapping schemes for grids in spherical coordinates, *Mon Wea Rev*, **7**, No 129, pp 2204-2210.

Josey S A, Kent E C and Taylor P K, 1998: The Southampton Oceanography Centre (SOC) Ocean–Atmosphere Heat, Momentum and Freshwater Flux Atlas, *Southampton Oceanography Centre Report No 6*, Southampton, UK, 30pp & figs.

Josey S A, Kent E C and Taylor P K, 2002: Wind stress forcing of the ocean in the SOC climatology: comparisons with the NCE-NCAR, ECMWF, UWM/COADS, and Hellerman and Rosenstein datasets, *Journal of Physical Oceanography*, **32**, pp 1993-2019.

Kalnay E et al, 1996: The NCEP/NCAR 40-year reanalysis project, *Bull Amer Met Soc*, **77**, pp 437-471.

Killworth, P D, Smeed, D A and Nurser A J G, 2000: The Effects on Ocean Models of Relaxation toward Observations at the Surface, *Journal of Physical Oceanography*, **30**, No. 1, pp. 160-174.

Large W G and Pond S, 1981: Open Ocean Momentum Flux Measurements in Moderate to Strong Winds, *Journal of Physical Oceanography*, **11**, pp 324-336.

Large W G and Pond S, 1982: Sensible and Latent Heat Flux Measurements over the Ocean, *Journal of Physical Oceanography*, **12**, pp 464-482.

Large W G and Yeager S G, 2004: Diurnal to Decadal Global Forcing for Ocean and Sea-Ice Models: The Data Sets and Flux Climatologies, *NCAR Technical Note NCAR/TN-460+STR*, pp 62 & figs.

Lohmann G, Gerdes R and Chen D, 1996: Sensitivity of the thermohaline circulation in coupled oceanic GCM – atmospheric EBM experiments, Clim Dyn, **12**, pp 403-416.

Madec G, Delecluse P, Imbard M and Levy C, 1998: OPA8.1 Ocean General Circulation Model Reference Model, *IPSL Tech Note 1*, 91 pp.

Martin G, Dearden C, Greeves C, Hinton T, Inness P, James P, Pope V, Ringer M, Slingo J, Stratton R and Yang G-Y, 2004: Evaluation of the atmospheric performance of HadGAM1/GEM1, *Met Office HCTN 54*.

Mikolajewicz U and Maier-Reimer E, 1994: Mixed boundary conditions in ocean general circulation models and their influence on the stability of the model's conveyor belt, *Journal of Geophysical Research*, **99**, No C11, pp 22633-22644.

Moore A M and Reason C J C, 1993: The reponse of a Global Ocean General Circulation Model to Climatological Surface Boundary Conditions for Temperature and Salinity, *Journal of Physical Oceanography*, **23**, pp 300-328.

Mullerworth S, 2006: FLUME Implementation Project Documentation http://www-hc/~hadsm/FLUMEProject/projectDocs/index.html

North G R, 1988: Lessons for Energy Balance Models, *Proceedings of the NATO Advanced Study Institute on physically based modelling and simulation of climate and climatic change*. Part 2. Erice, Italy.

Oberhuber J M, 1988: An atlas based on the COADS data set: the budgets of heat, buoyancy and turbulent kinetic energy at the surface of the global ocean, *Max-Plank-Institut fur Meteorologie Report No 15*, 20 pp & figs.

Philander, S G H and Seigel, A D, 1985: Simulation of El Nino of 1982-1983. In *Coupled Ocean-Atmosphere Models* (ed. J.C.J. Nihoul). Amsterdam: Elsevier.

Power S B and Kleeman R, 1993: Multiple Equilibria in a Global General Circulation Model, *Journal of Physical Oceanography*, **23**, pp 1670-1681.

PREDICATE project, 1999: http://www.met.rdg.ac.uk/~rowan/fp5/predicate.html

Rahmstorf S and Willebrand J, 1995: The role of temperature feedback in stabilizing the thermohaline circulation, *Journal of Physical Oceanography*, **25**, pp 787-805.

Reed R K, 1977: On estimating insolation over the ocean, *Journal of Physical Oceanography*, **7** pp 482-485.

Roullet G and Madec G, 2000: Salt conservation, free surface, and varying levels: a new formulation for ocean general circulation models, *Journal of Geophysical Research*, **105**, No C10, pp 23927-23942.

Schopf P S, 1983: On equatorial waves and El Nino. II: Effects of air-sea thermal coupling, *Journal of Physical Oceanography*, **13**, pp 1878-1893.

Seager R, Blumenthal M B and Kushnir Y, 1995: An Advective Atmospheric Mixed Layer Model for Ocean Modeling Purposes: Global Simulation of Surface Heat Fluxes , *Journal of Climate*, **8**, No 8, pp 1951-1964.

Smith S D, 1980: Wind Stress and Heat Flux over the Ocean in Gale Force Winds, *Journal of Physical Oceanography*, **10**, pp 709-726.

Smith S D, 1988: Coefficients for Sea Surface Wind Stress, Heat Flux, and wind Profiles as a Function of Wind Speed and Temperature, *Journal of Geophysical Research*, **93**, No C10, pp 15467-15472.

Stocker T F, Wright D G and Mysak L A, 1992: A Zonally Averaged, Coupled Ocean-Atmosphere Model for Paleoclimate Studies, *Journal of Climate*, **5**, pp 773-797.

Trenberth K E, Caron J M and Stepanaik D P, 2001a: The atmospheric energy budget and implications for surface fluxes and ocean heat transports, *Climate Dynamics*, **17**, pp 259-276.

Trenberth K E and Caron J M, 2001b: Estimates of Meridional Atmosphere and Ocean Heat Transports, *Journal of Climate*, **14**, No 3, pp 3433-3443.

Wijffels S, 2001: Ocean Transport of Fresh Water, Chapter 6.2 of *Ocean Circulation and Climate*, eds Siedler G, Church J and Gould J, International Geophysical Series,, Academic Press, **77**, pp 475-488.

Xie P P and Arkin P A, 1997: Global Precipitation: A 17-Year Monthly Analysis Based on Gauge Observations, Satellite Estimates, and Numerical Model Outputs, *Bull Amer Met Soc*, **78**, No 11, pp 2539-2558.

Zhang S, Greatbatch R and Lin C, 1993: A Re-examination of the Polar Halocline Catastrophe and Implications for Coupled Ocean-Atmosphere Modeling, *Journal of Physical Oceanography*, **23**, pp 287-299.

SOC ADJUSTED CLIMATOLOGY

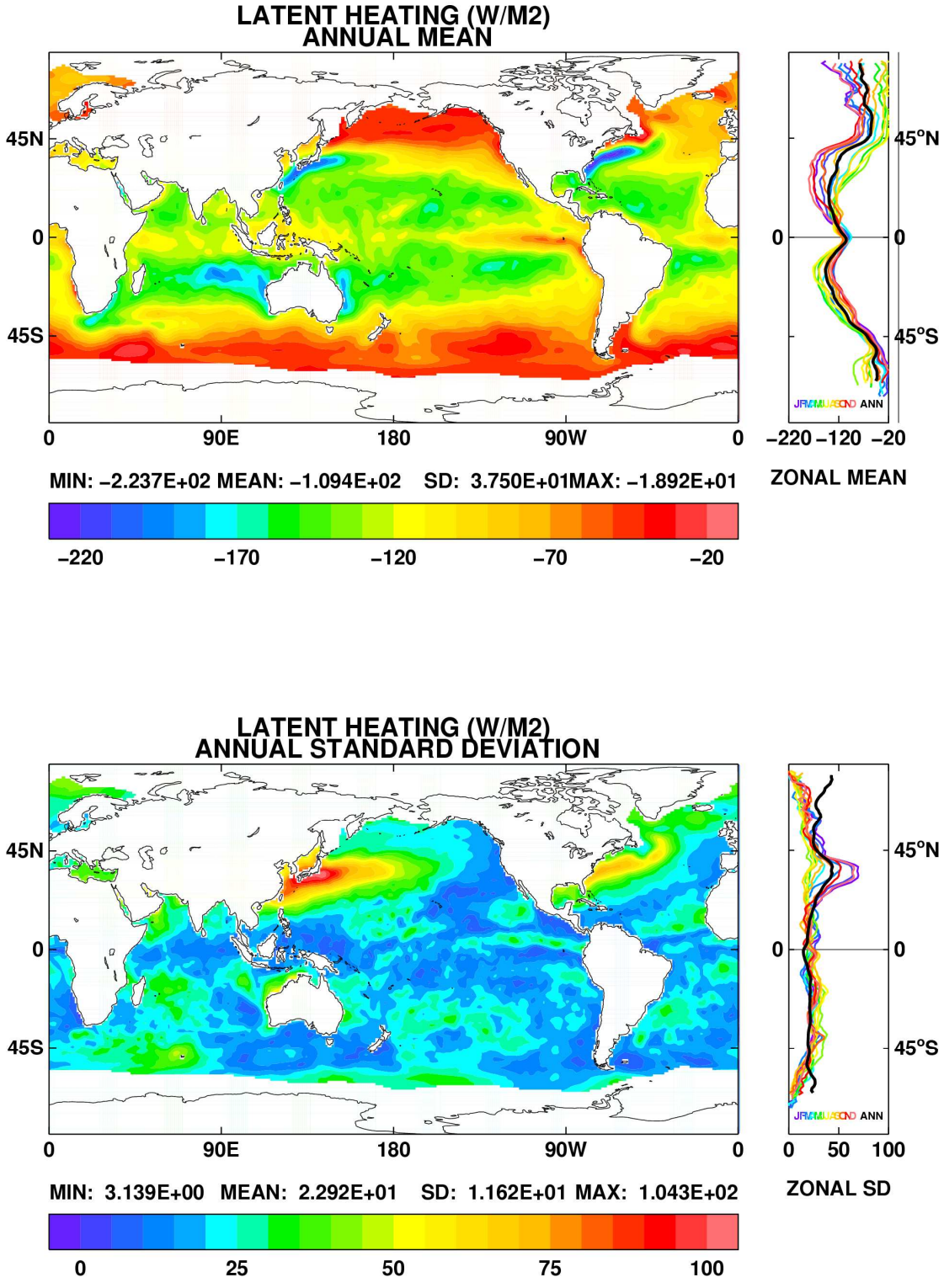

Fig 1a: Latent heating in adjusted SOC dataset.
Top panel – mean; bottom panel – standard deviation.

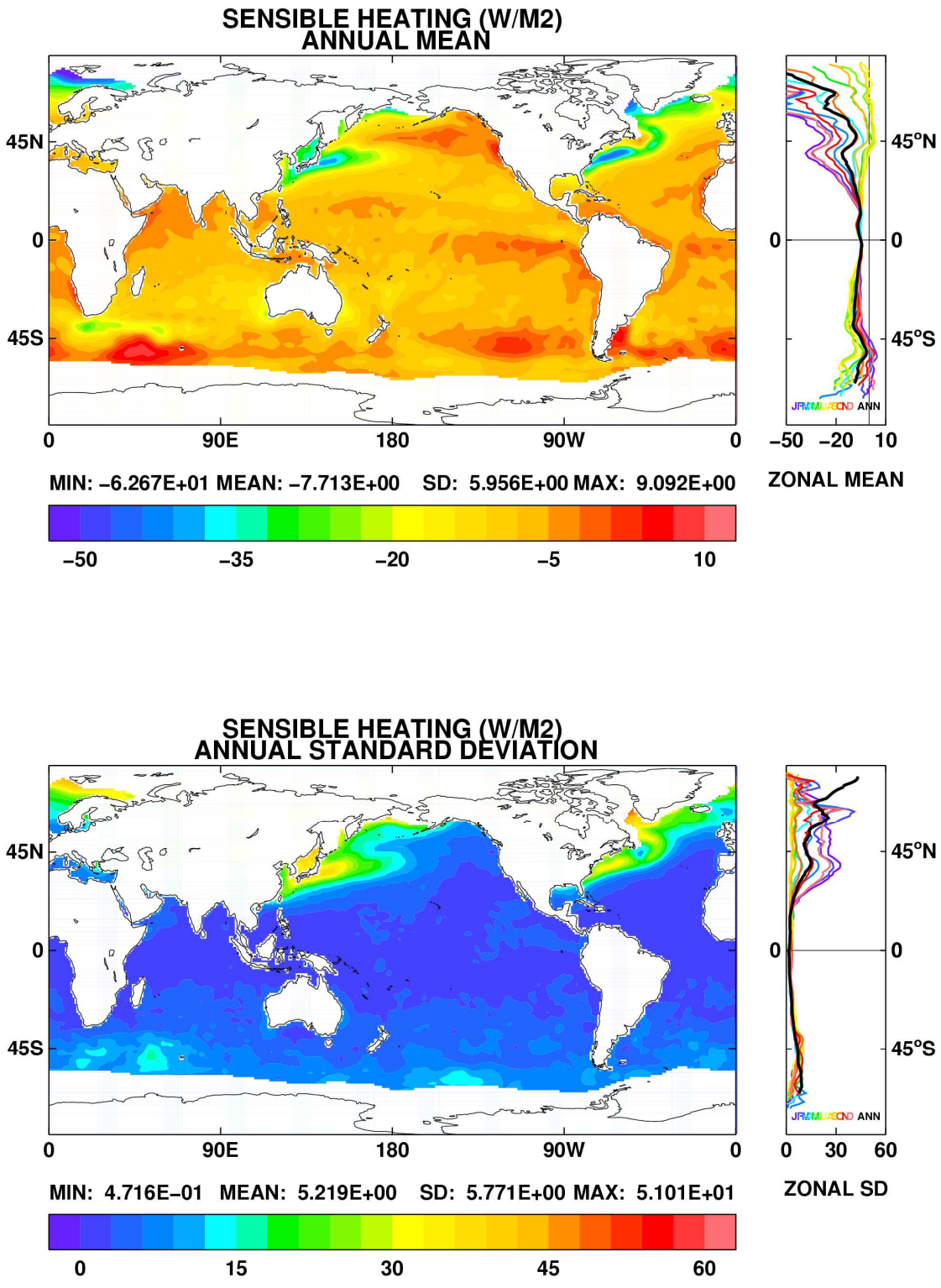

Fig 1b: As Fig 1a but for sensible heating.

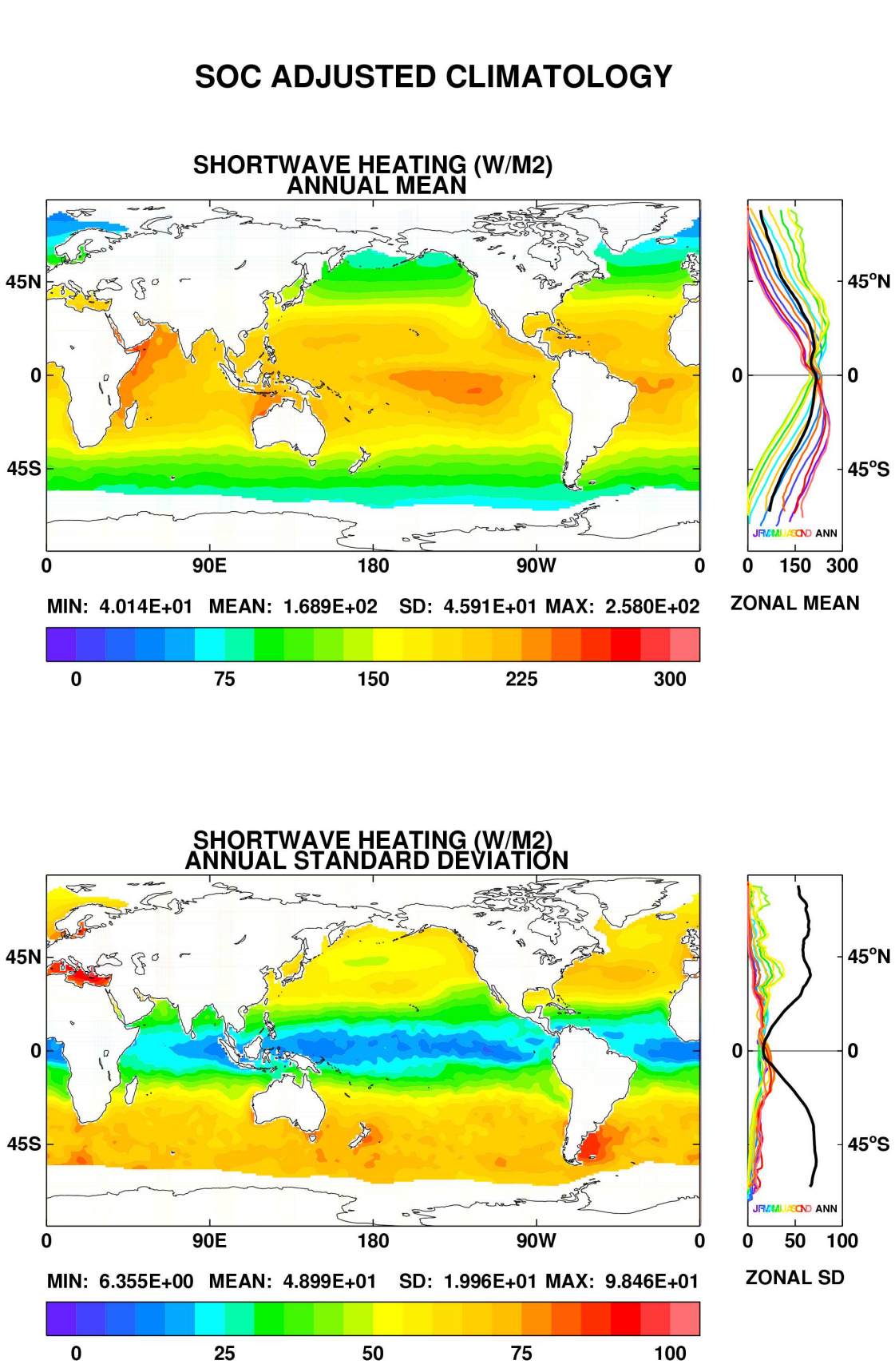

Fig 1c: As Fig 1a but for shortwave heating.

SOC ADJUSTED CLIMATOLOGY

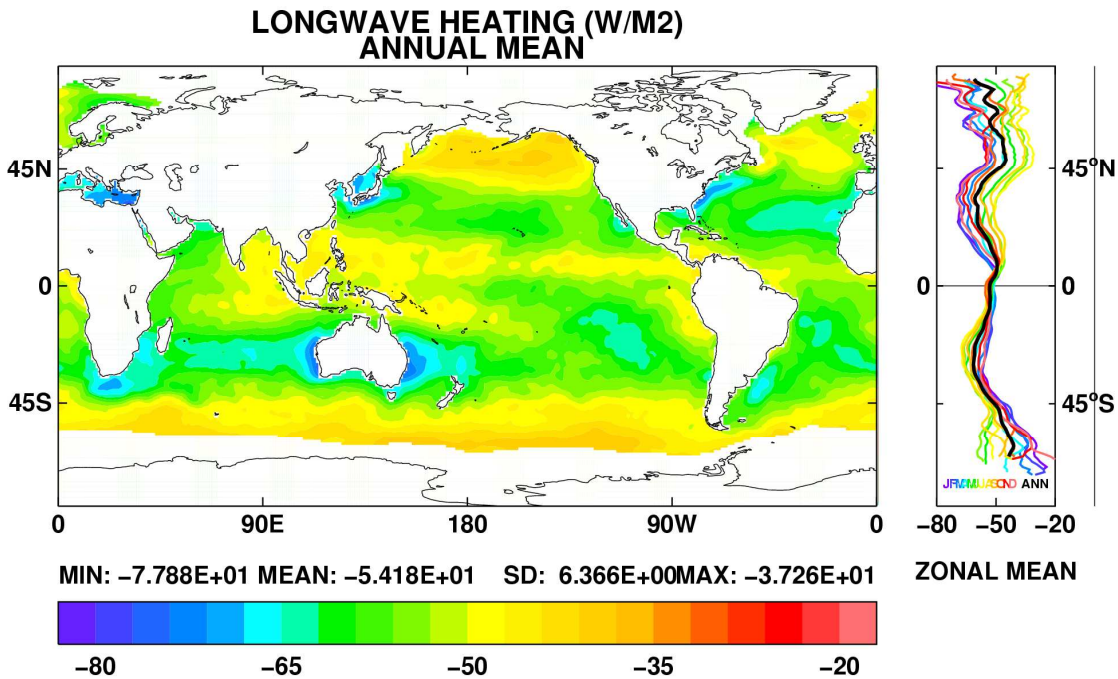

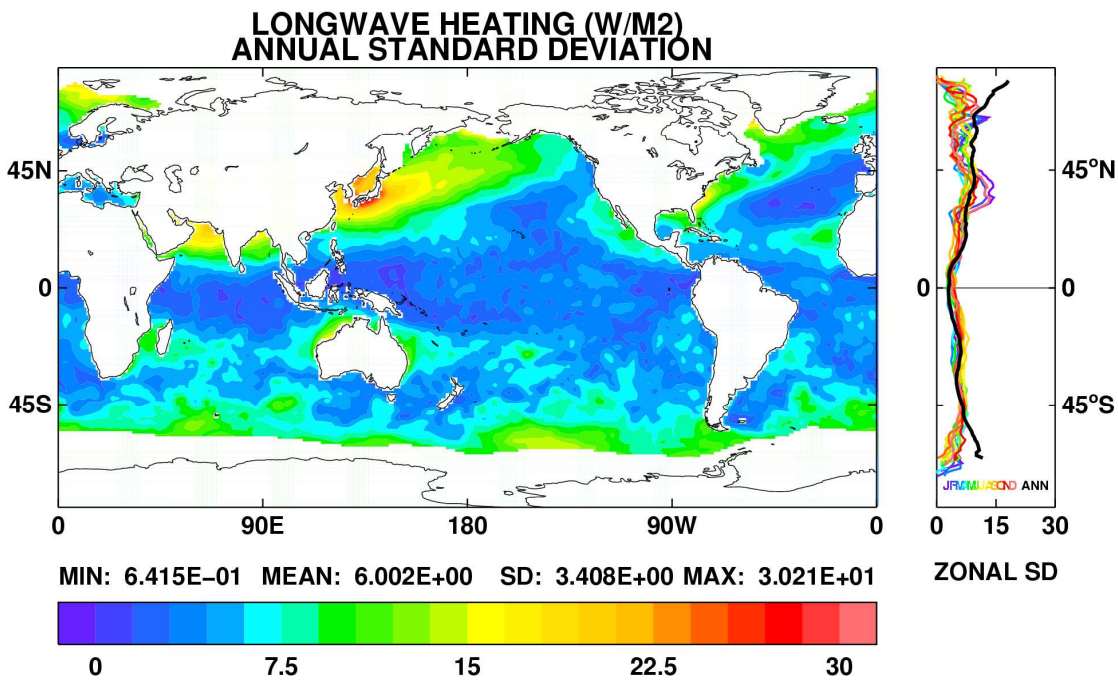

Fig 1d: As Fig 1a but for longwave heating.

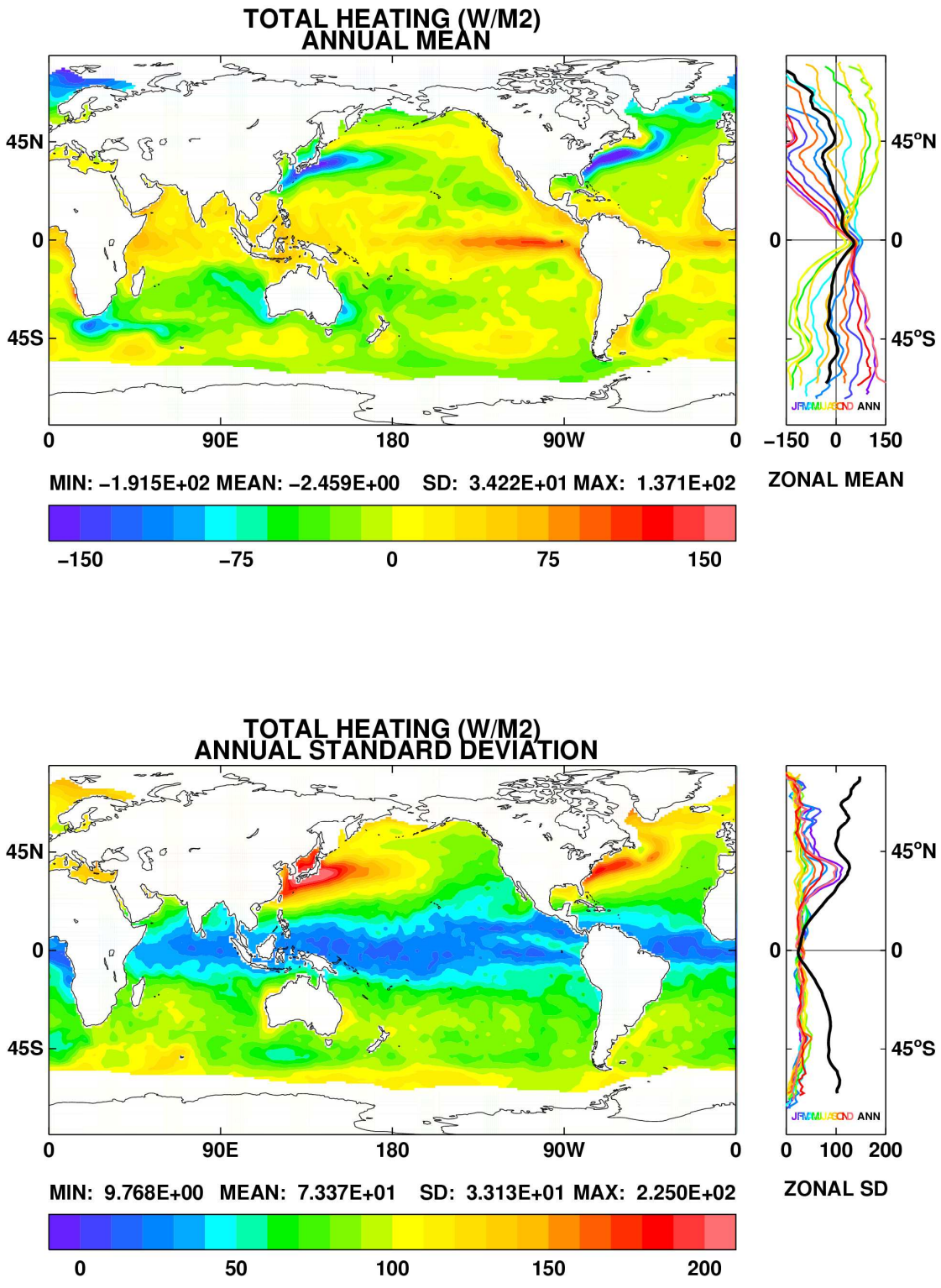

Fig 1e: As Fig 1a but for total (LH+SH+SW+LW) heating.

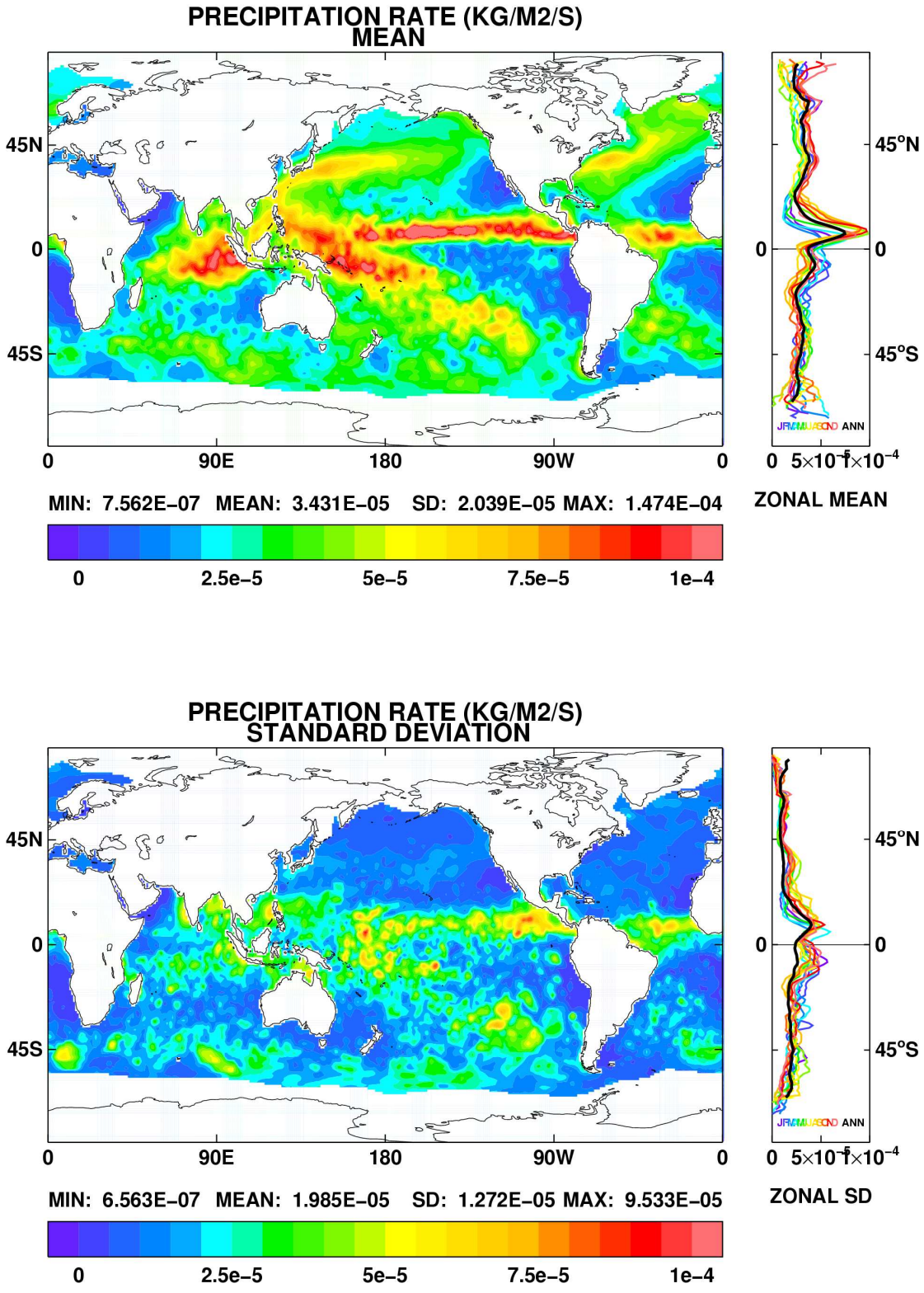

Fig 1f: As Fig 1a but for precipitation rate.

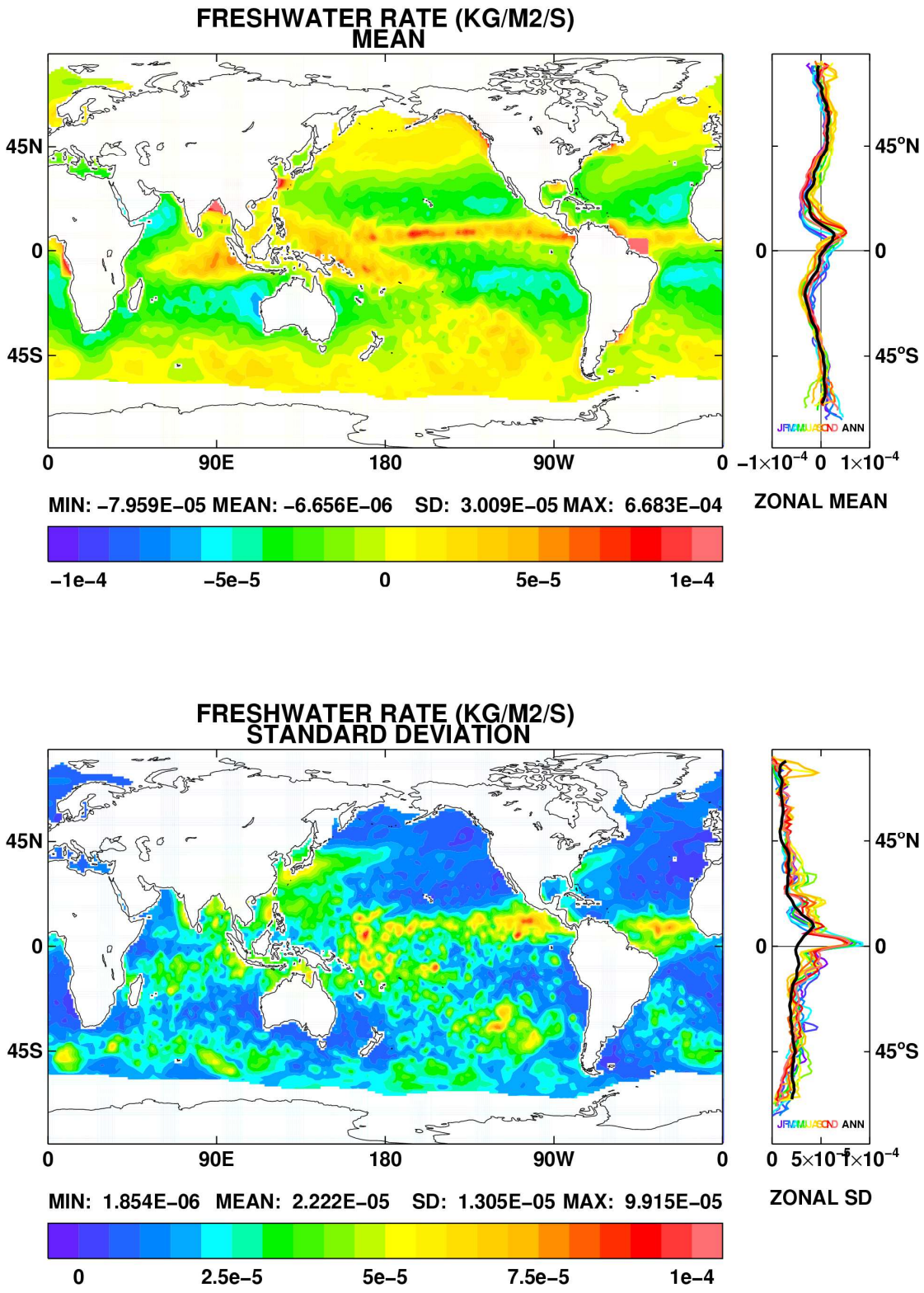

Fig 1g: As Fig 1a but for total freshwater (P-E+R) rate.

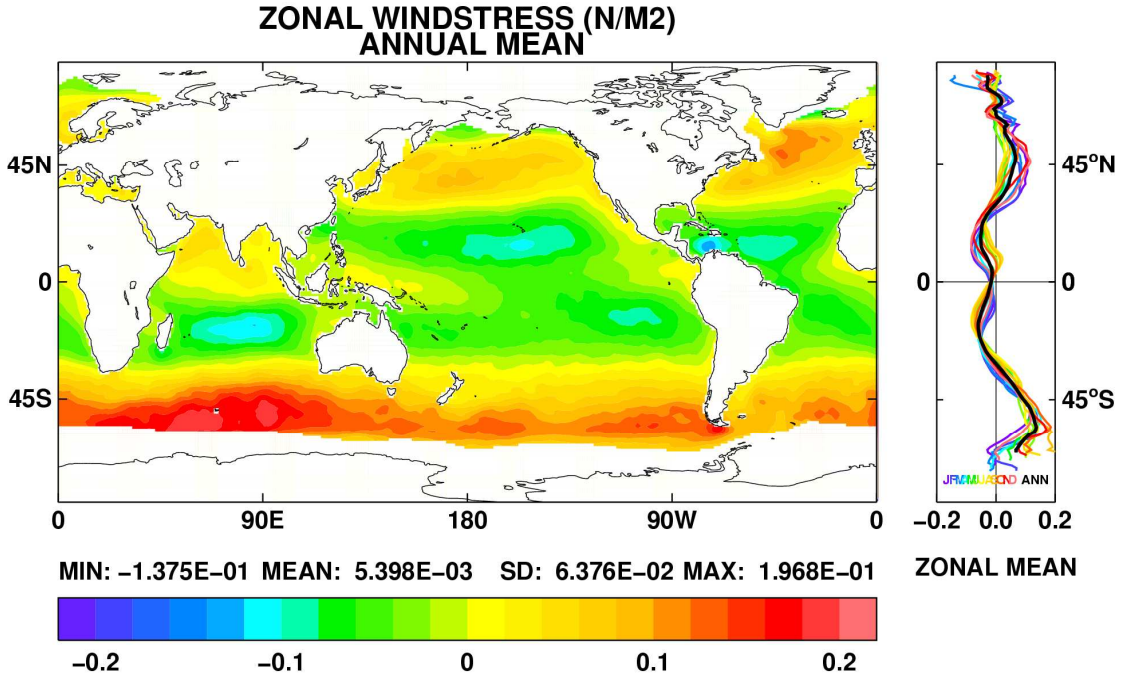

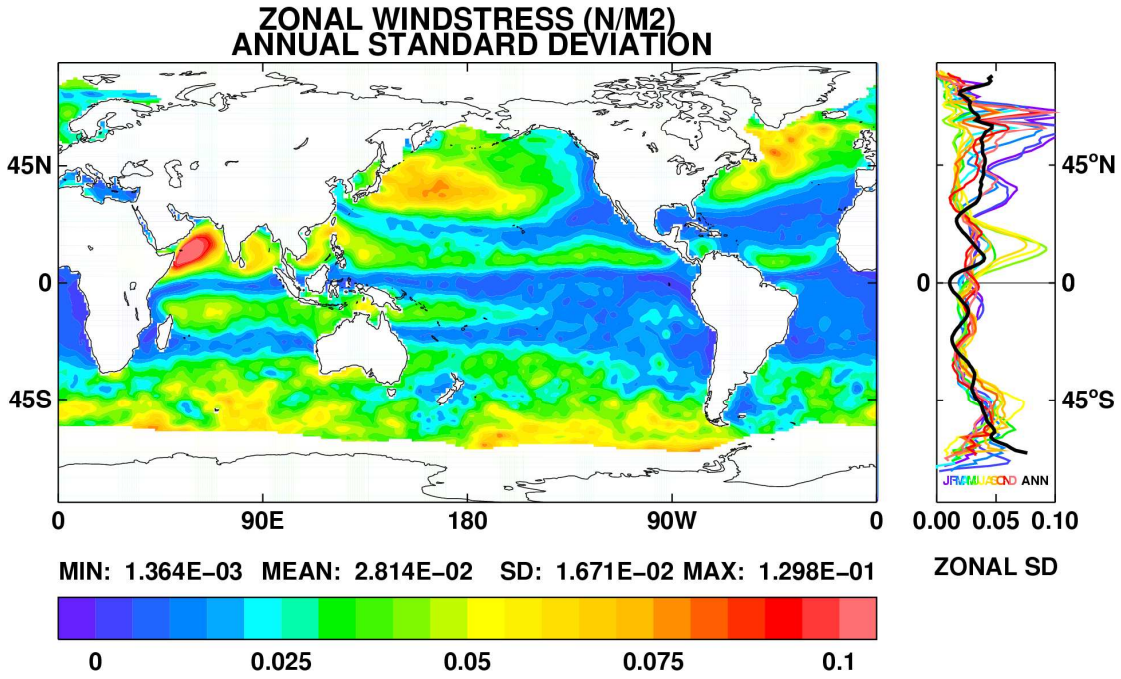

Fig 1h: As Fig 1a but for zonal wind stress.

SOC ADJUSTED CLIMATOLOGY

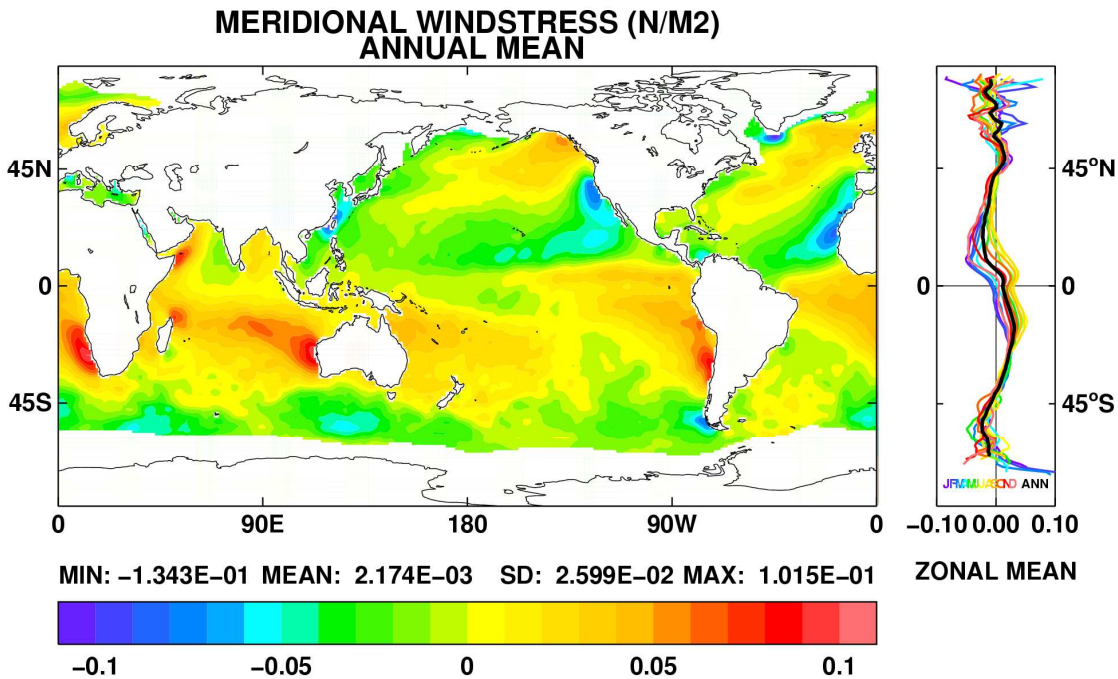

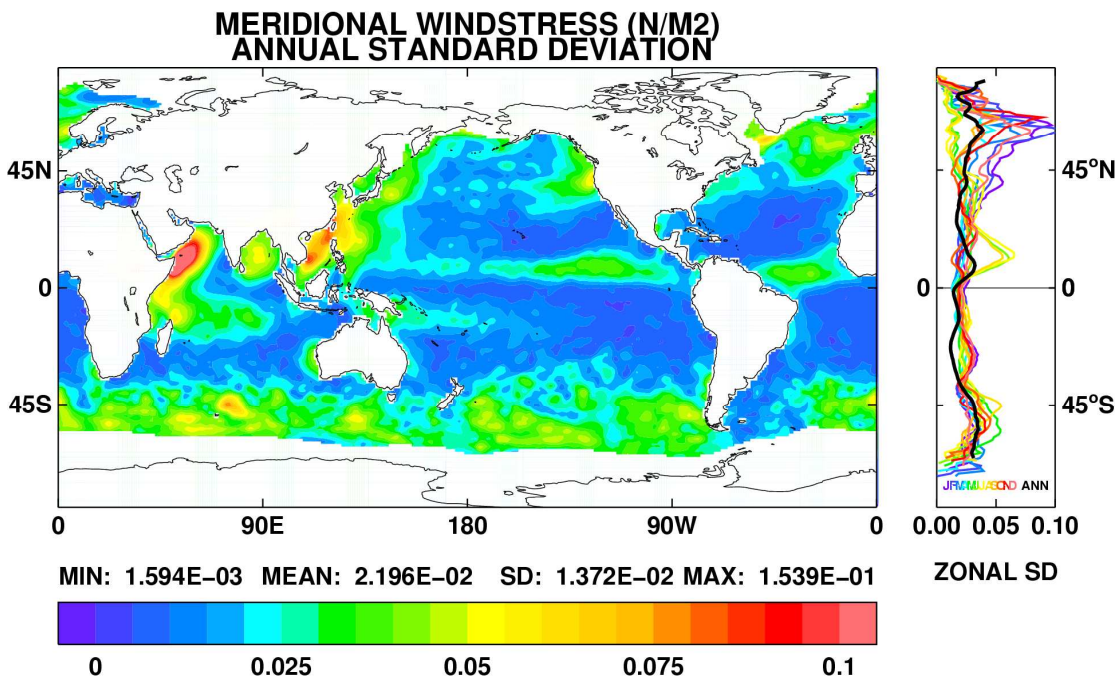

Fig 1i: As Fig 1a but for meridional wind stress.

This page is intentionally left blank.

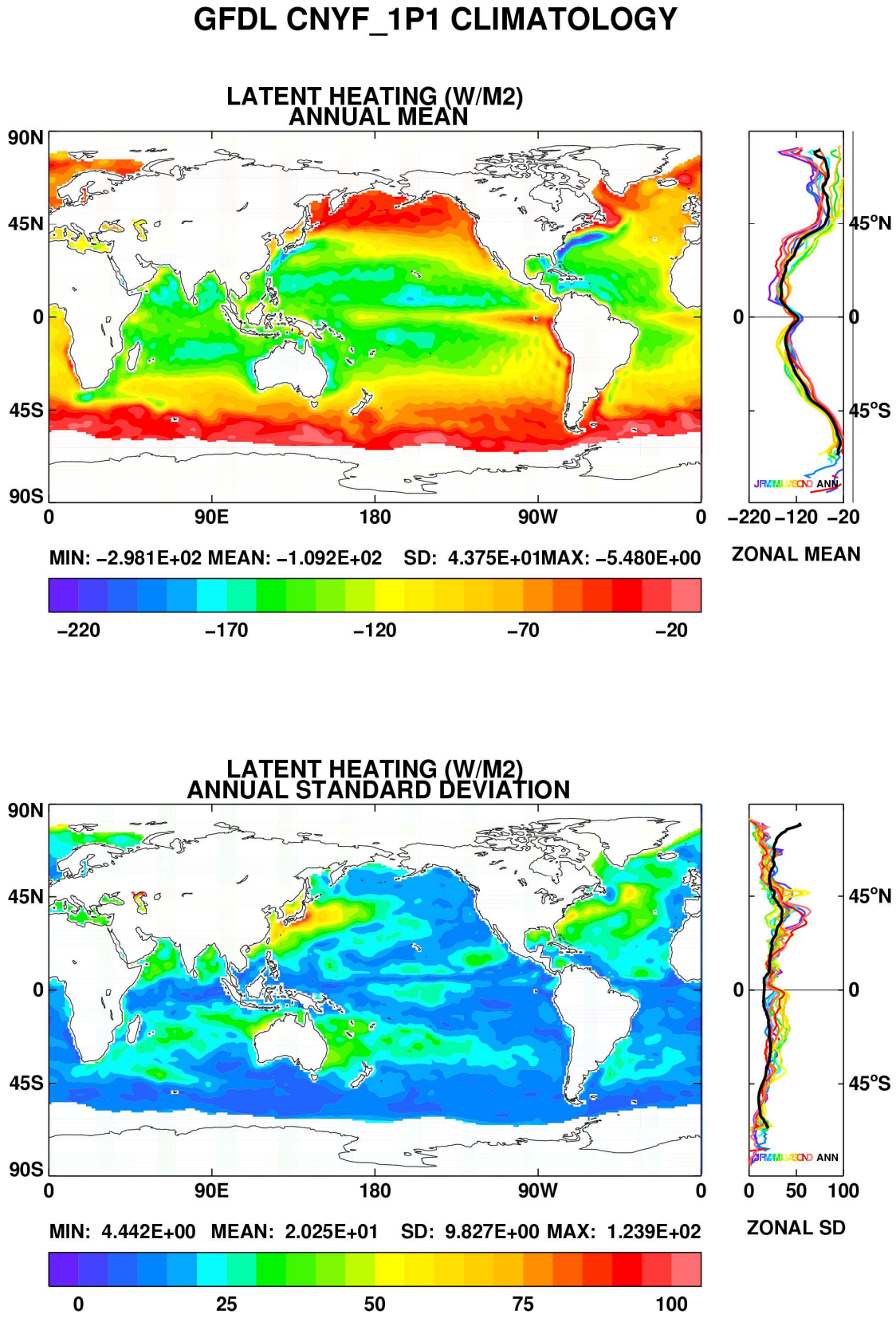

Fig 2a: Latent heating in GFDL CNYF dataset.
Top panel – mean; bottom panel – standard deviation.

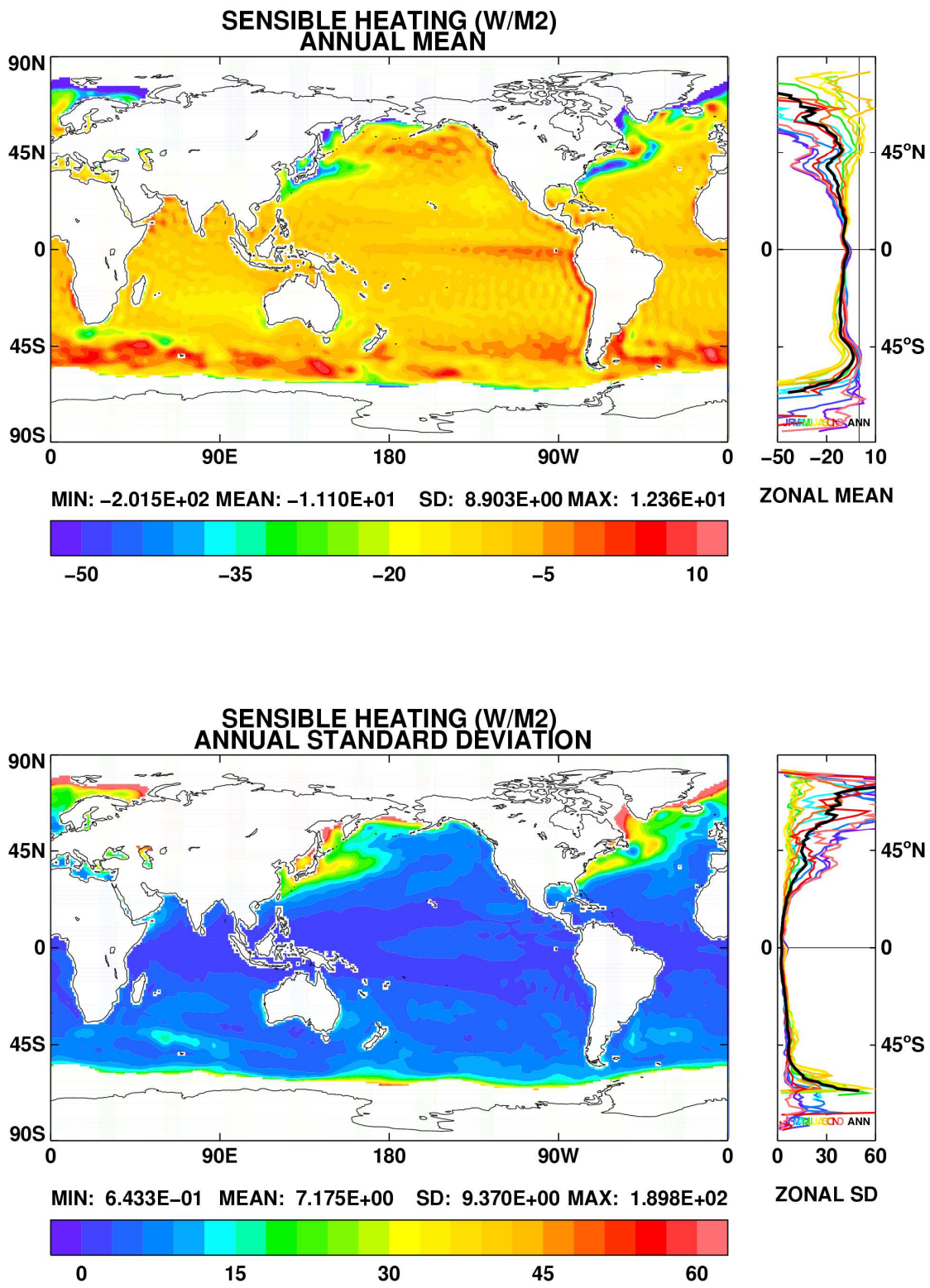

Fig 2b: As Fig 2a but for sensible heating.

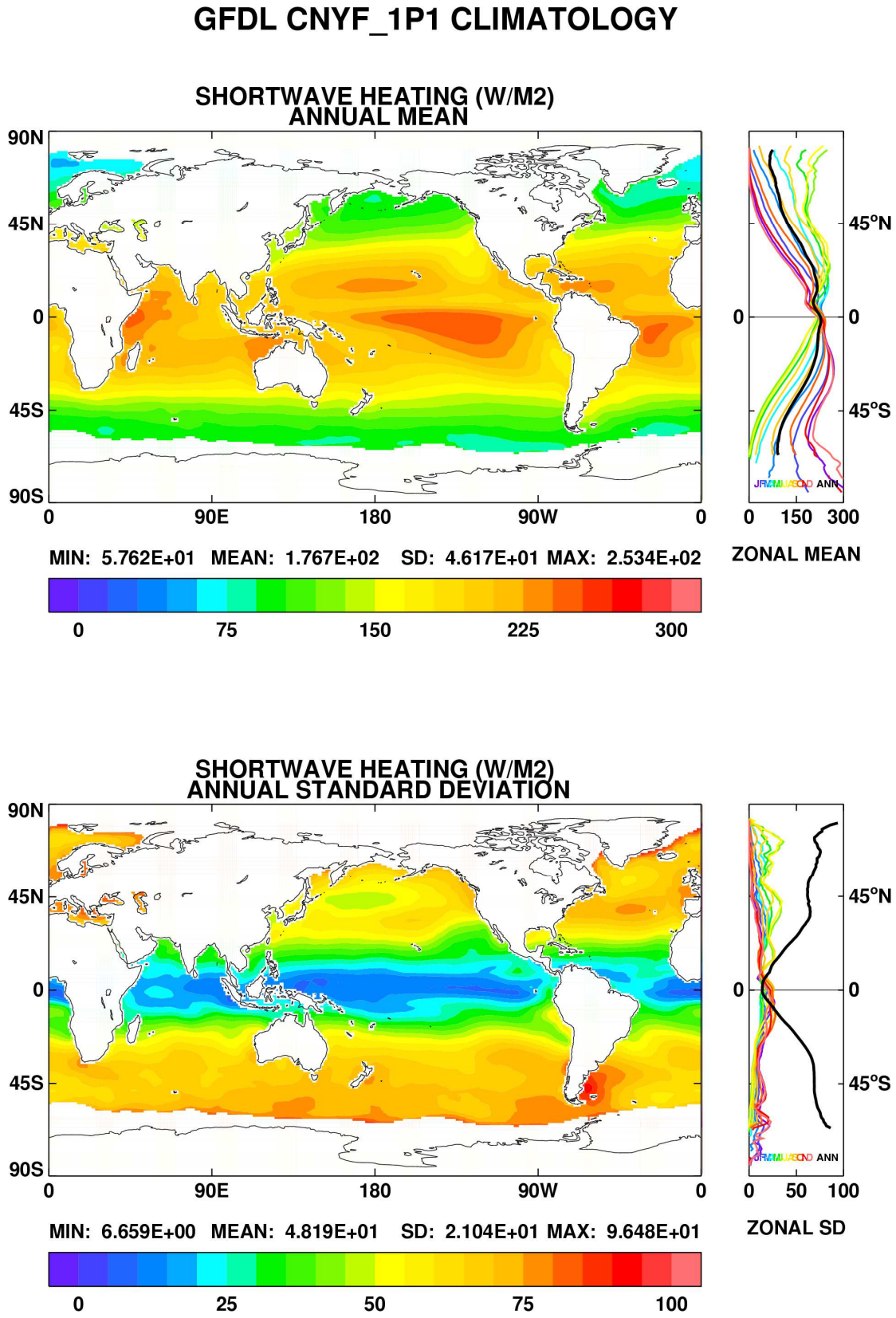

Fig 2c: As Fig 2a but for shortwave heating.

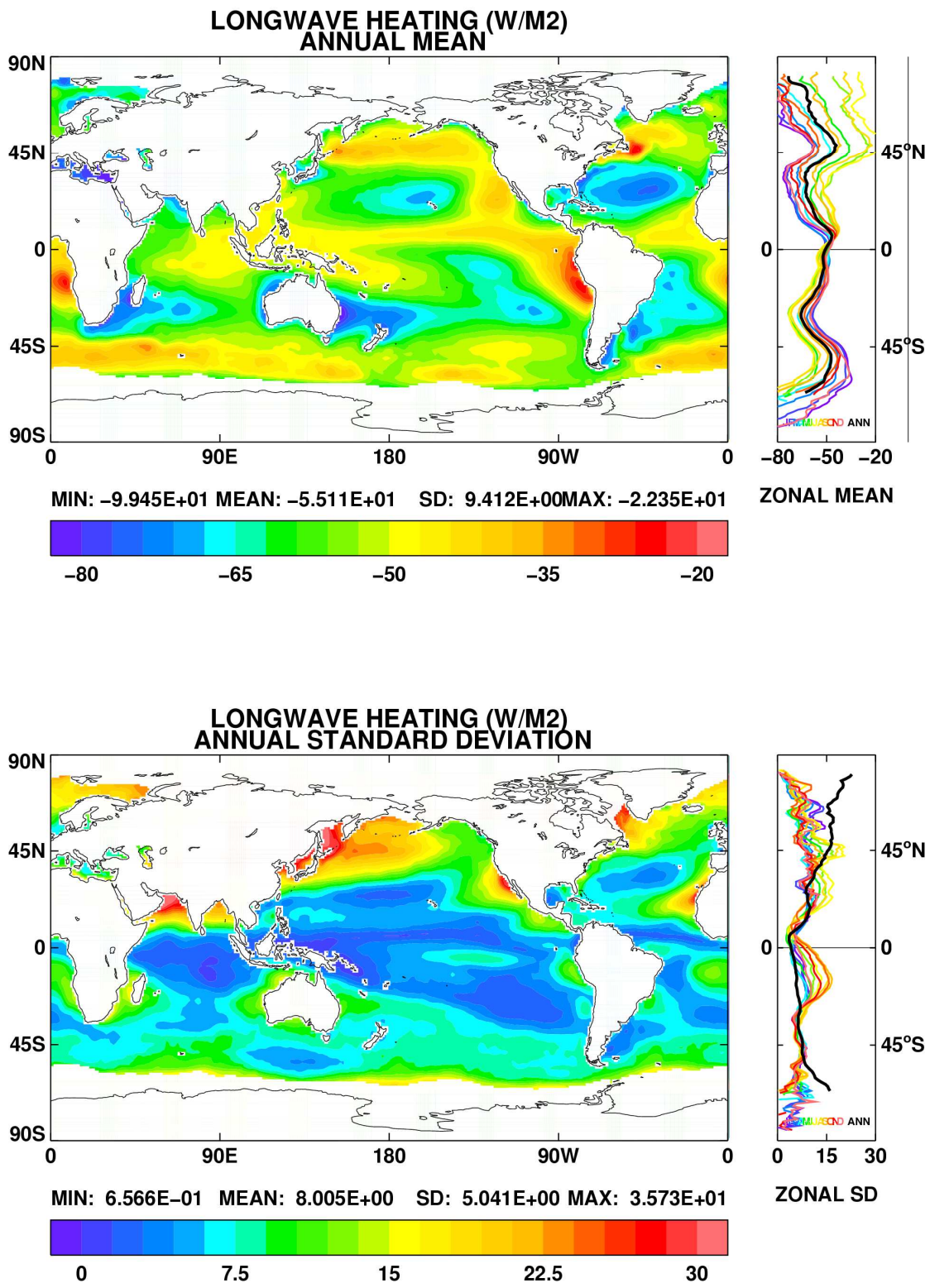

Fig 2d: As Fig 2a but for longwave heating.

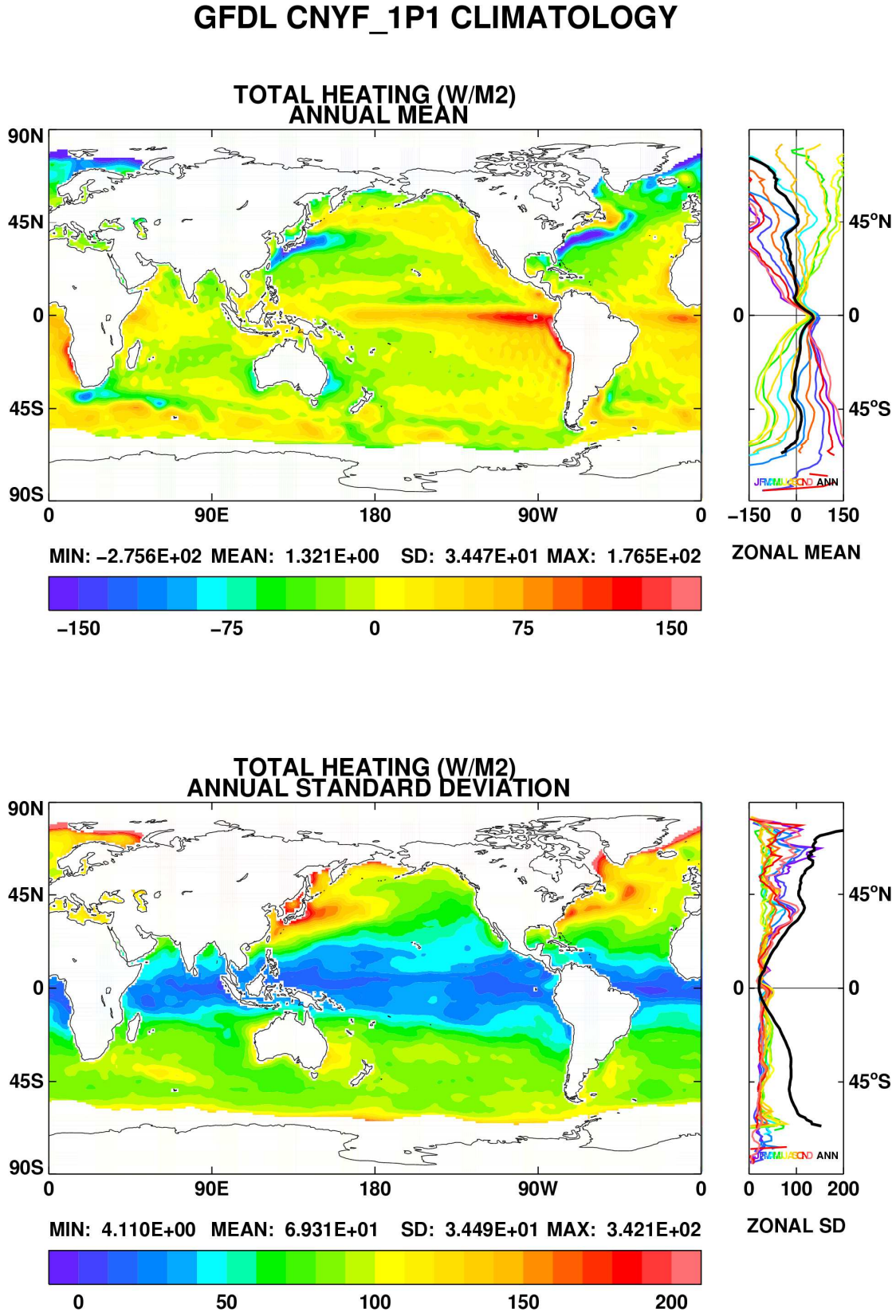

Fig 2e: As Fig 2a but for total (LH+SH+SW+LW) heating.

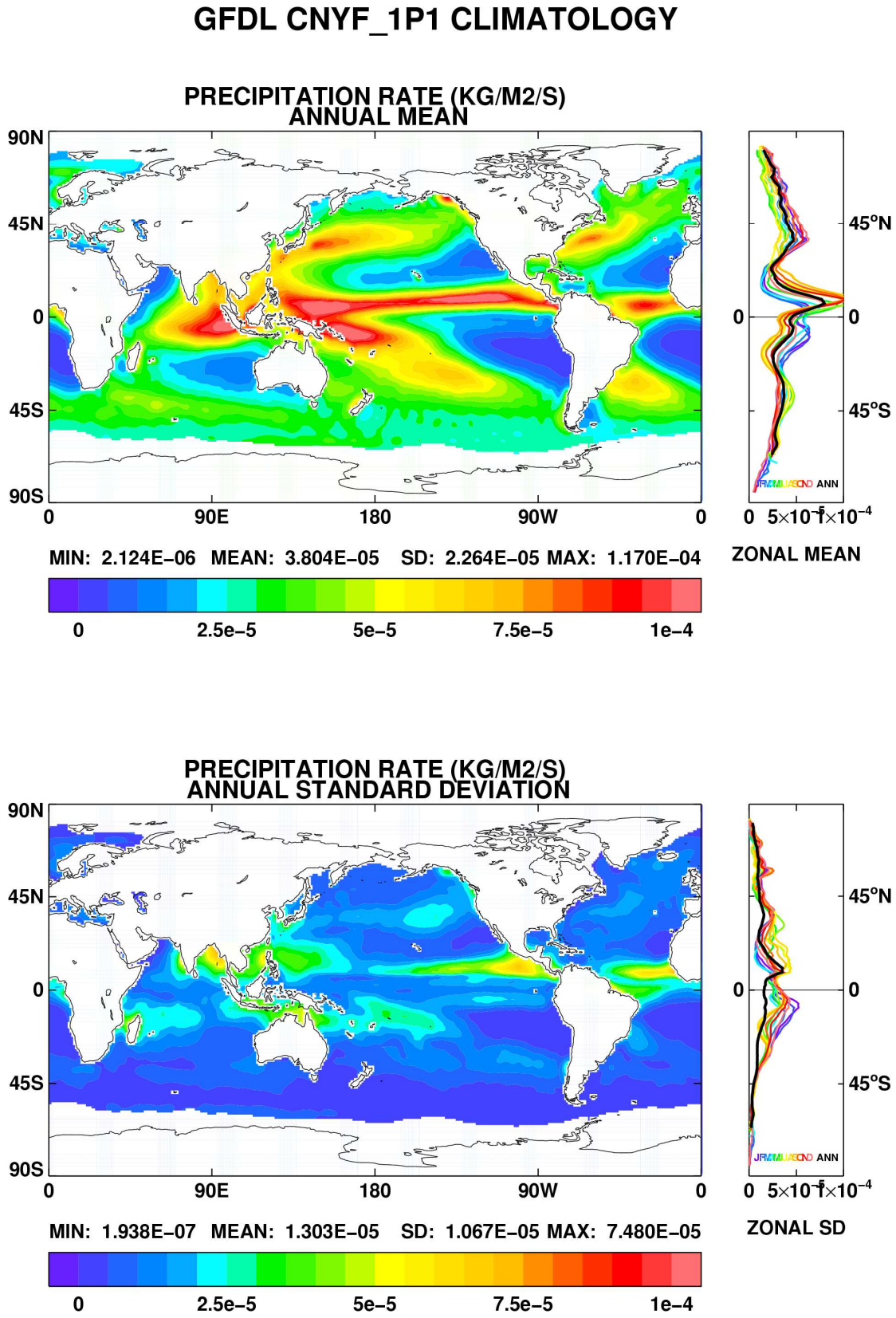

Fig 2f: As Fig 2a but for precipitation rate.

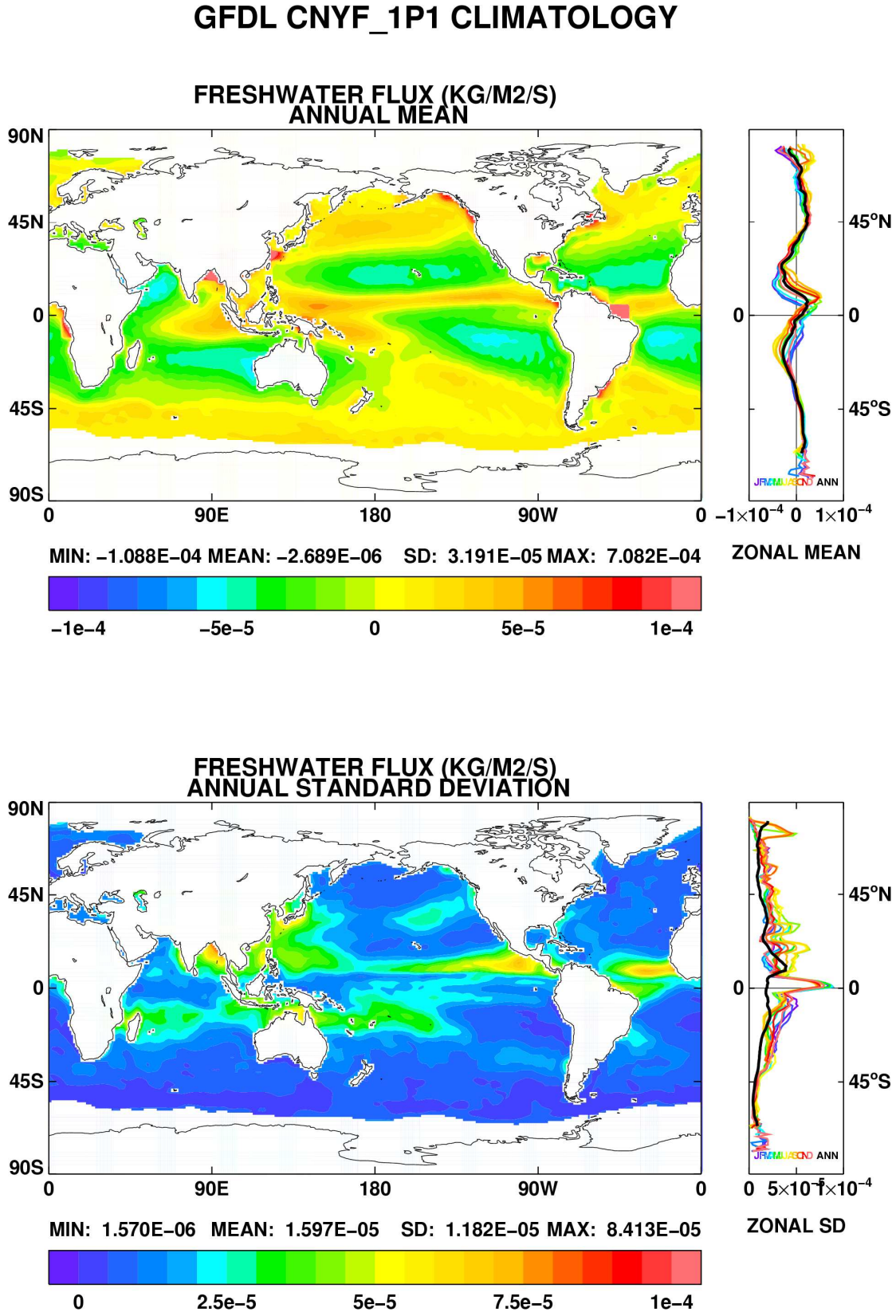

Fig 2g: As Fig 2a but for total freshwater (P-E+R) rate.

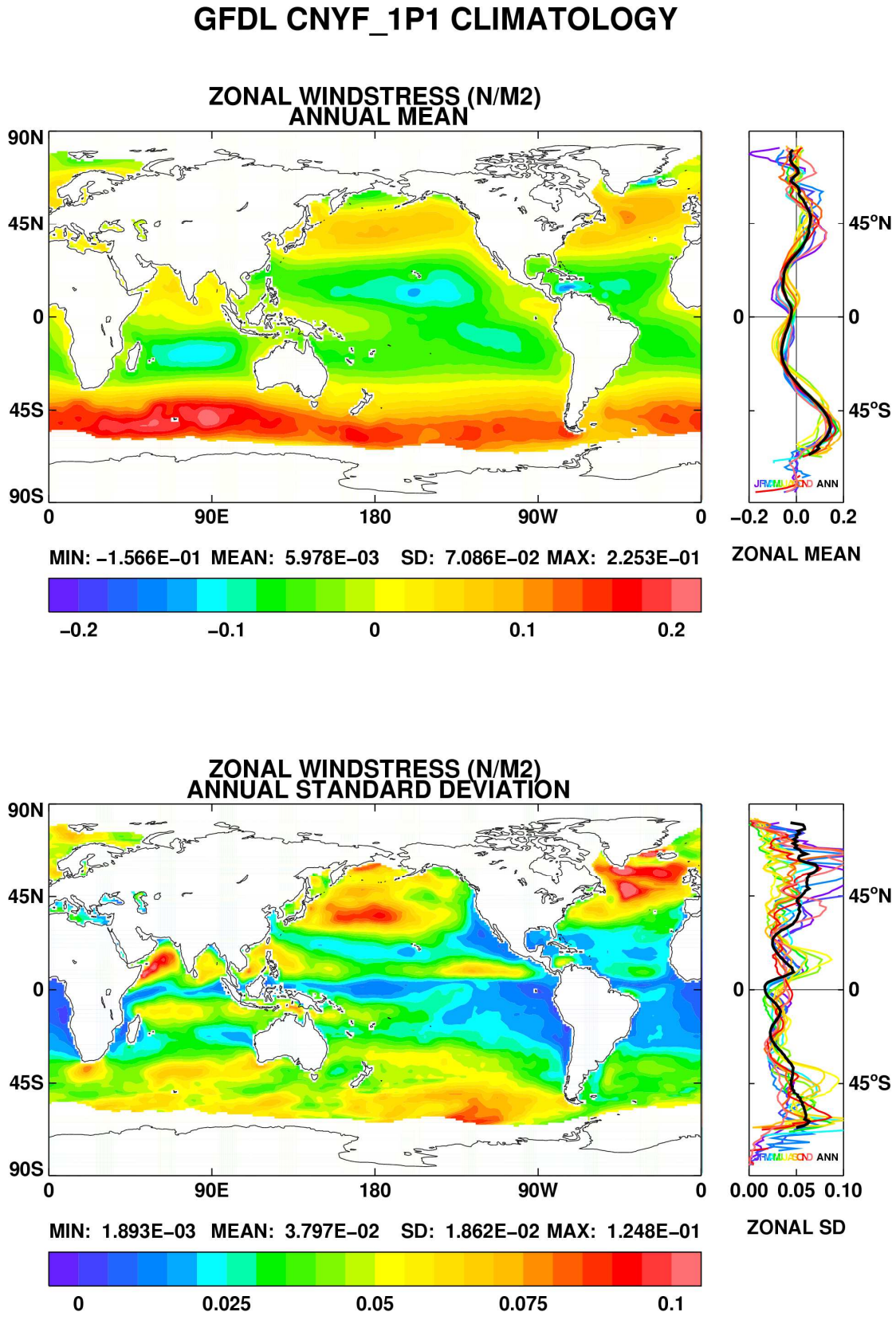

Fig 2h: As Fig 2a but for zonal wind stress.

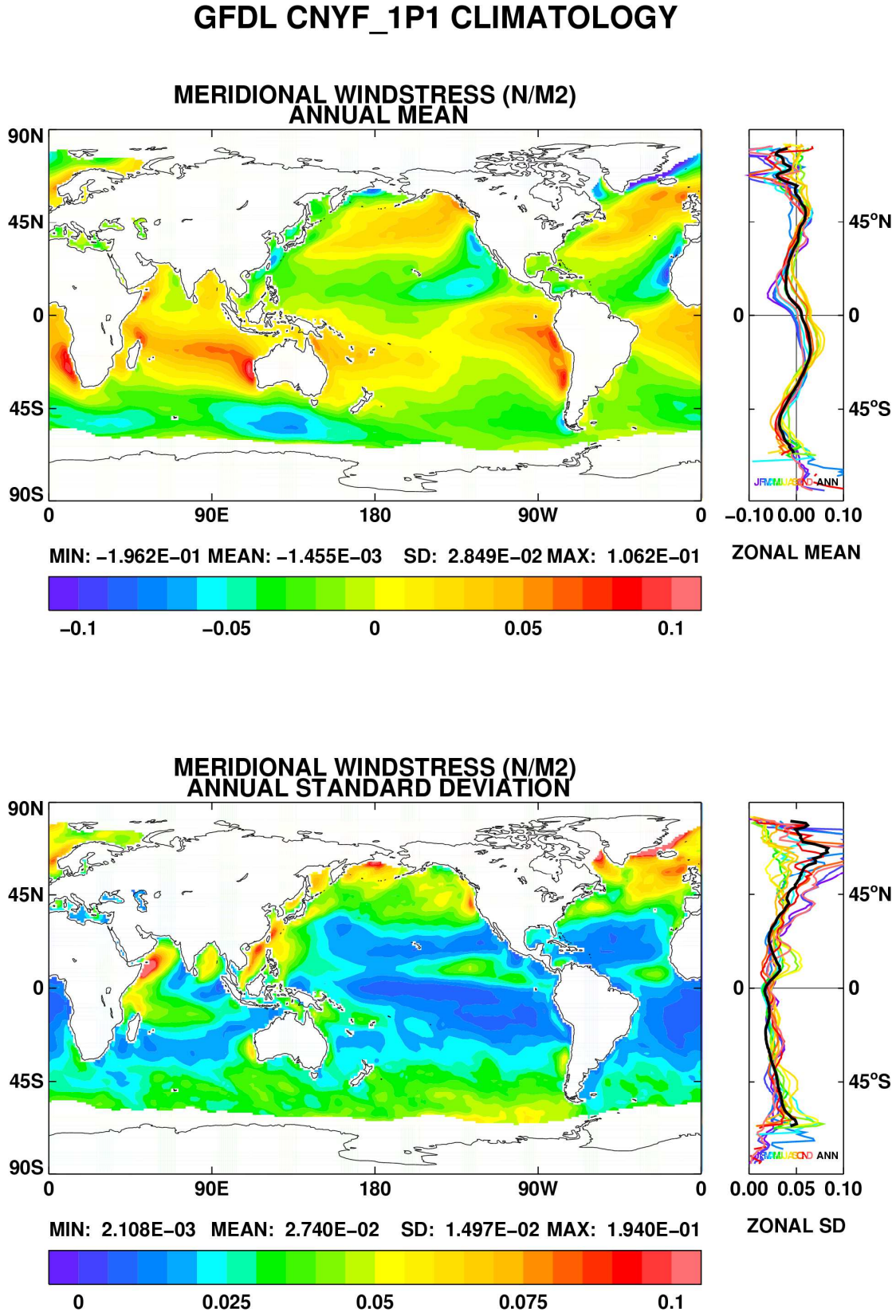

Fig 2i: As Fig 2a but for meridional wind stress.

This page is intentionally left blank.

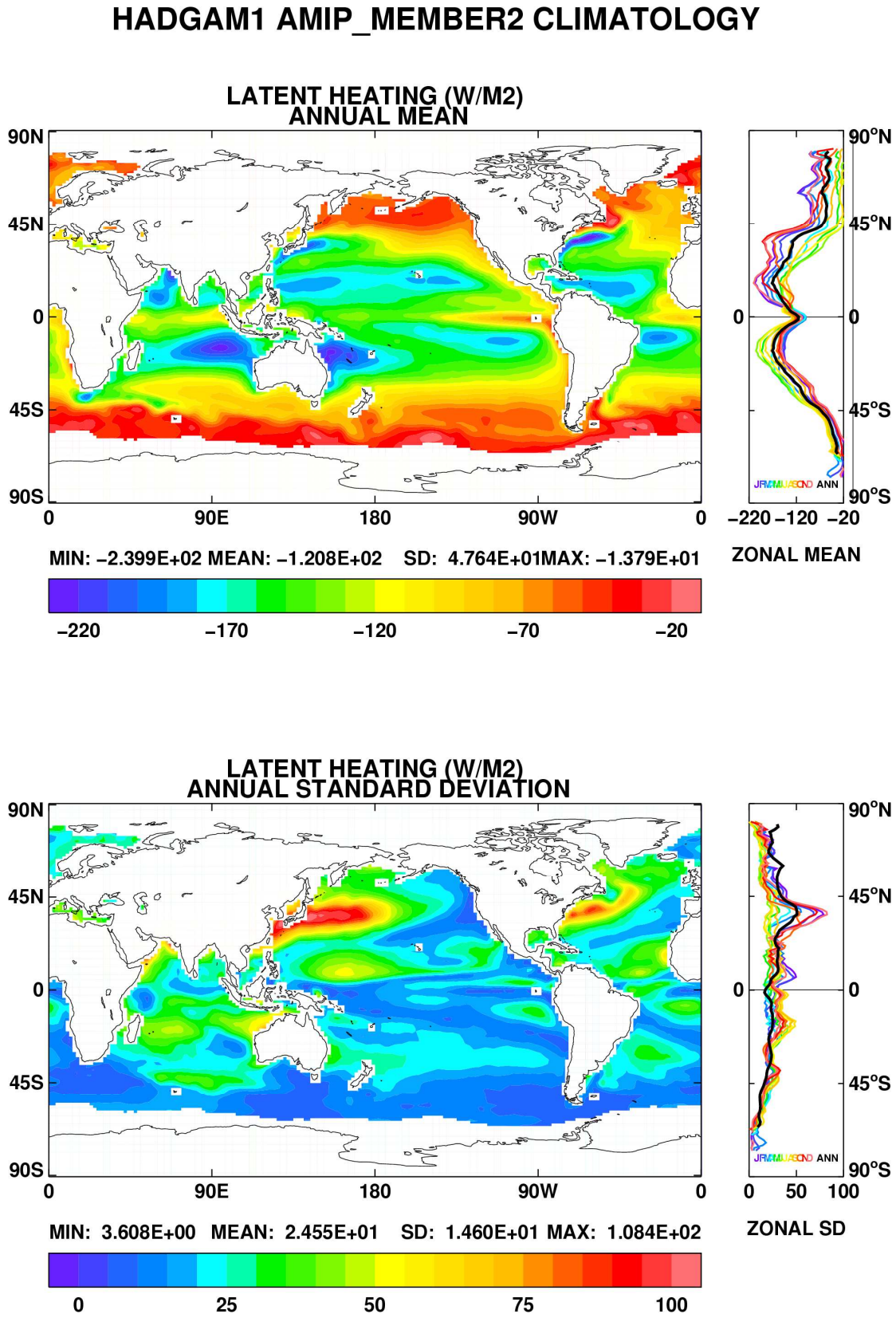

Fig 3a: Latent heating in HadGAM1 AMIP2 dataset.
Top panel – mean; bottom panel – standard deviation.

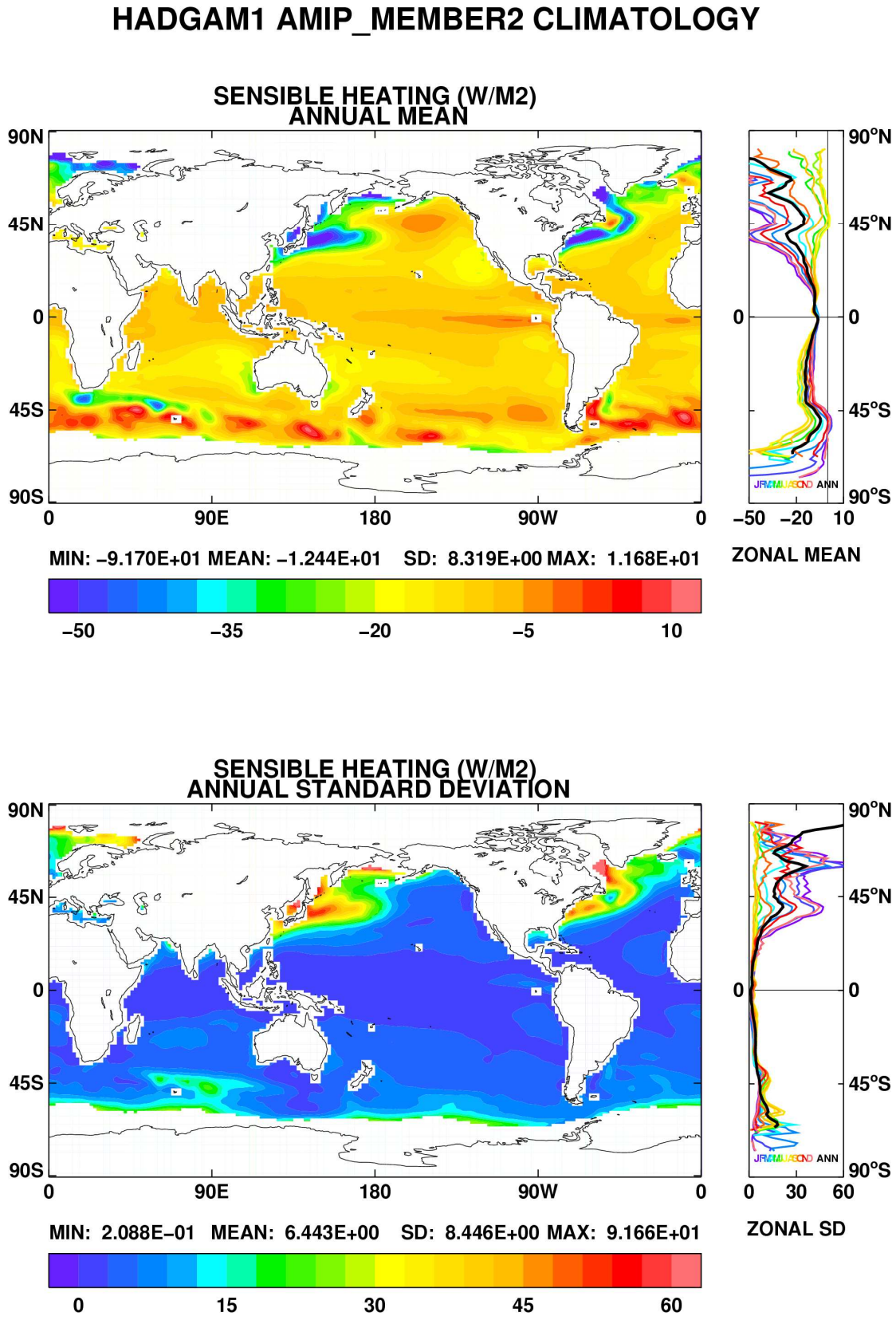

Fig 3b: As Fig 3a but for sensible heating.

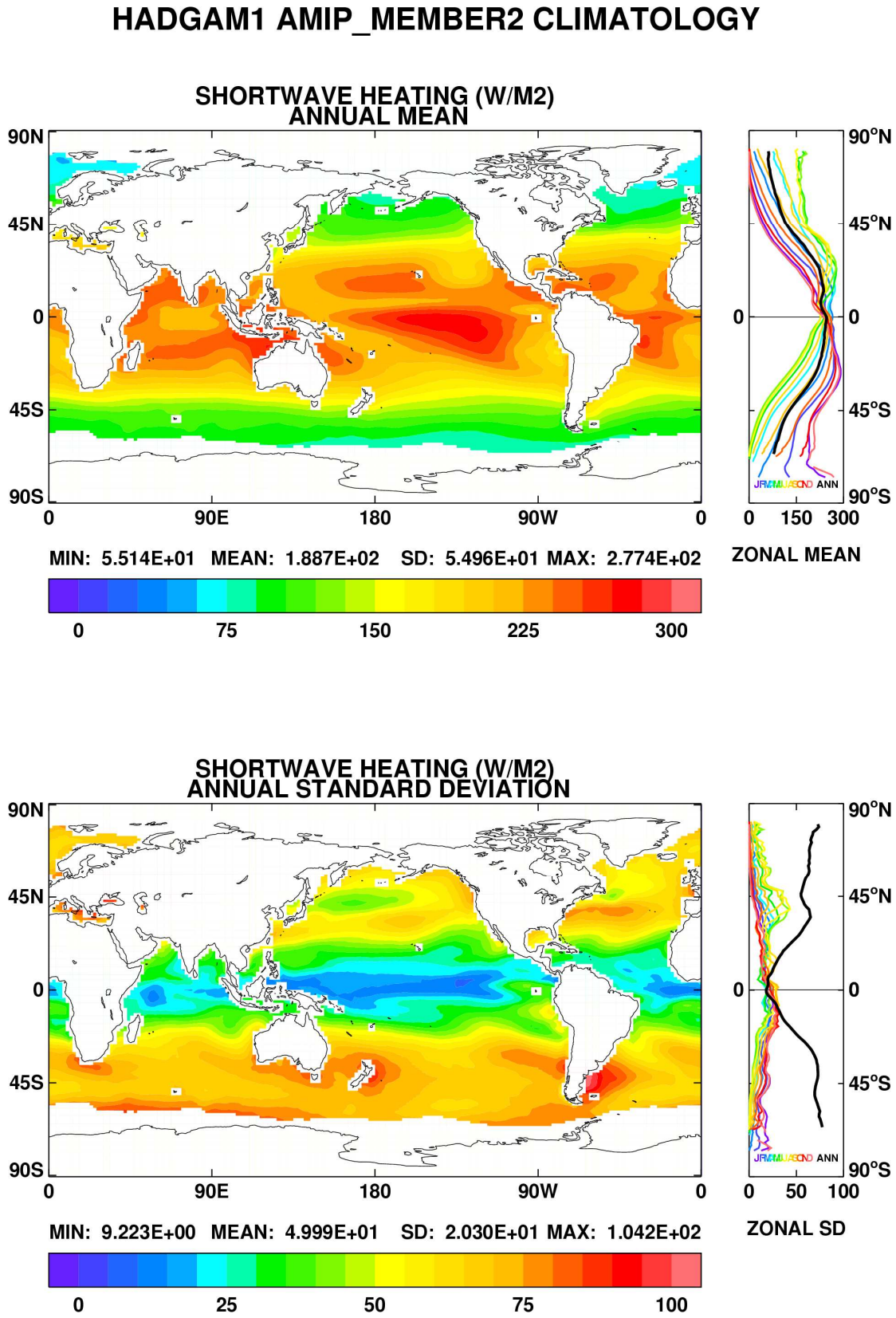

Fig 3c: As Fig 3a but for shortwave heating.

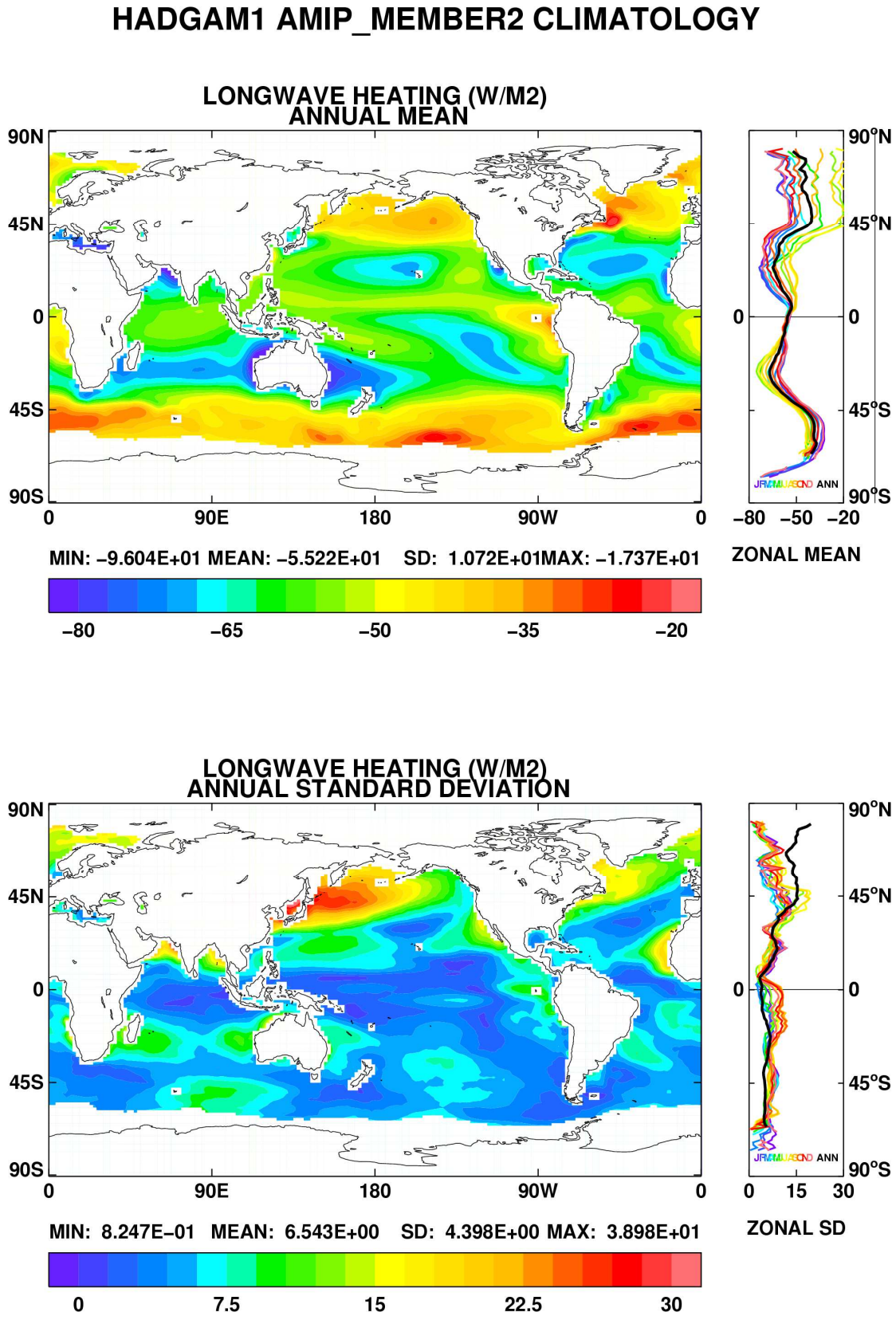

Fig 3d: As Fig 3a but for longwave heating.

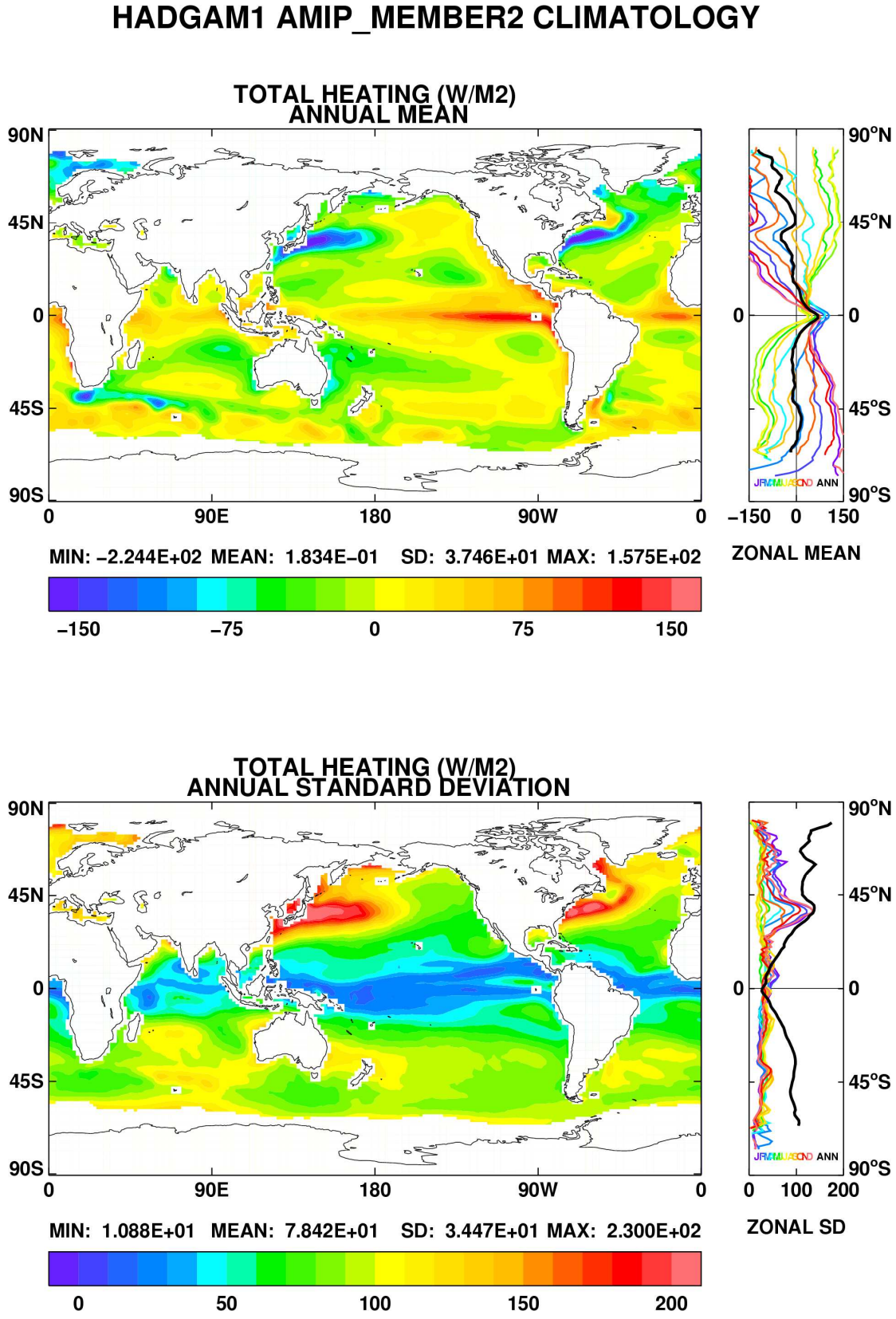

Fig 3e: As Fig 3a but for total (LH+SH+SW+LW) heating.

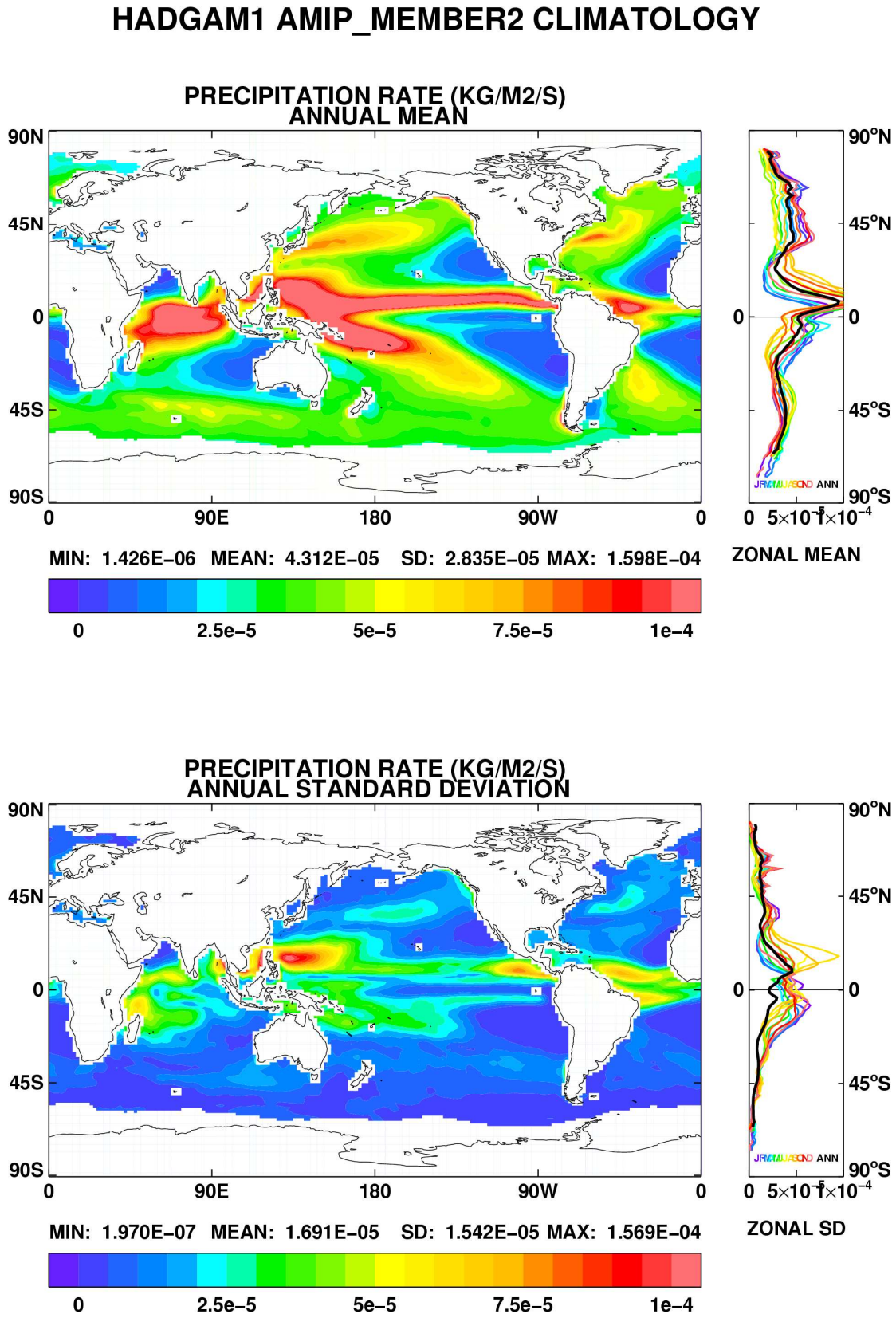

Fig 3f: As Fig 3a but for precipitation rate.

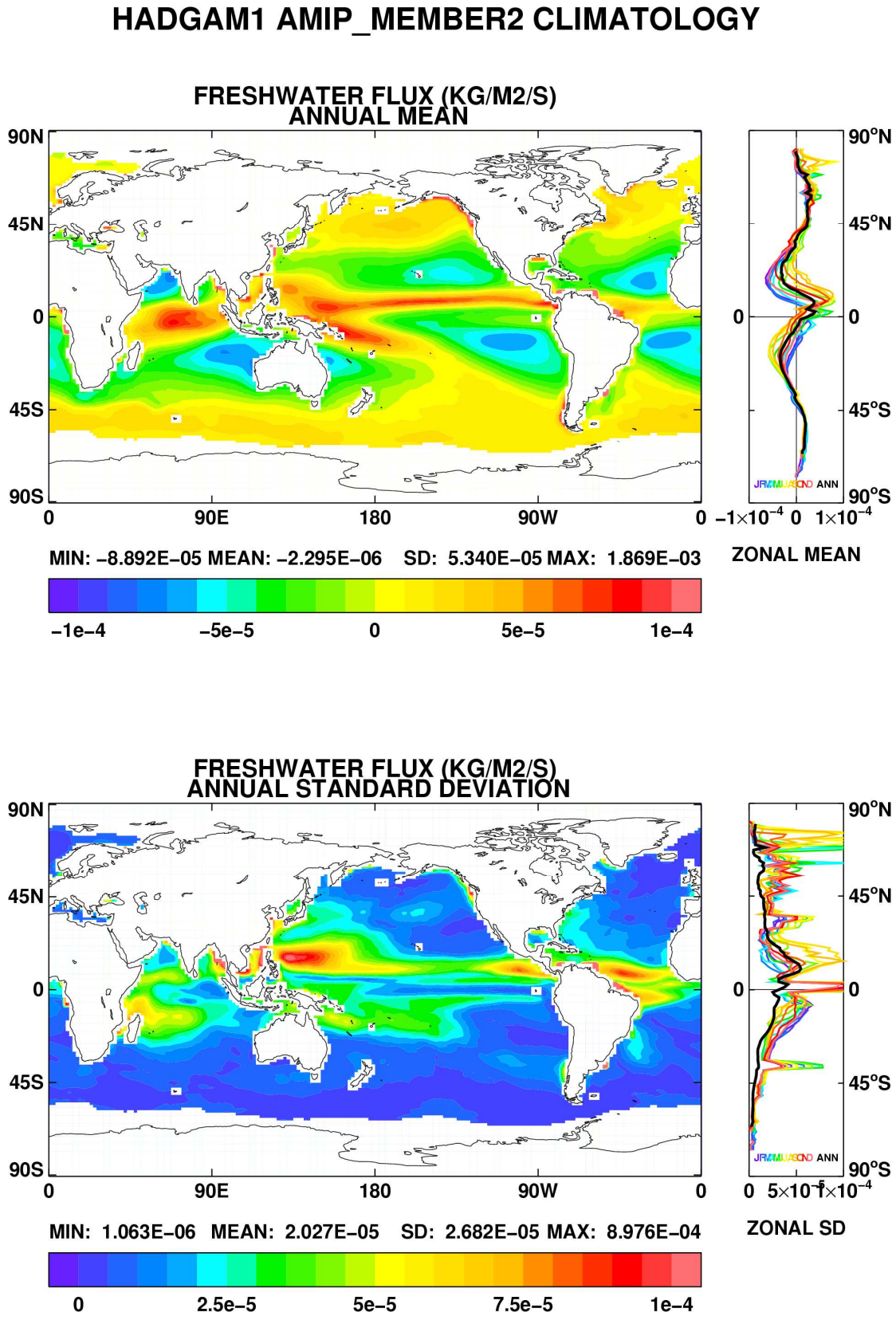

Fig 3g: As Fig 3a but for total freshwater (P-E+R) rate.

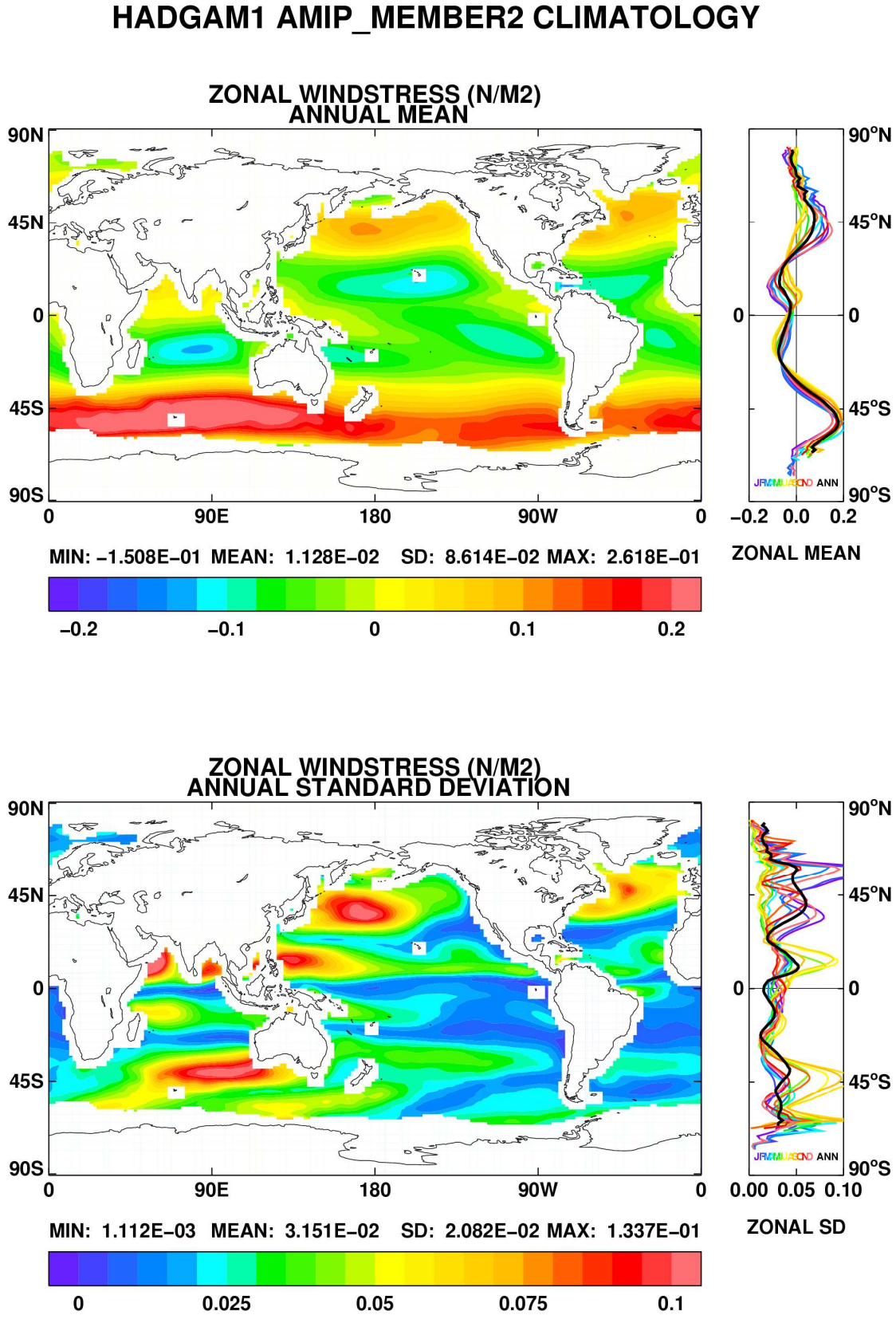

Fig 3h: As Fig 3a but for zonal wind stress.

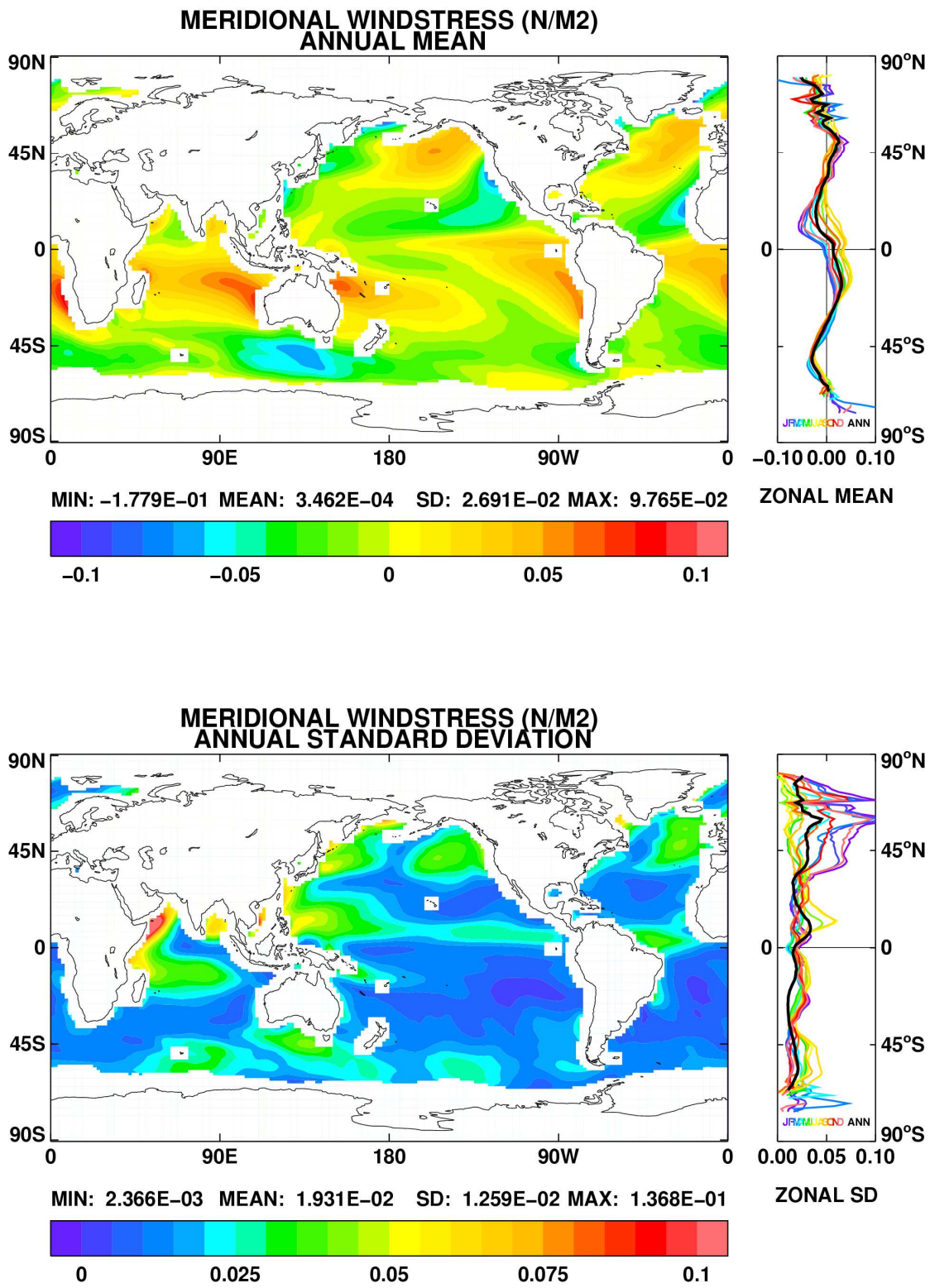

Fig 3i: As Fig 3a but for meridional wind stress.

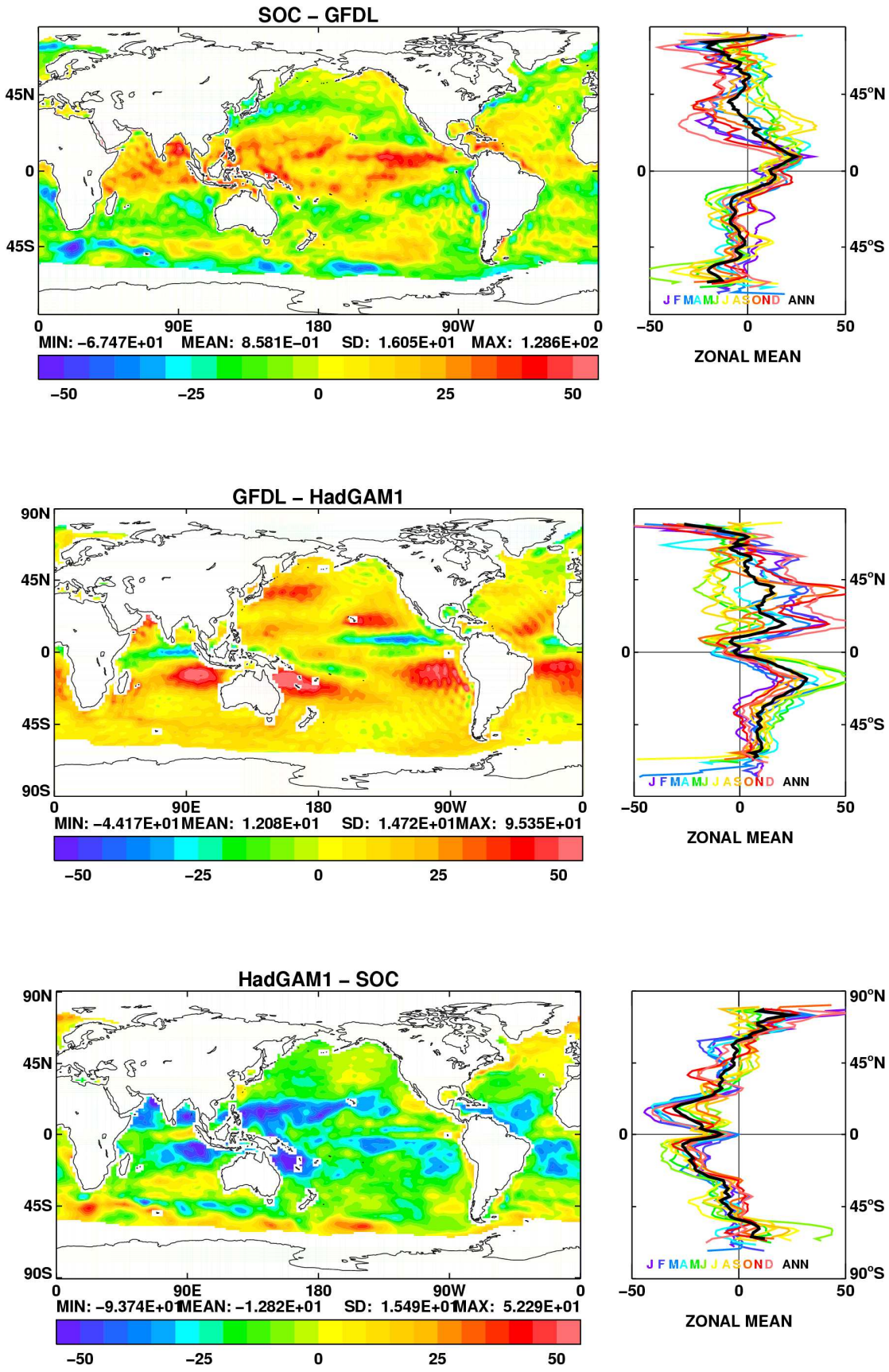

Fig 4a: Differences in annual mean latent heating between the 3 datasets.

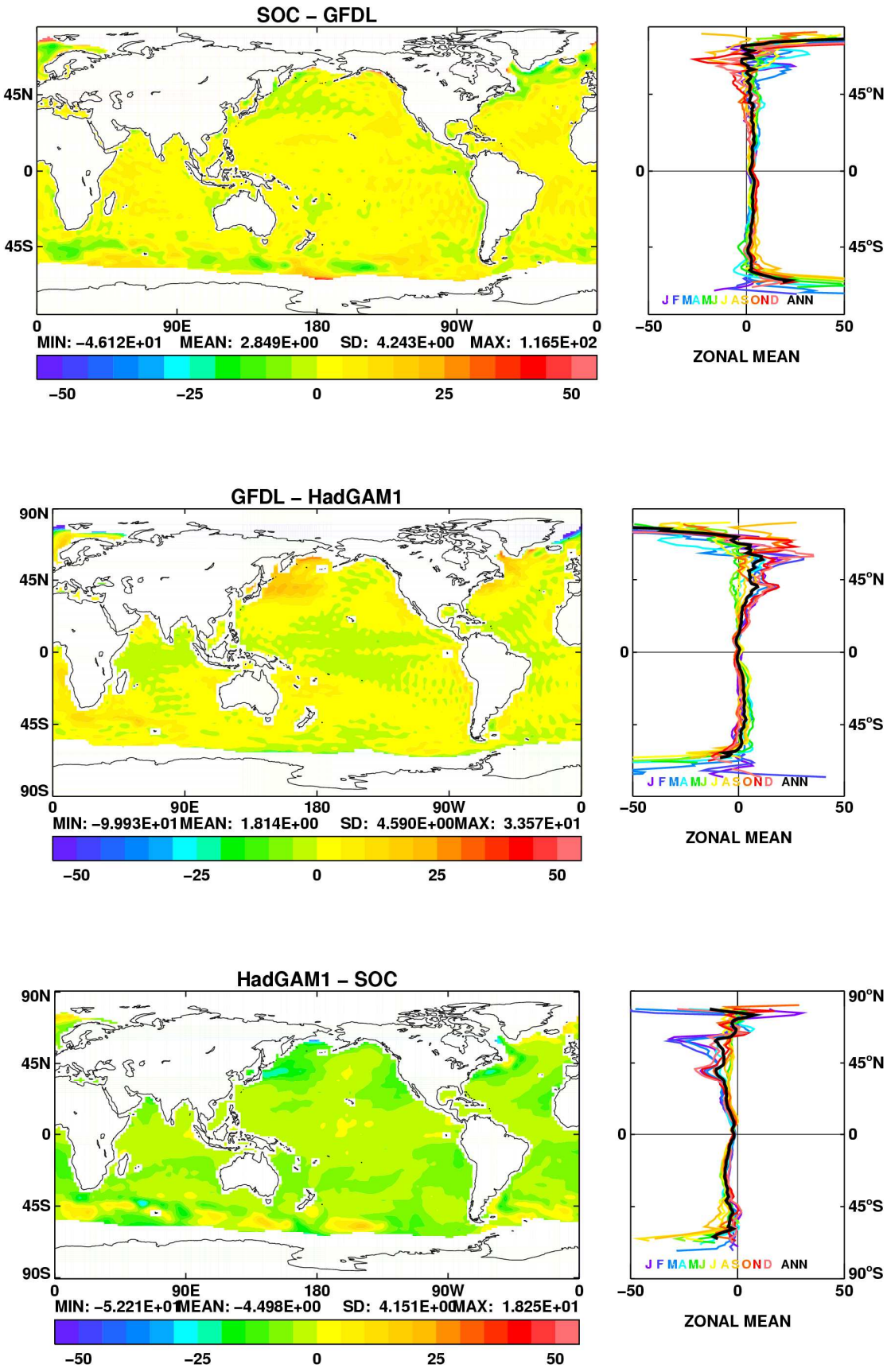

Fig 4b: As Fig 4a but for sensible heating.

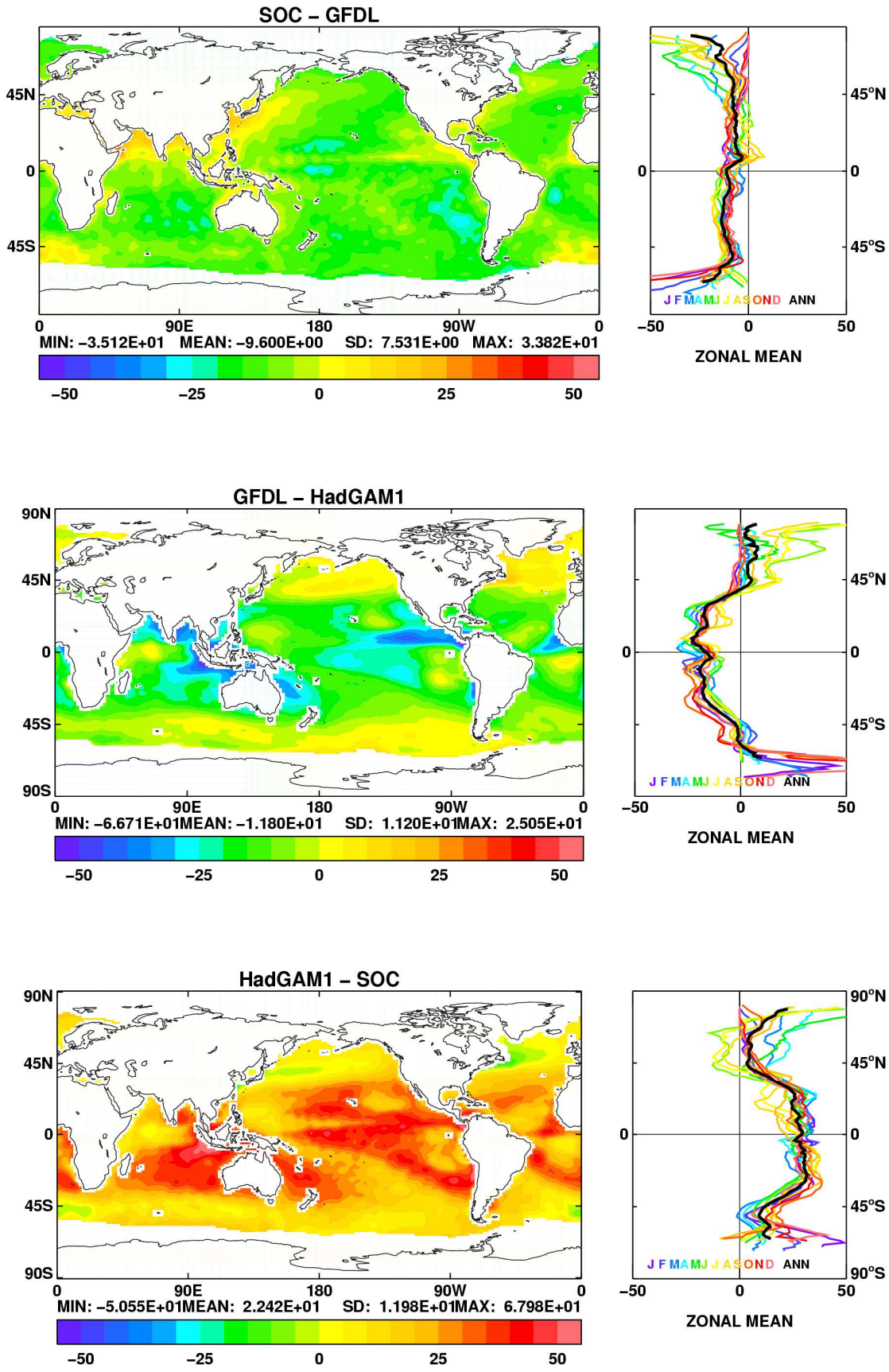

Fig 4c: As Fig 4a but for SW heating.

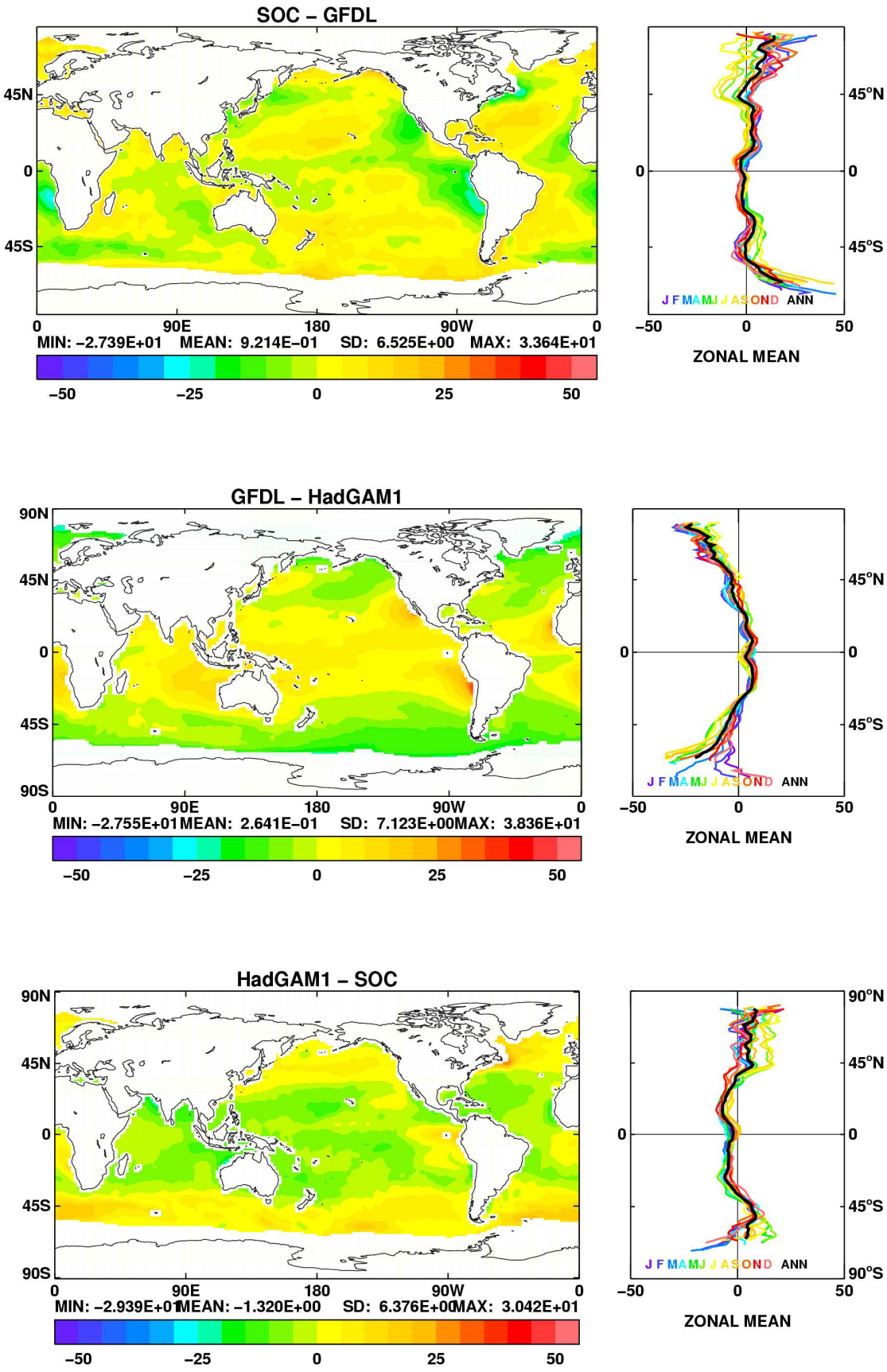

Fig 4d: As Fig 4a but for LW heating.

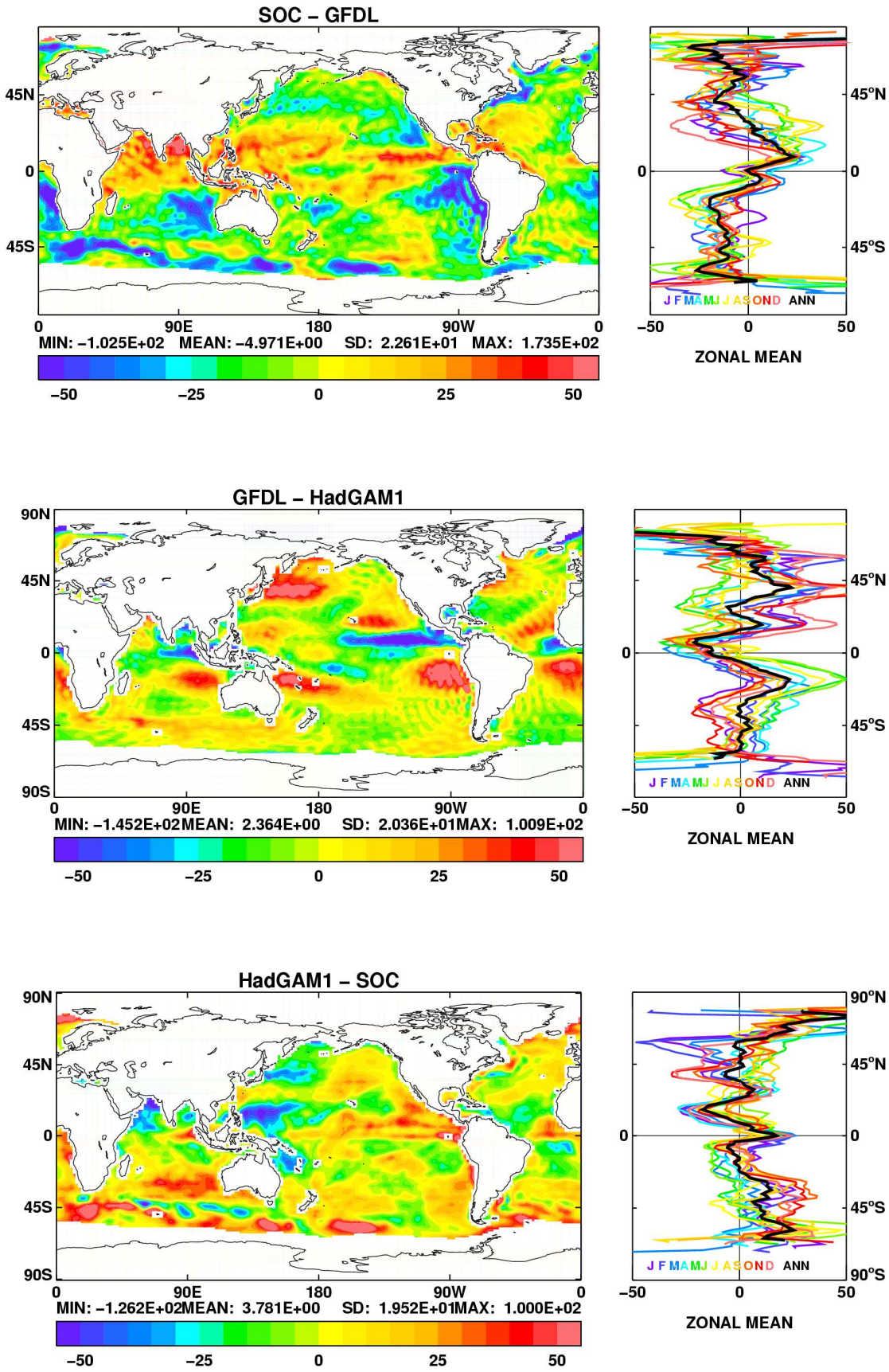

Fig 4e: As Fig 4a but for total heating.

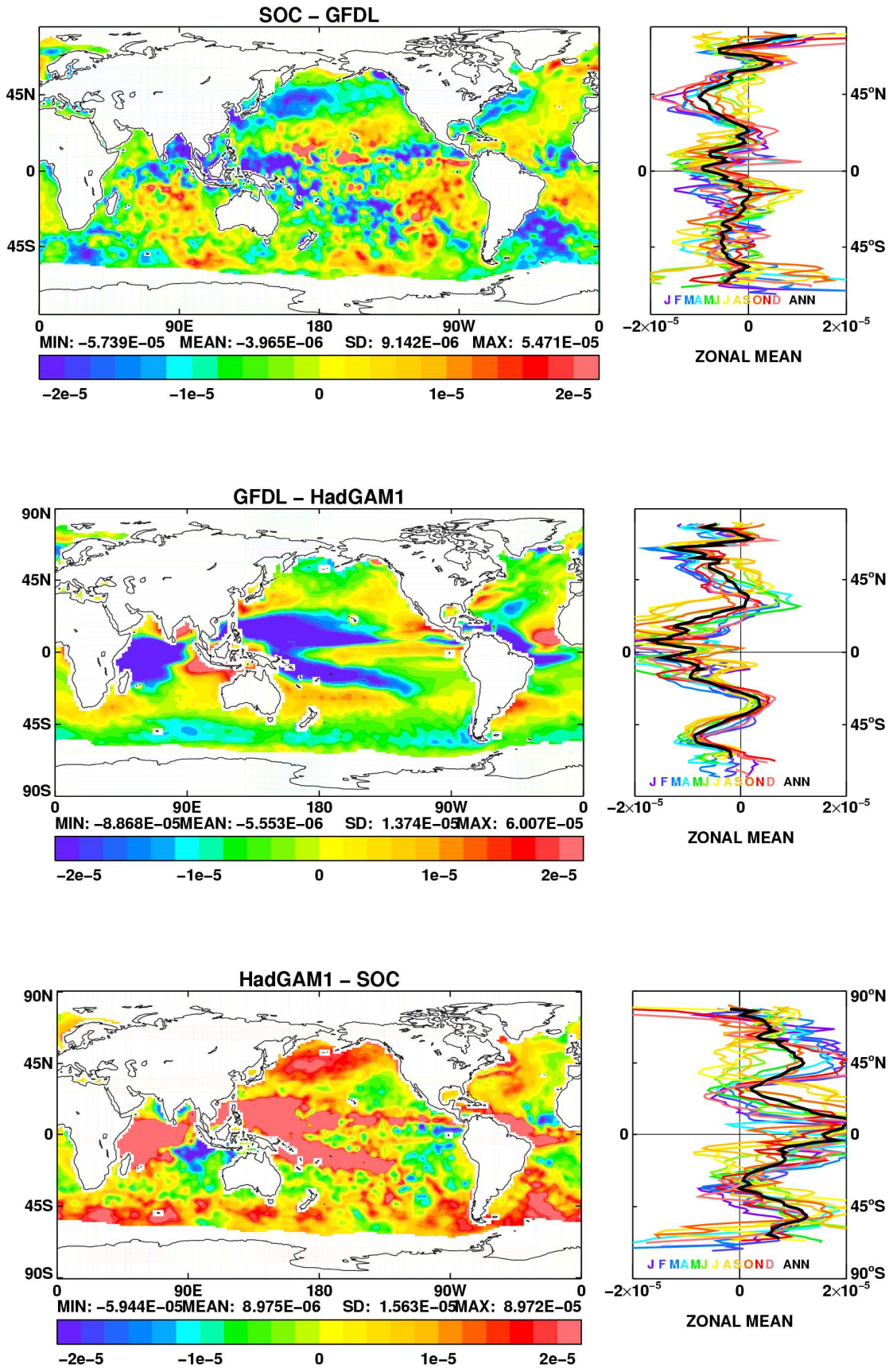

Fig 4f: As Fig 4a but for precipitation rate.

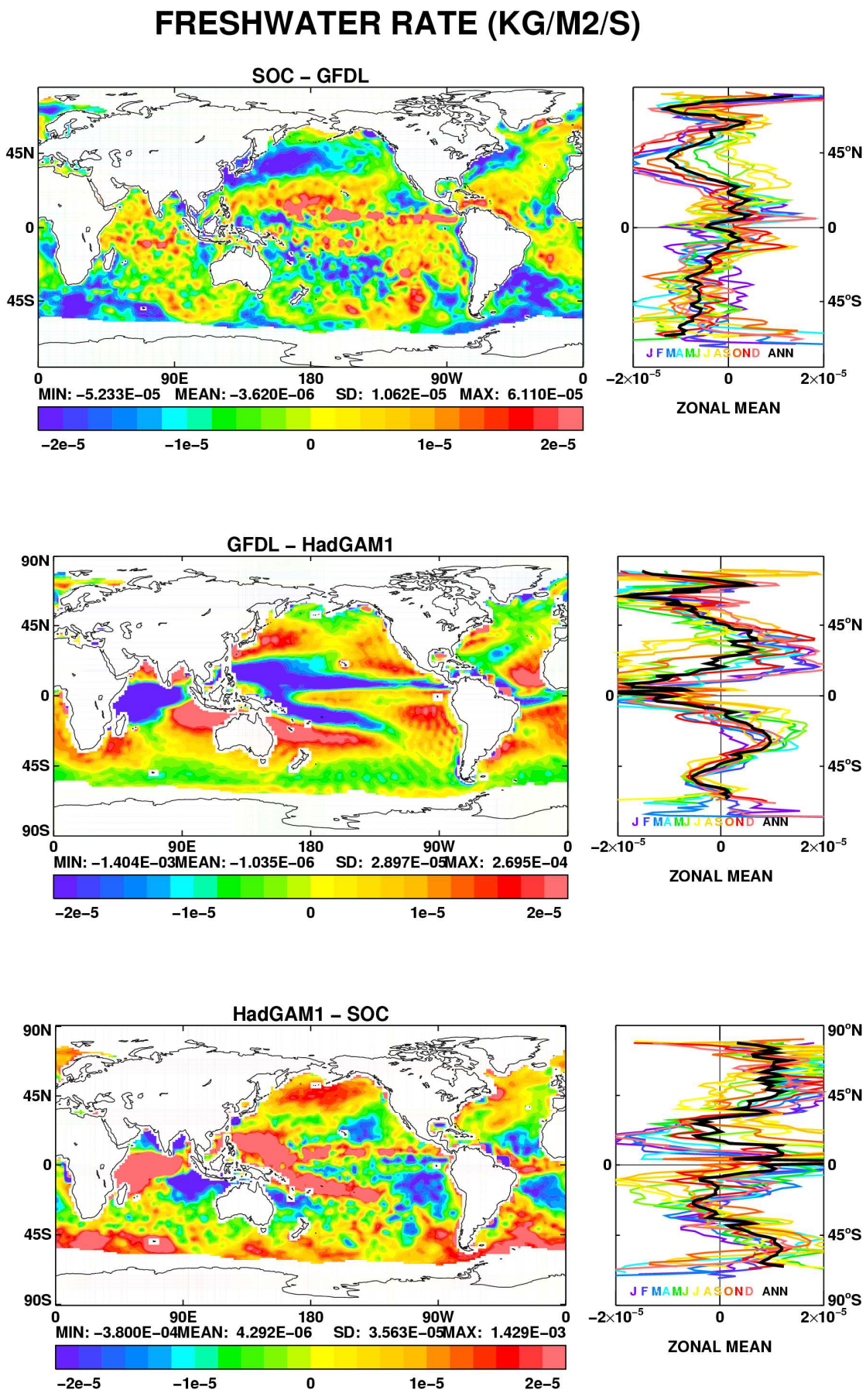

Fig 4g: As Fig 4a but for total freshwater rate.

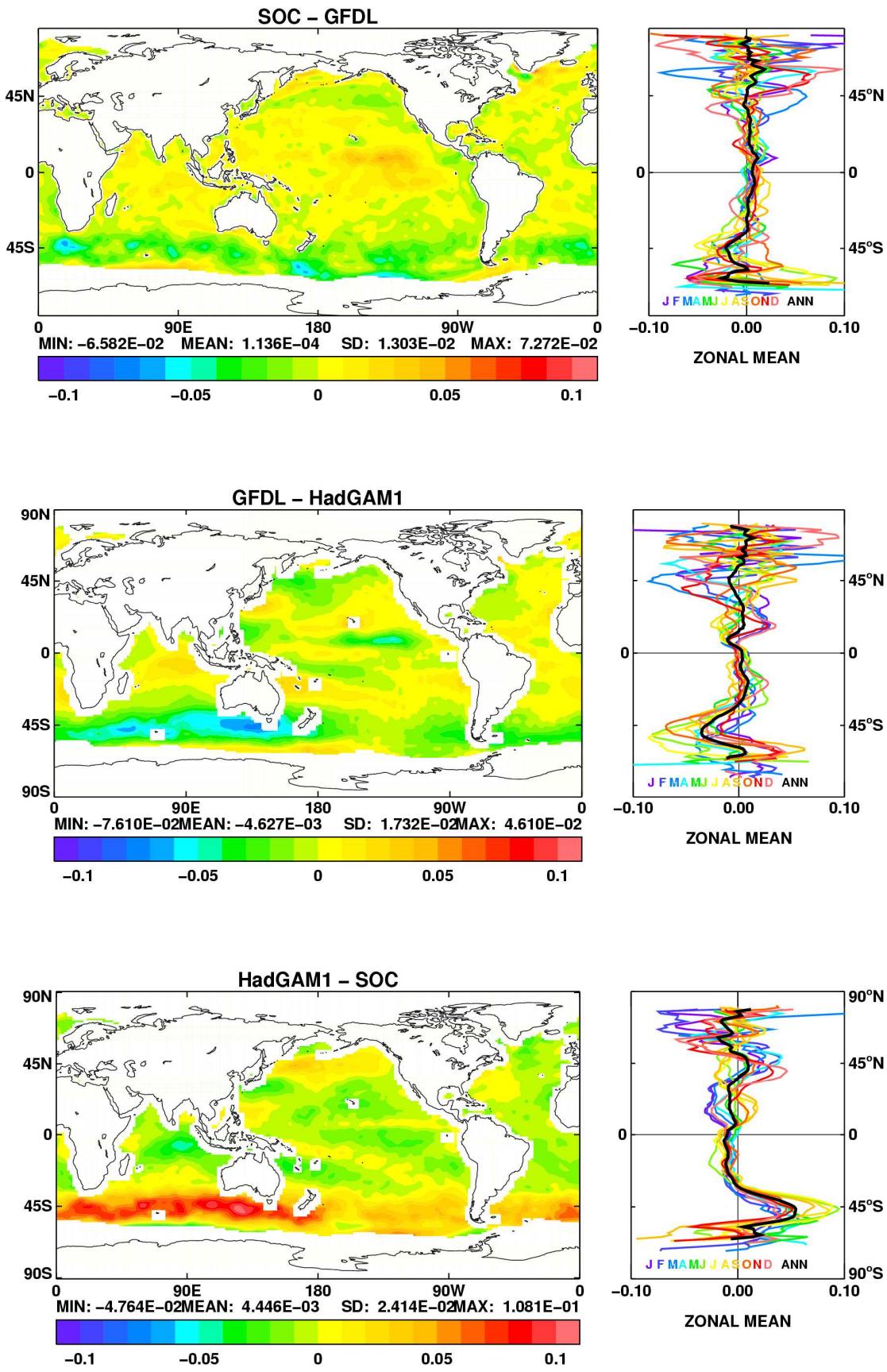

Fig 4h: As Fig 4a but for zonal windstress.

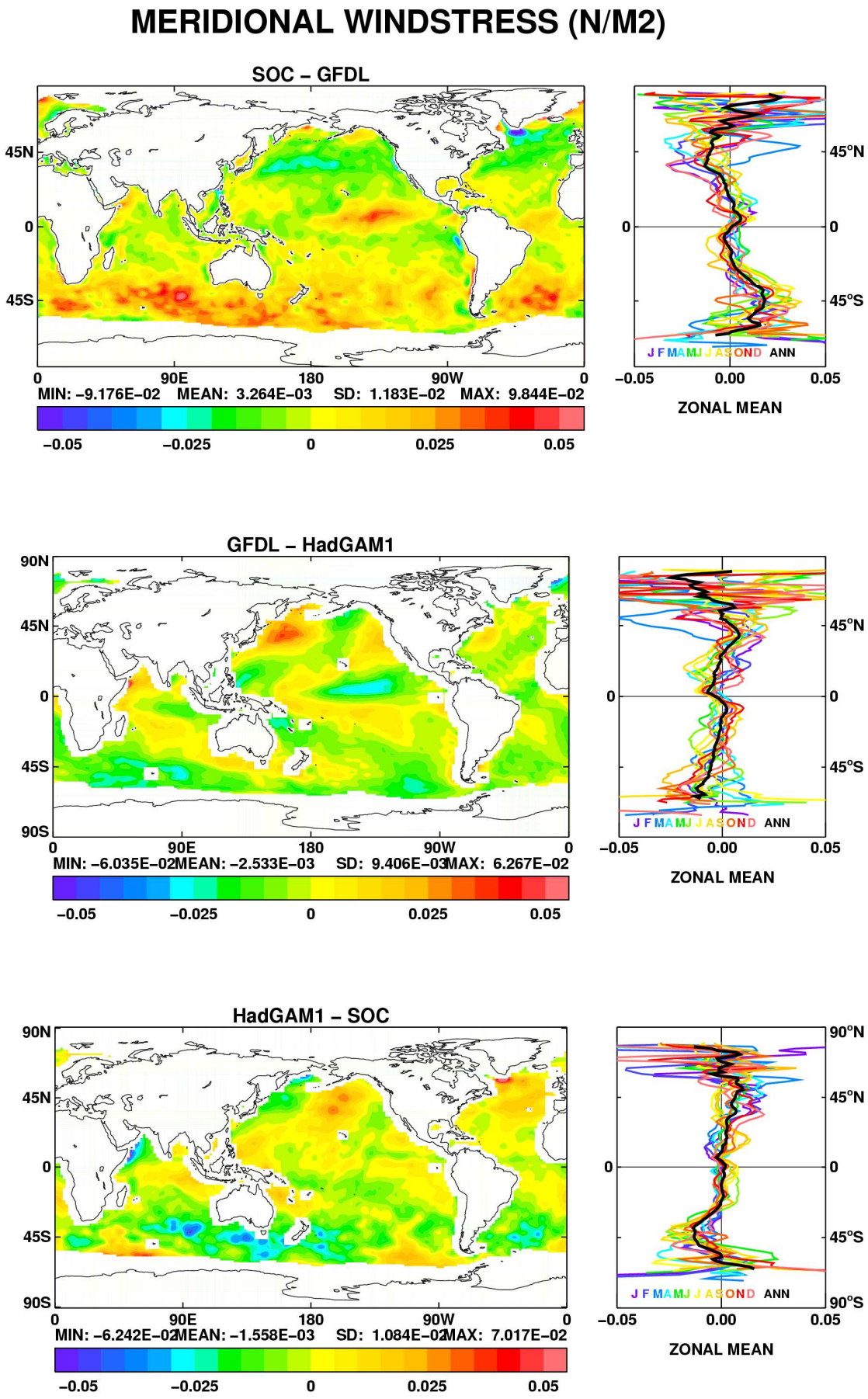

Fig 4i: As Fig 4a but for meridional windstress.

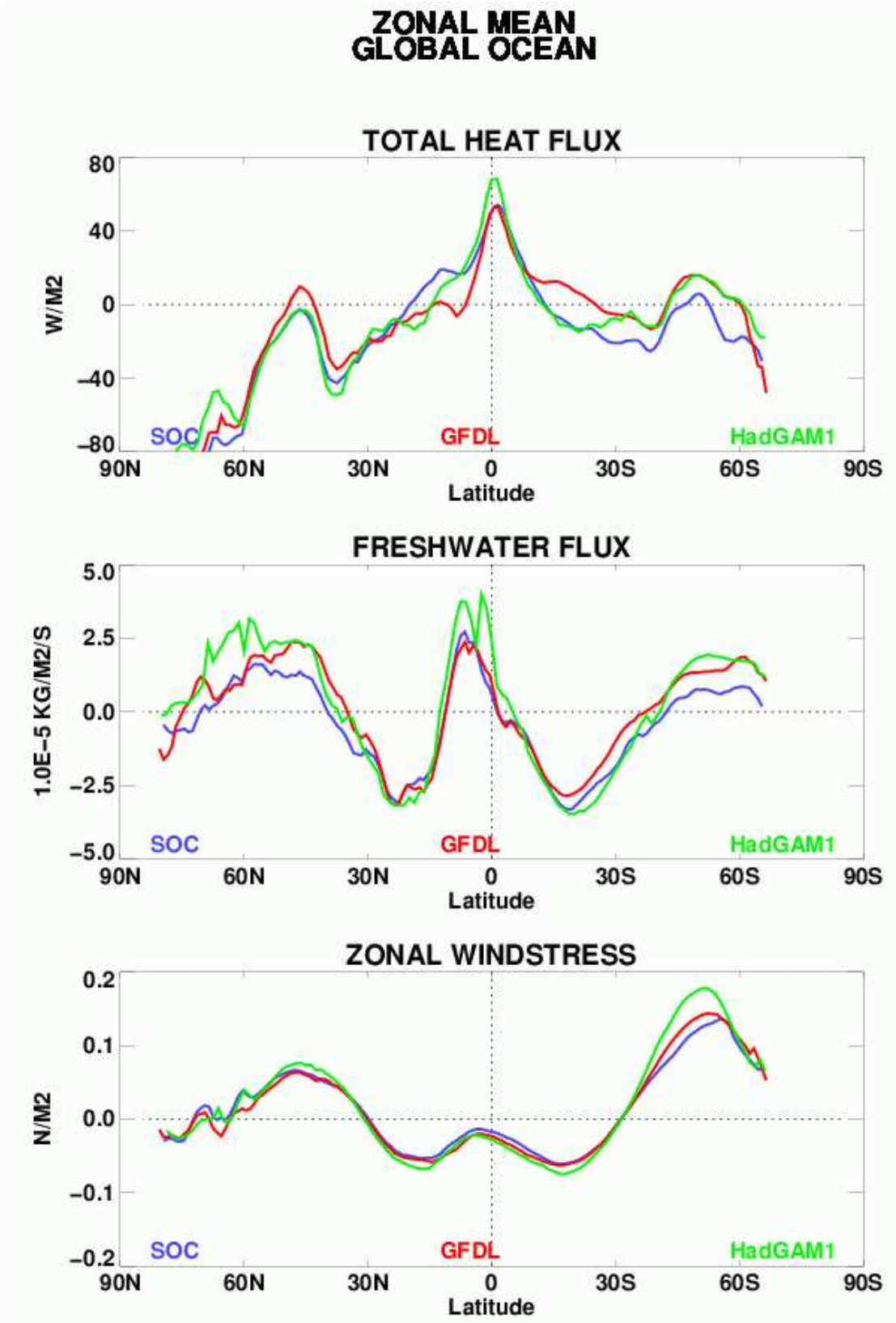

Fig 5: Zonal mean total heat flux, total freshwater flux and zonal windstress for the SOC, GFDL and HadGAM1 datasets.

SOC ADJUSTED FLUXES

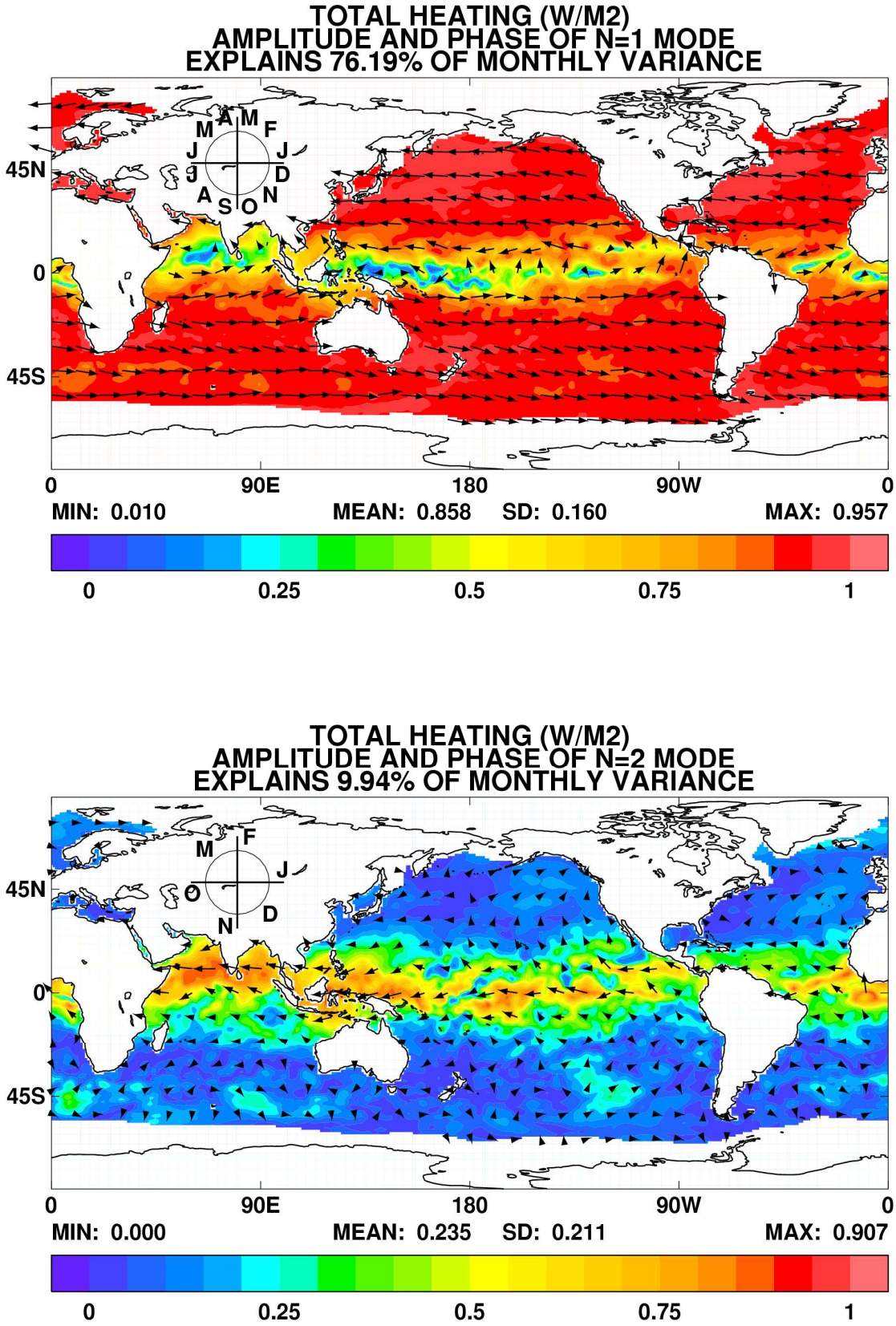

Fig 6.1a: Normalised amplitude and phase for annual and biannual modes of total heat input. SOC fluxes.

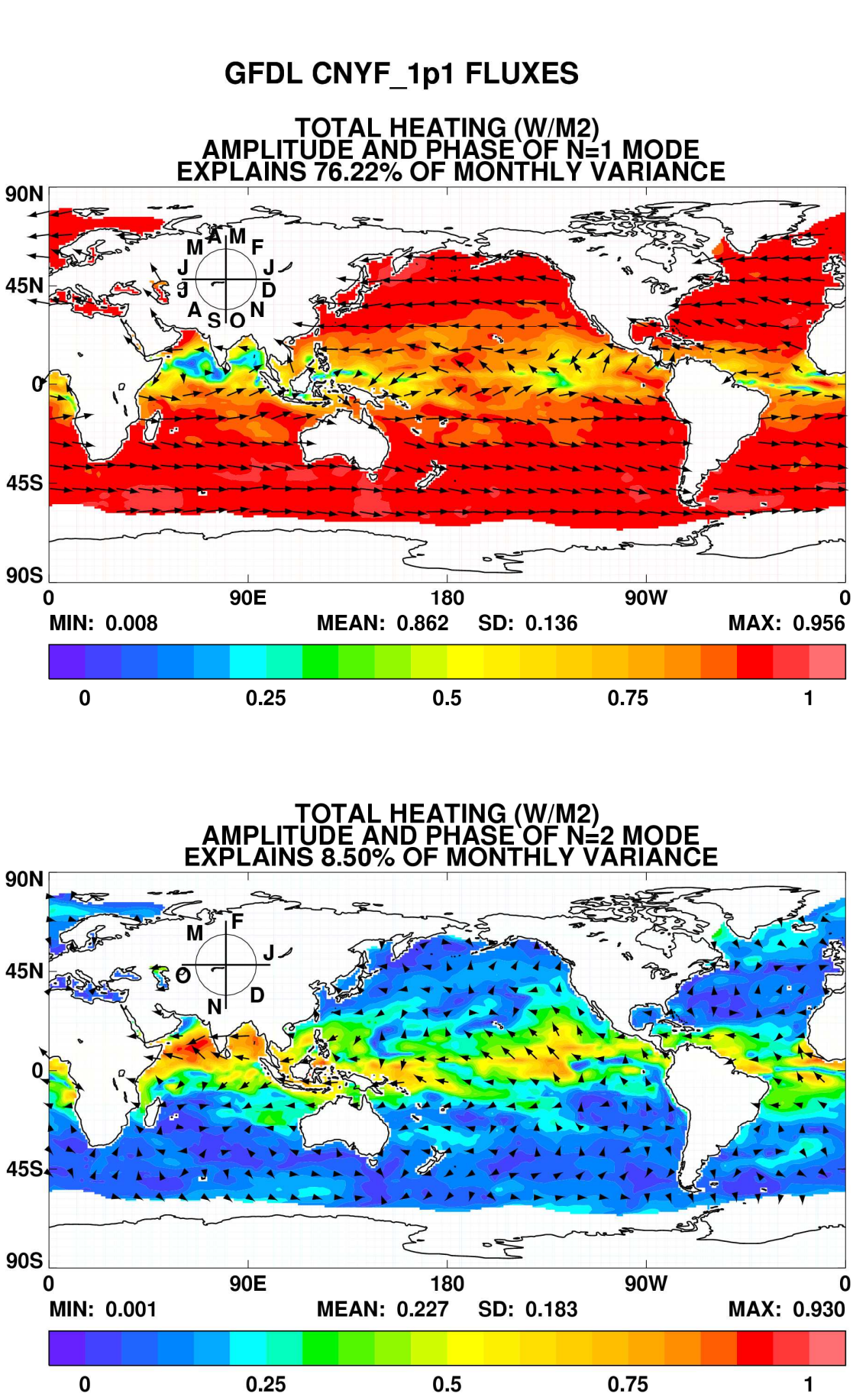

Fig 6.1b: Normalised amplitude and phase for annual and biannual modes of total heat input. GFDL fluxes.

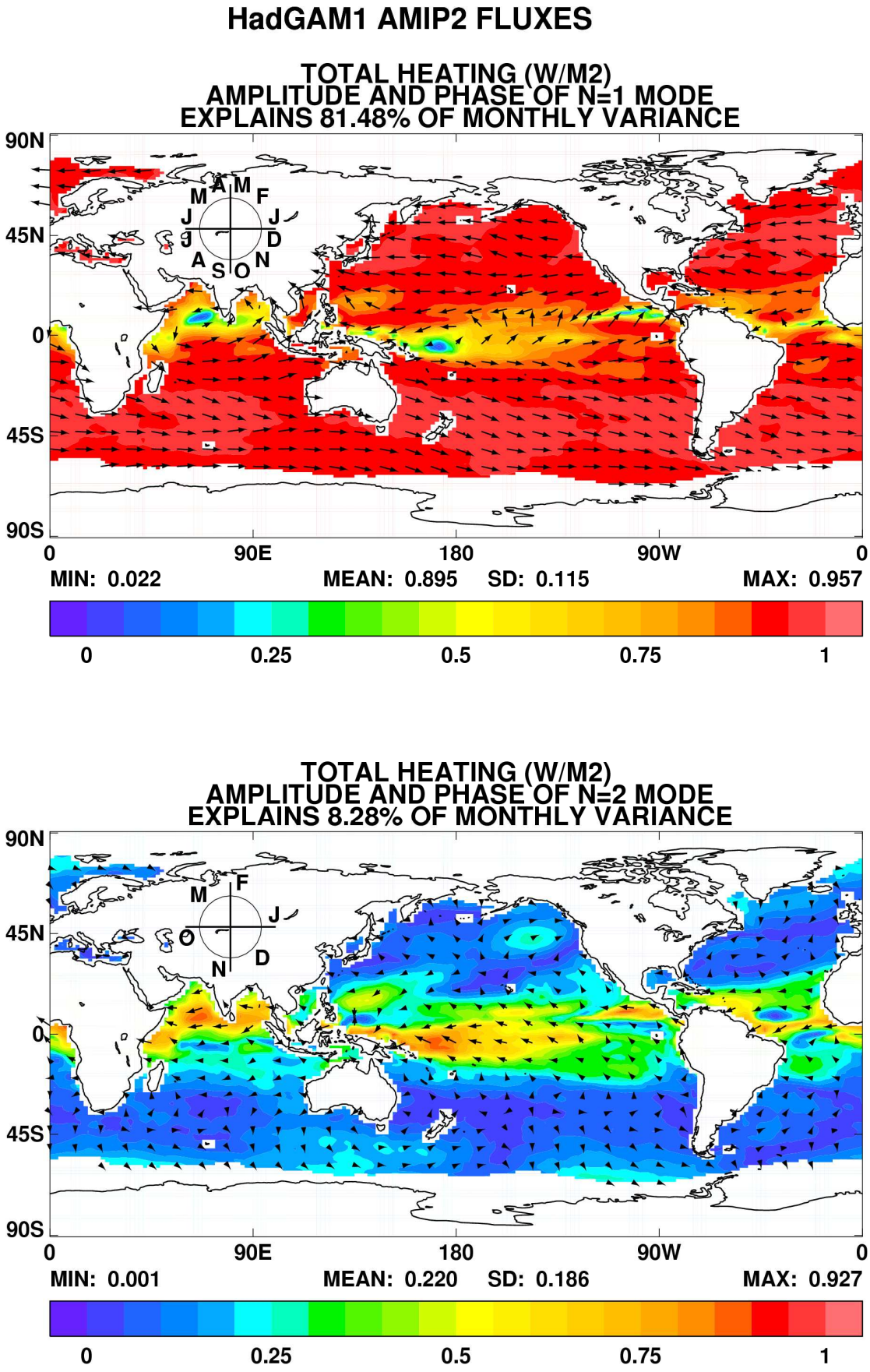

Fig 6.1c: Normalised amplitude and phase for annual and biannual modes of total heat input. HadGAM1 fluxes.

SOC ADJUSTED FLUXES

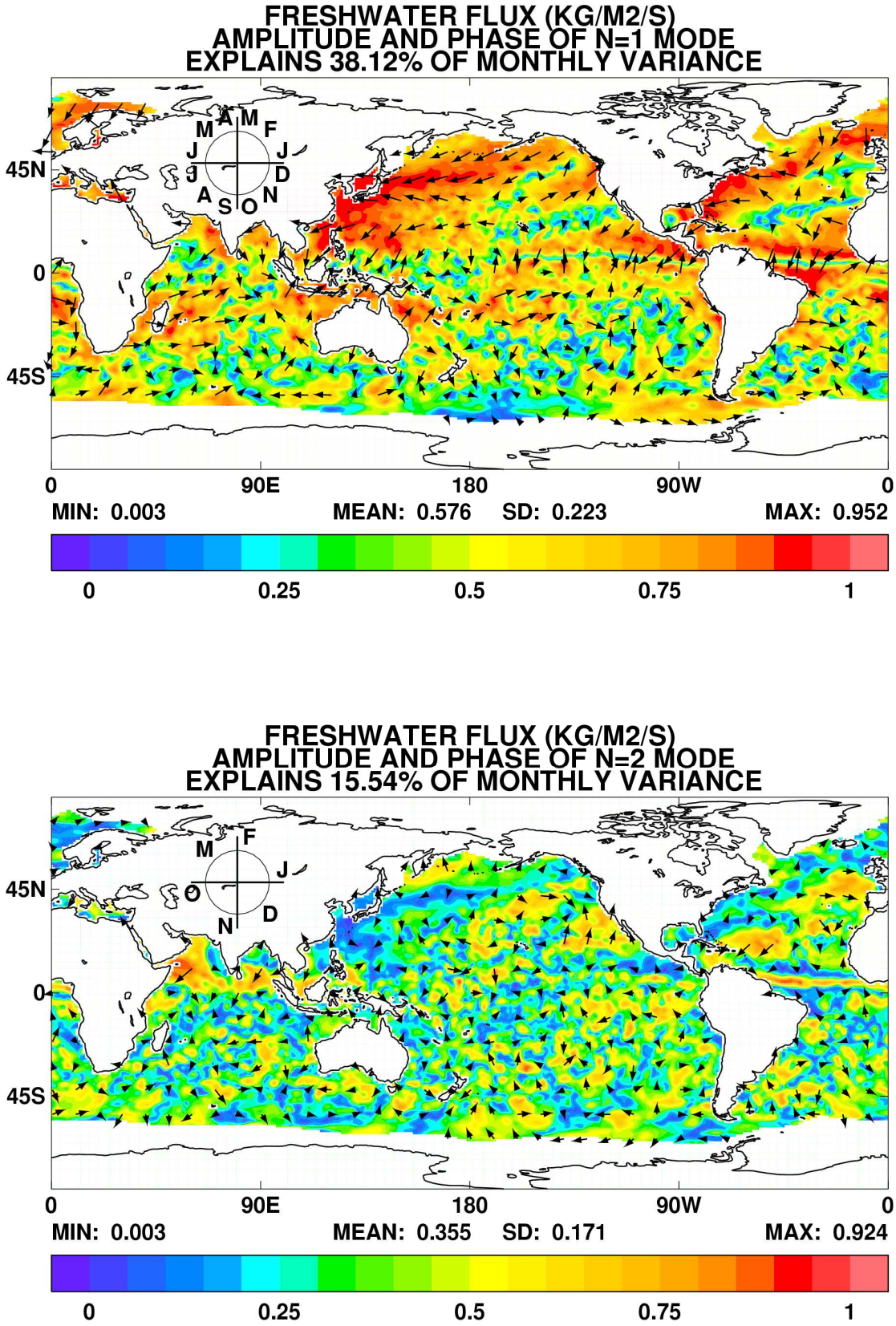

Fig 6.2a: Normalised amplitude and phase for annual and biannual modes of total freshwater input. SOC fluxes.

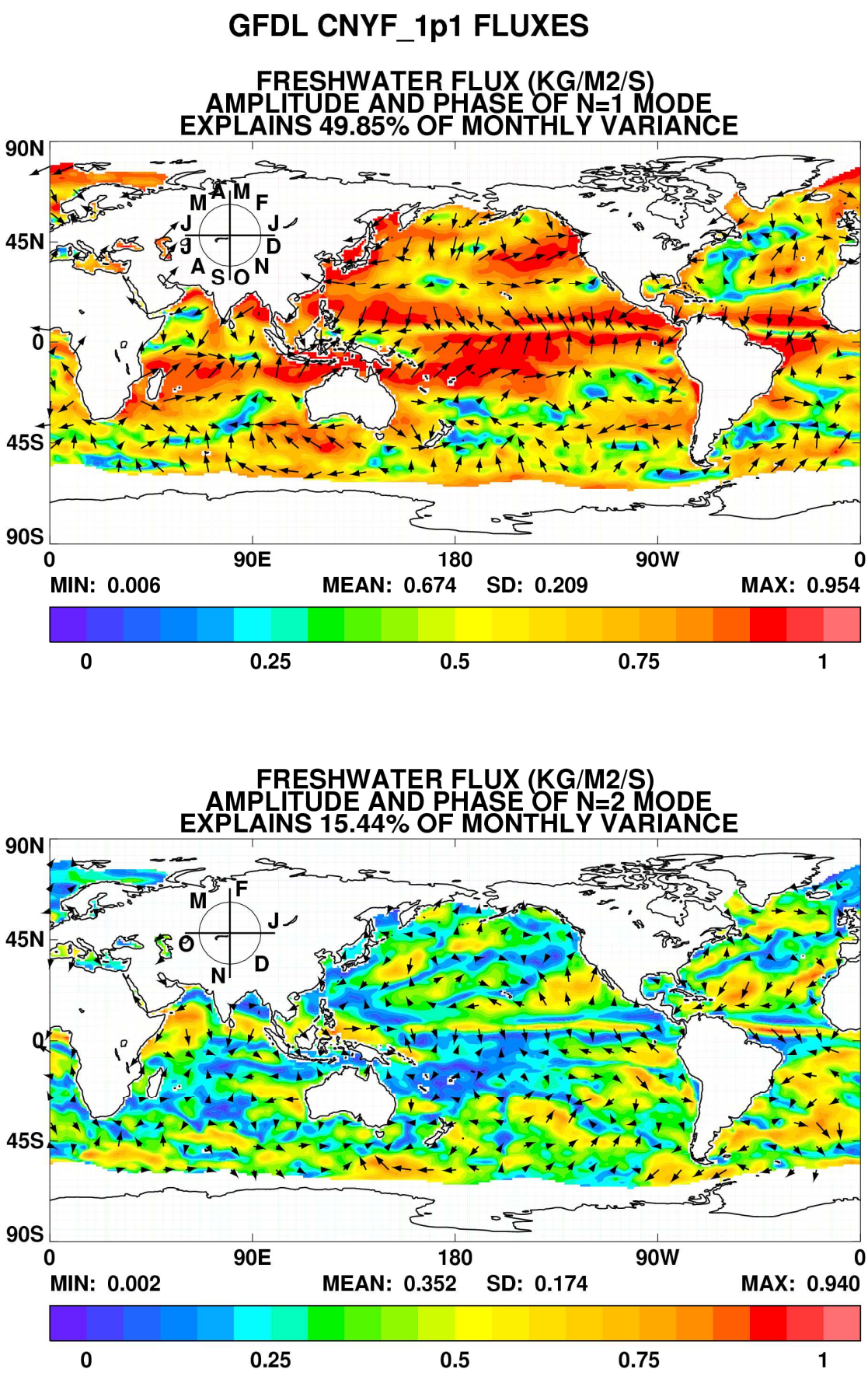

Fig 6.2b: Normalised amplitude and phase for annual and biannual modes of total freshwater input. GFDL fluxes.

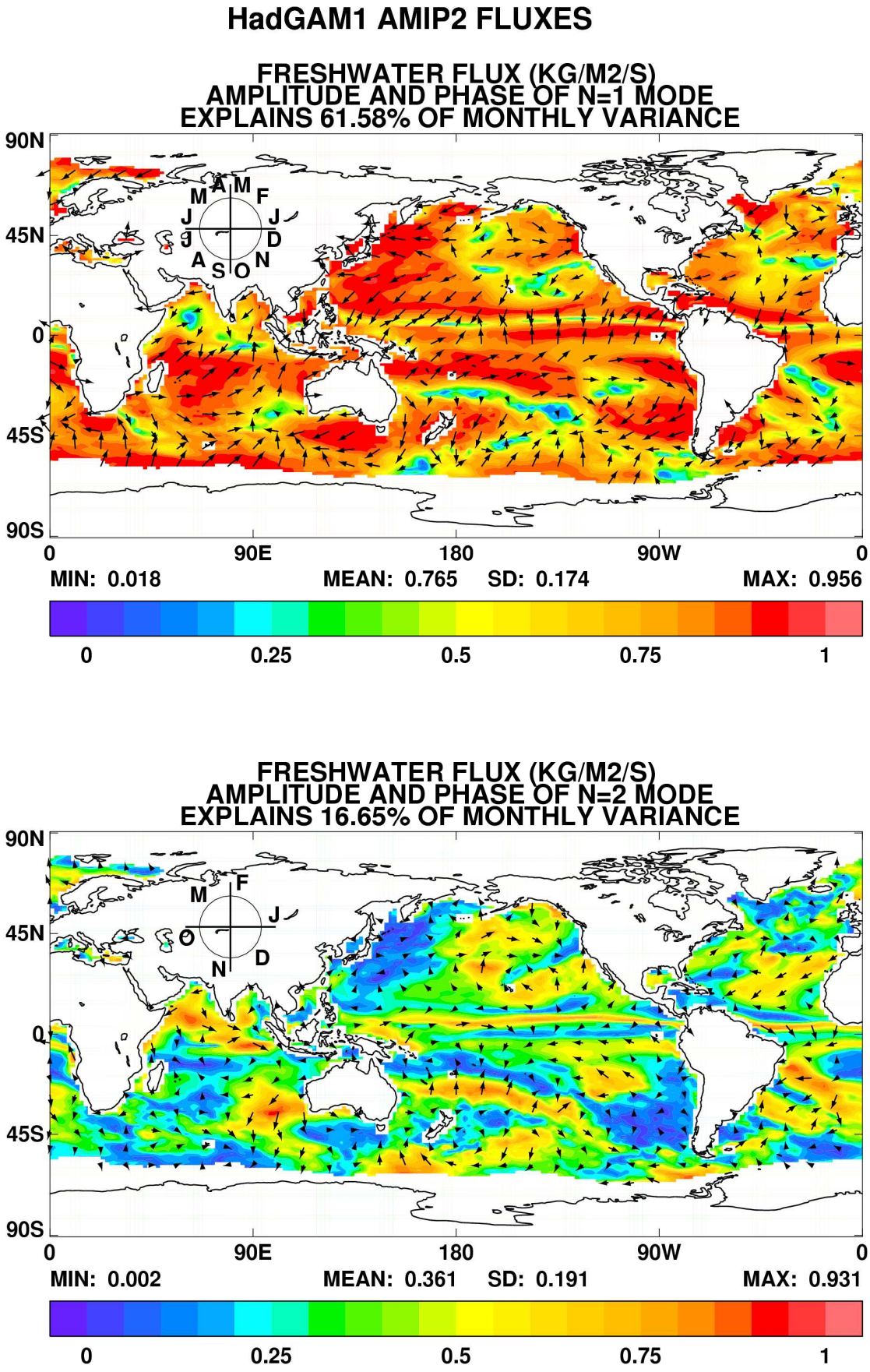

Fig 6.2c: Normalised amplitude and phase for annual and biannual modes of total freshwater input. HadGAM1 fluxes.

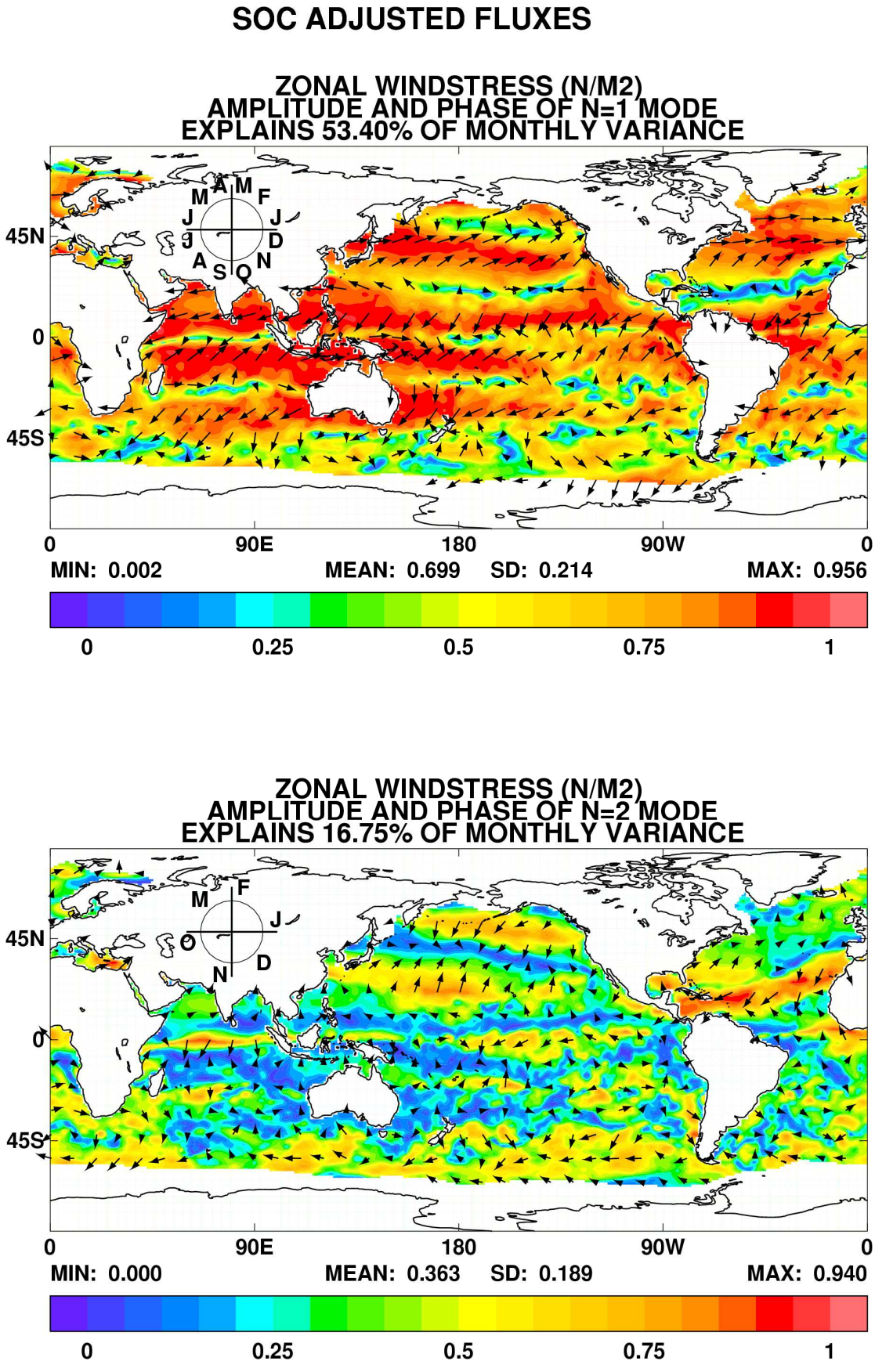

Fig 6.3a: Normalised amplitude and phase for annual and biannual modes of zonal windstress. SOC fluxes.

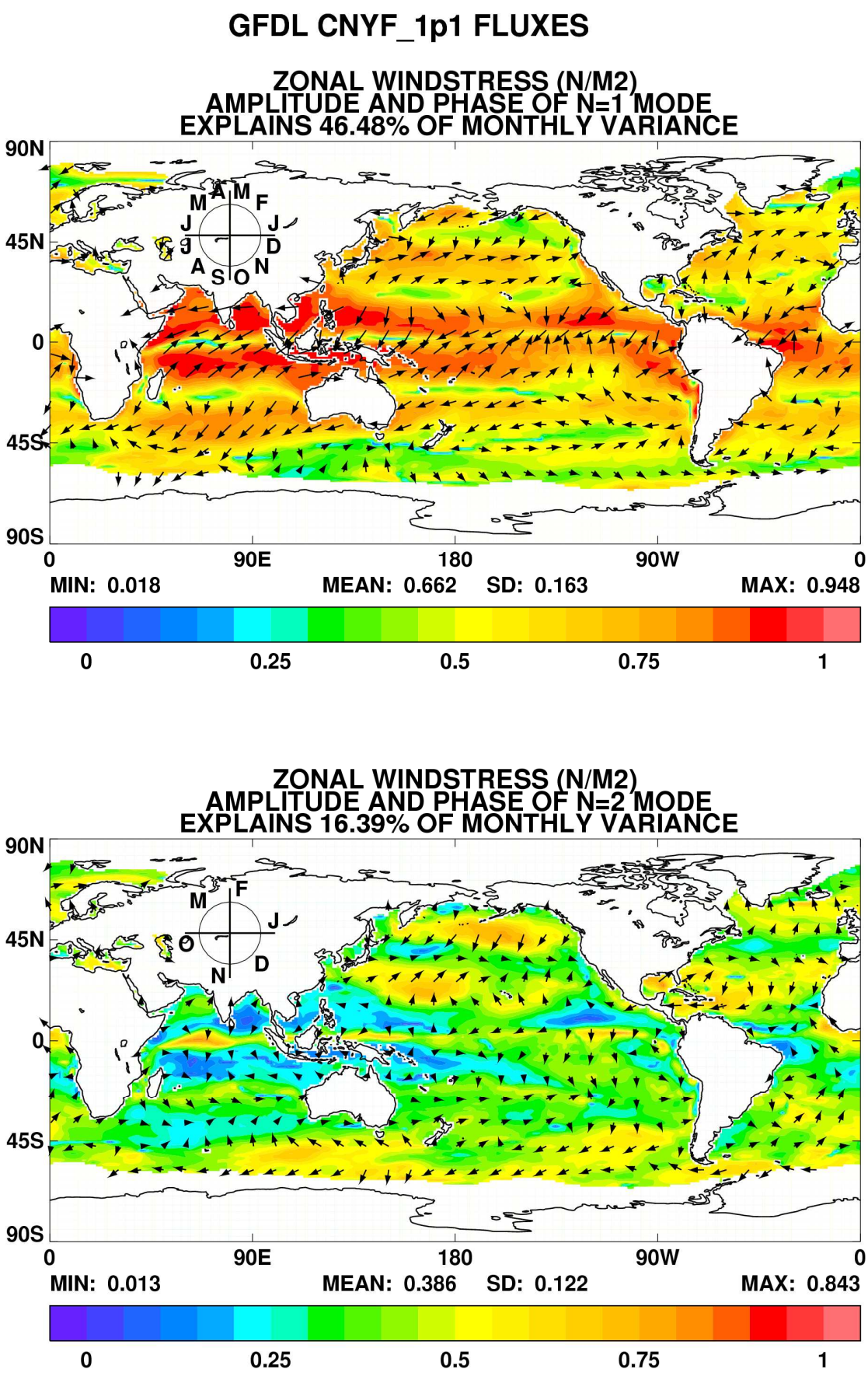

Fig 6.3b: Normalised amplitude and phase for annual and biannual modes of zonal windstress. GFDL fluxes.

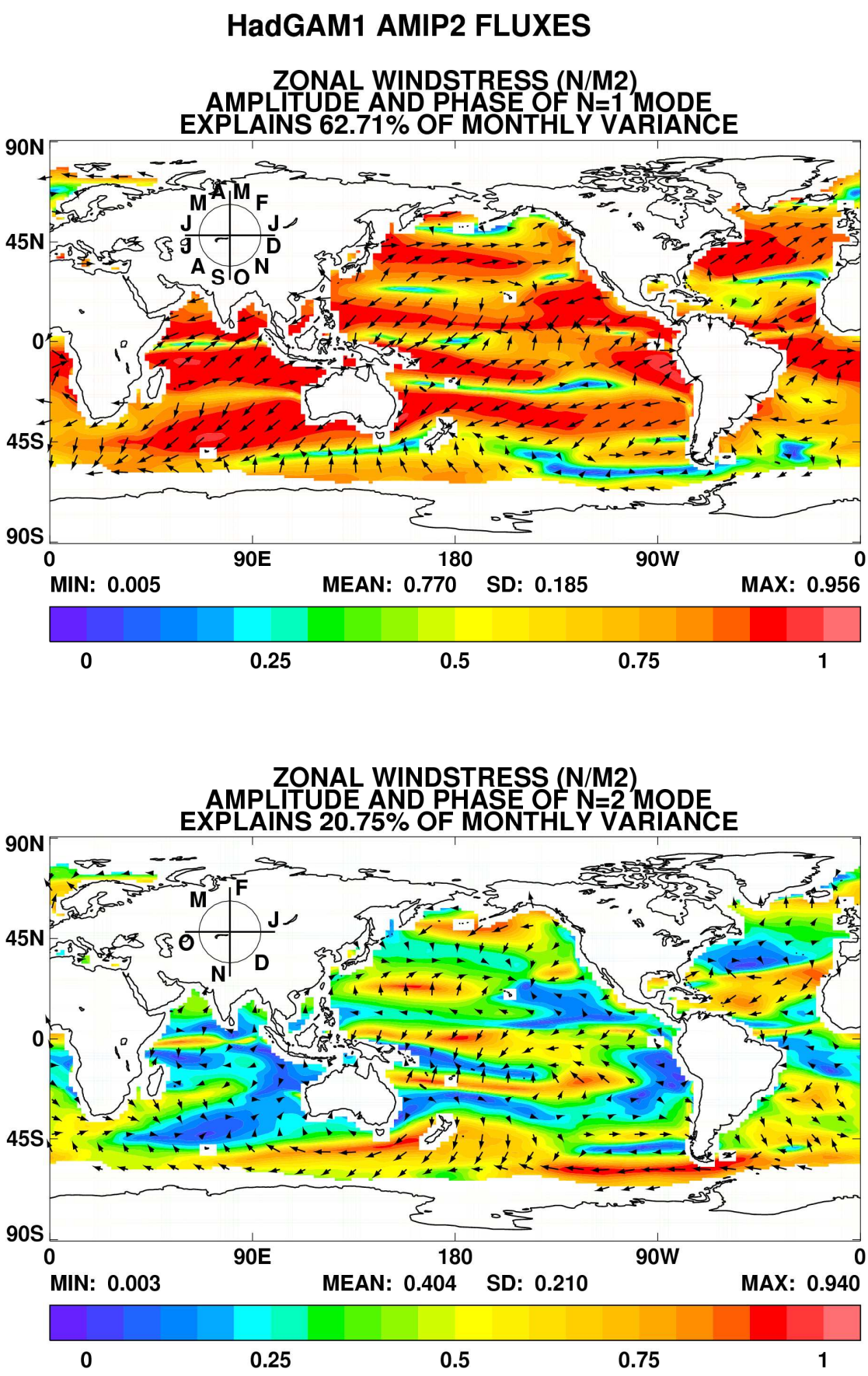

Fig 6.3c: Normalised amplitude and phase for annual and biannual modes of zonal windstress. HadGAM1 fluxes.

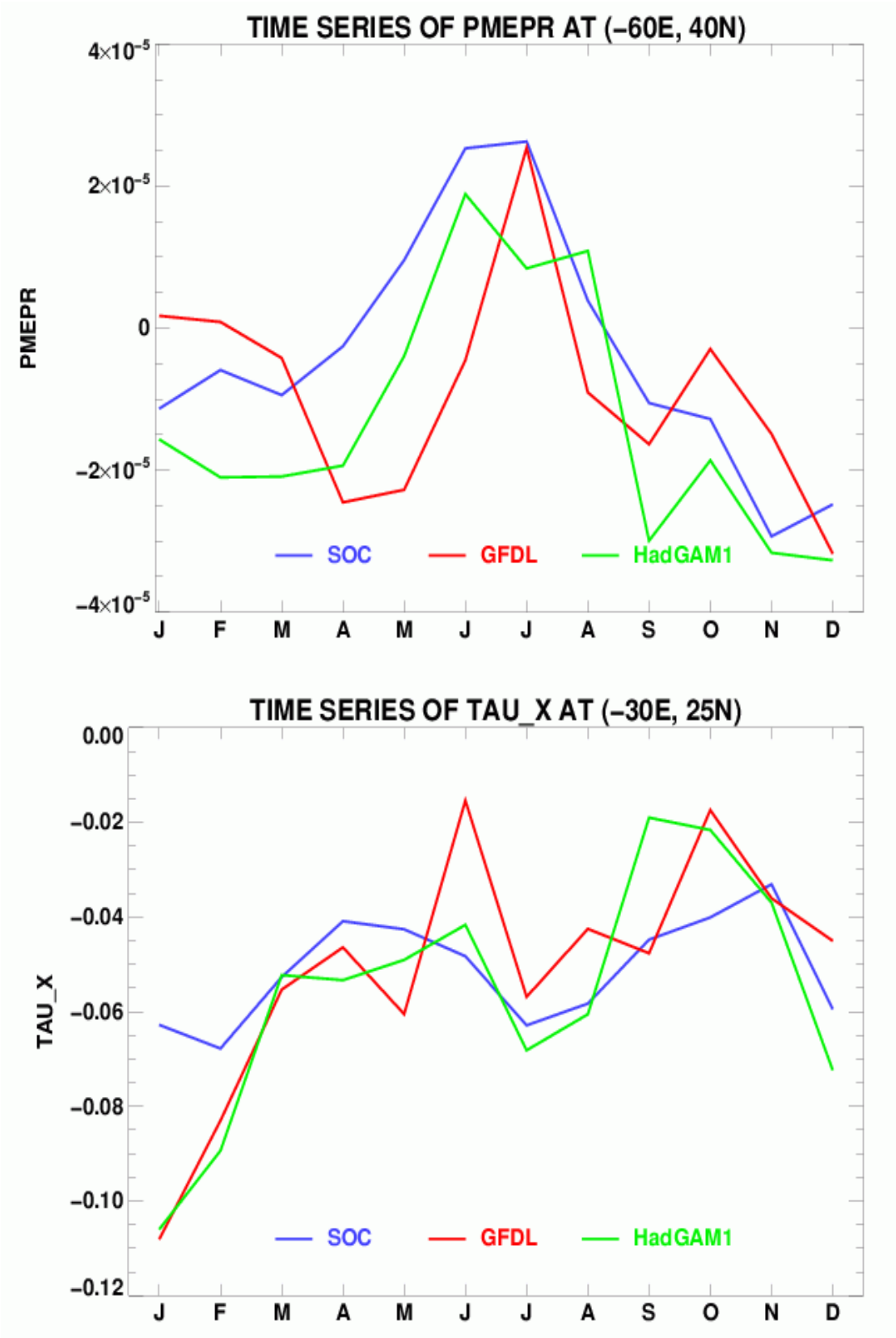

Fig 7: Timeseries of net freshwater at (60W, 40N) (top panel) and zonal windstress at (30W, 25N) (bottom panel) for the three datasets.

Appendix A: Bulk formulae

Haney's calculation of the relaxation parameter λ, and the estimation of turbulent air-sea fluxes of heat and momentum, both depend on the use of bulk formulae. These involve an "Ohm's law" approximation in which the "current" of a quantity is proportional to the "potential difference" which drives it. More precisely, the atmosphere-to-ocean sensible heat, latent heat and momentum fluxes are given in terms of the differences in temperature, specific humidity and wind between the sea surface and atmosphere at a given reference height:

$$SH = \rho_A \, c_p \, C_S \, V_A \, (T_A - SST) \qquad (A.1)$$

$$LH = \rho_A \, L_v \, C_L \, V_A \, (q_A - q_{sat}(SST)) \qquad (A.2)$$

$$\tau = \rho_A \, C_D \, V_A \, \mathbf{V_A} \qquad (A.3)$$

In the above, $\mathbf{V_A}$ is the velocity of air relative to the sea surface, c_p is the air heat capacity at constant pressure, L_v is the latent heat of vaporisation of water and the other symbols have their usual meanings. C_S, C_L and C_D, dimensionless quantities of order 10^{-3}, are called *transfer* or *exchange coefficients*. They depend on the atmospheric parameters T_A, q_A and $\mathbf{V_A}$, the height at which they're measured, and on the stability of the atmosphere. Note that all fluxes have a dependence on the wind speed V_A.

Haney (1971) used the sum of formulae like A.1, A.2 and analogous expressions for SW (eg Reed, 1977) and LW (eg Clark et al, 1974), with coefficients derived from climatological mean fields, to produce equation (1) for the total heat input into the ocean.

Many expressions for the drag coefficients have appeared in the literature, usually derived by calibration with respect to true flux measurements made from ships or platforms (eg Smith 1980; Large and Pond 1981, 1982; Fairall et al 1996 in the tropics). Blanc (1985) compared 10 published sets of bulk formulae by giving them all the same North Atlantic shipboard observations and calculating the heat and momentum fluxes that they produced. Mean differences of ~30% in basic stress and heat fluxes were found, with maximum differences of up to 100%. For "internal" parameters in the bulk formulae, such as roughness length and stability ratio, it was even worse. He concluded that "... it may [be] that we have already reached the inherent accuracy limitation of the bulk method because of the simplicity of the method's underlying assumptions." Nonetheless, bulk formulae remain the most widely used method of obtaining local, direct estimates of ocean surface heat fluxes from more routinely measurable quantities.

Appendix B: Adjustment of fluxes

Figure B.1 show the change in the SOC and GFDL total heat fluxes resulting from the adjustment procedures described in Sections 3.4, 5.1 and 5.2. For both datasets the change in the total heat input is dominated by increase in the latent cooling (not shown). The change (decrease) in SW heating in both datasets is about the same, although smoother and more extensive in SOC. The sensible heating hardly changes at all in either dataset. The LW cooling in the SOC dataset is increased almost everywhere by about 4W/m^2, but is largely unchanged in GFDL.

The GFDL changes in the total heating rate, Figure B.1, are clearly more concentrated in the tropics, with peak values twice as large as those of SOC. It has well-defined maxima at about ±5 degrees latitude, with the N Hemisphere maximum stronger than the S Hemisphere one. SOC is more N-S symmetrical than GFDL in the zonal mean, with its much broader maxima centred at about ±15 degrees. SOC has suffered a smaller change in the heat input in the Northern part of the Indian Ocean and a larger change in the Southern part. The heat flux has been changed (reduced) more over the Gulf Stream and Kuroshio Currents, and throughout the extratropics generally.

Despite the difference in spatial distribution of the SOC and GFDL adjustments, their global averages (-33 W/m^2 and -34 W/m^2 respectively) are very similar. The interesting question is whether the internal heating tendency (as revealed by the diagnosed Haney forcing) of an ocean model driven by unadjusted SOC or GFDL fluxes matches the changes displayed in Figure B.1. Since the model heating tendency describes what the model "wants" to do, an agreement between the two would suggest that the adjustment procedures were modifying the fields in a physically sensible way.

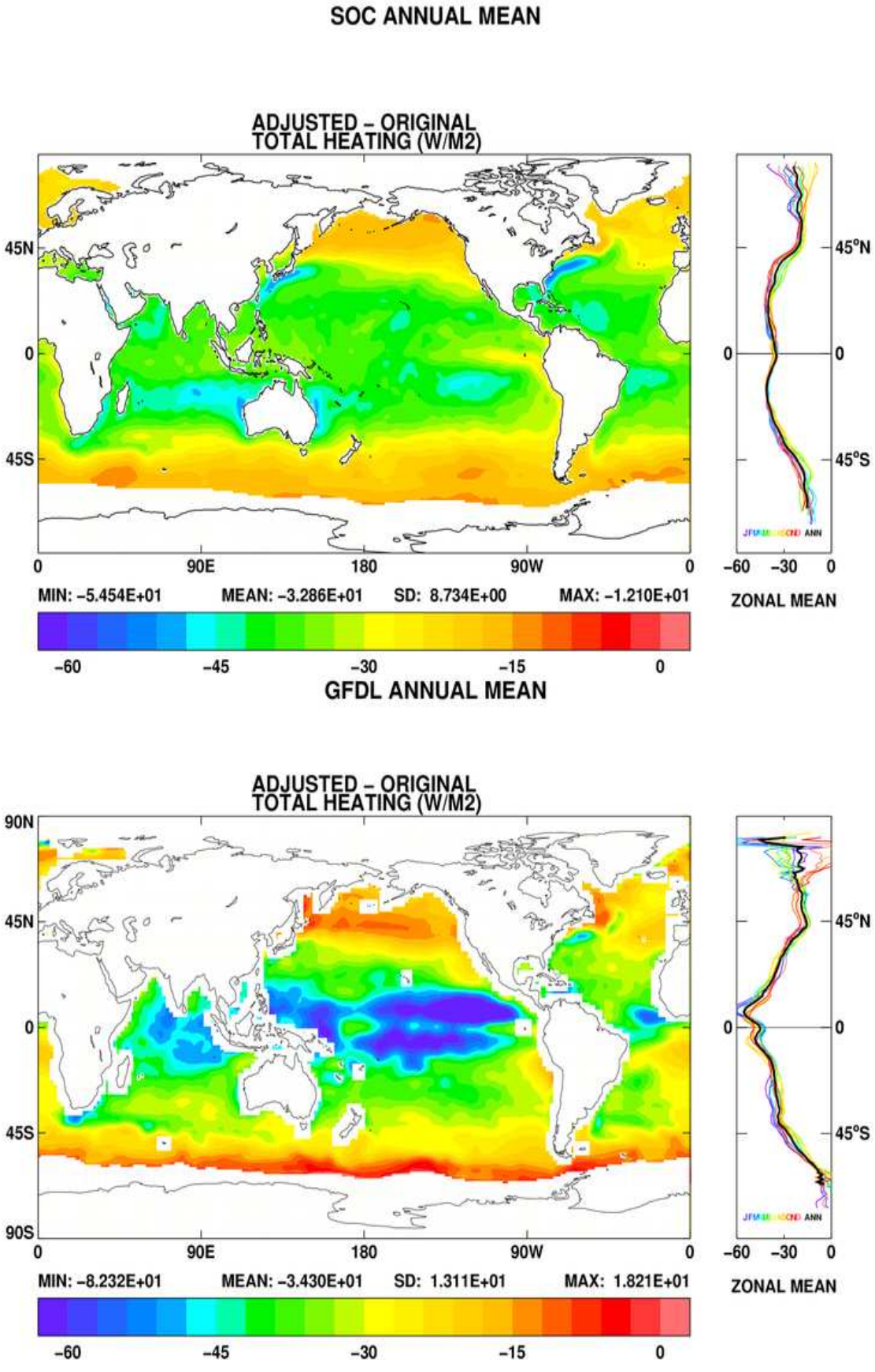

Fig B.1: Changes in annual mean total heat input effected by SOC (top) and GFDL (bottom) adjustment procedures.

Appendix C: Monthly means

For reference we present, without further comment, the monthly fields that make up the three flux datasets discussed in this report.

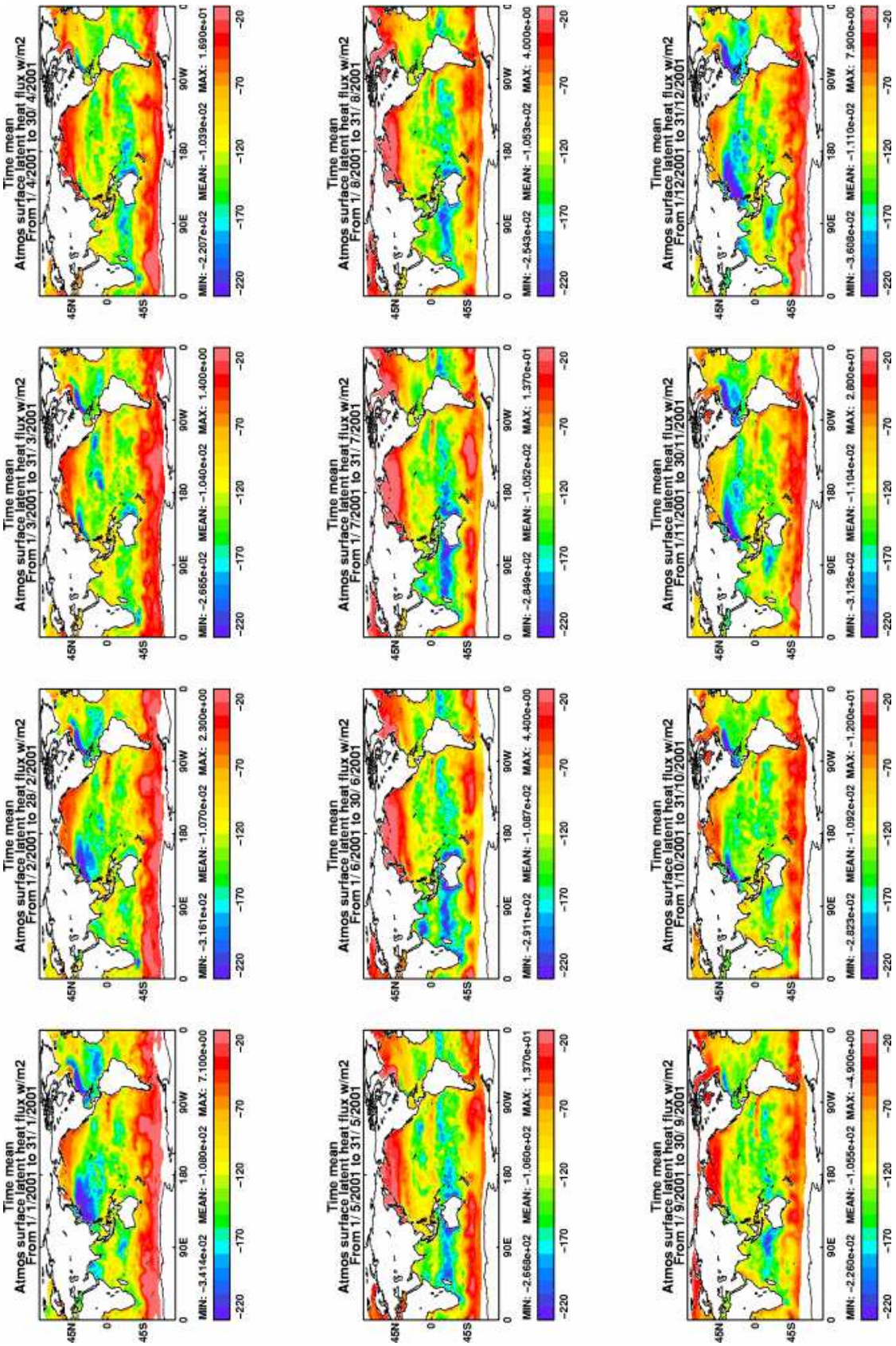

Fig C.1a: Monthly mean latent heating for adjusted SOC flux dataset.

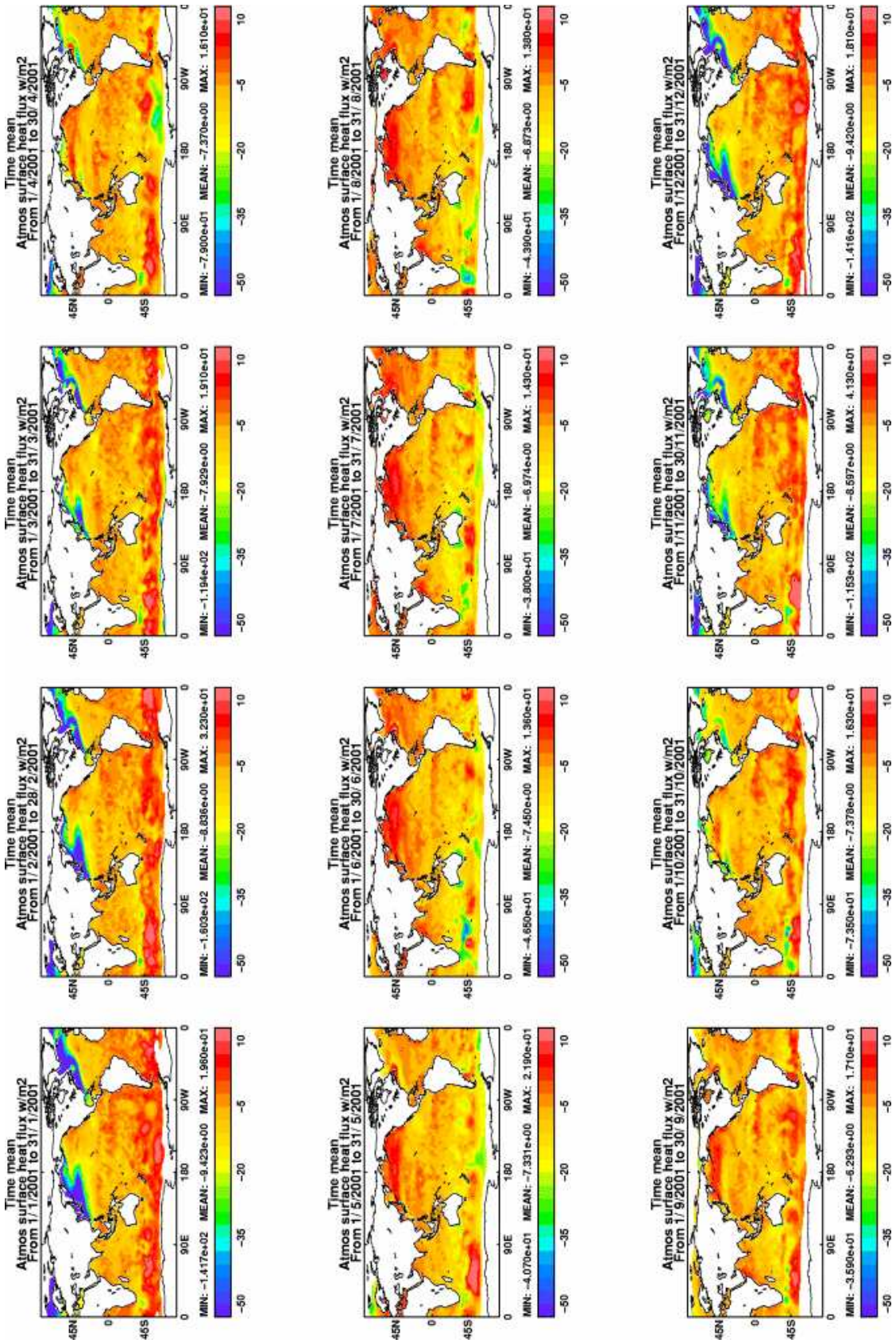

Fig C.1b: As Fig C.1a but for sensible heating.

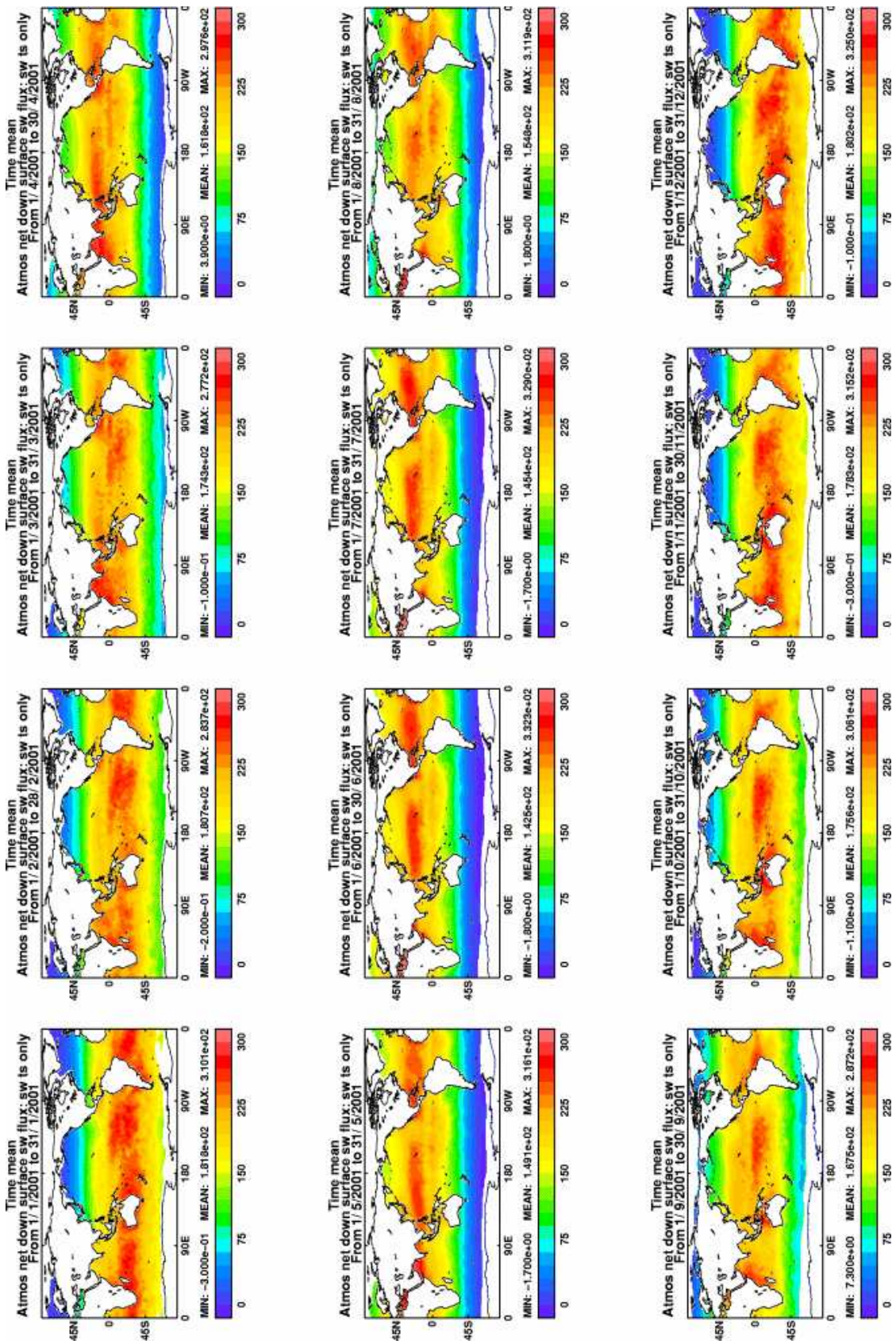

Fig C.1c: As Fig C.1a but for shortwave heating.

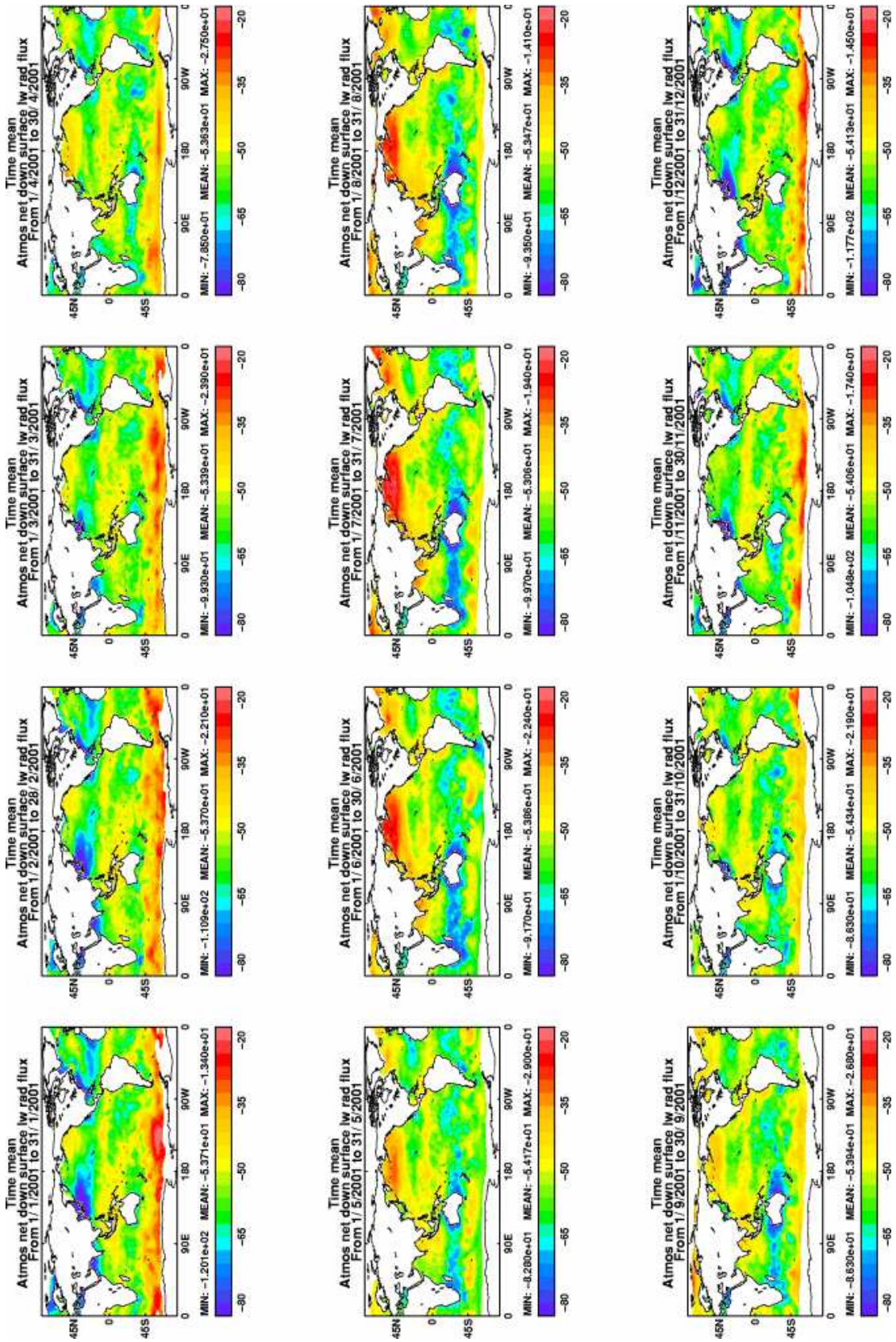

Fig C.1d: As Fig C.1a but for longwave heating.

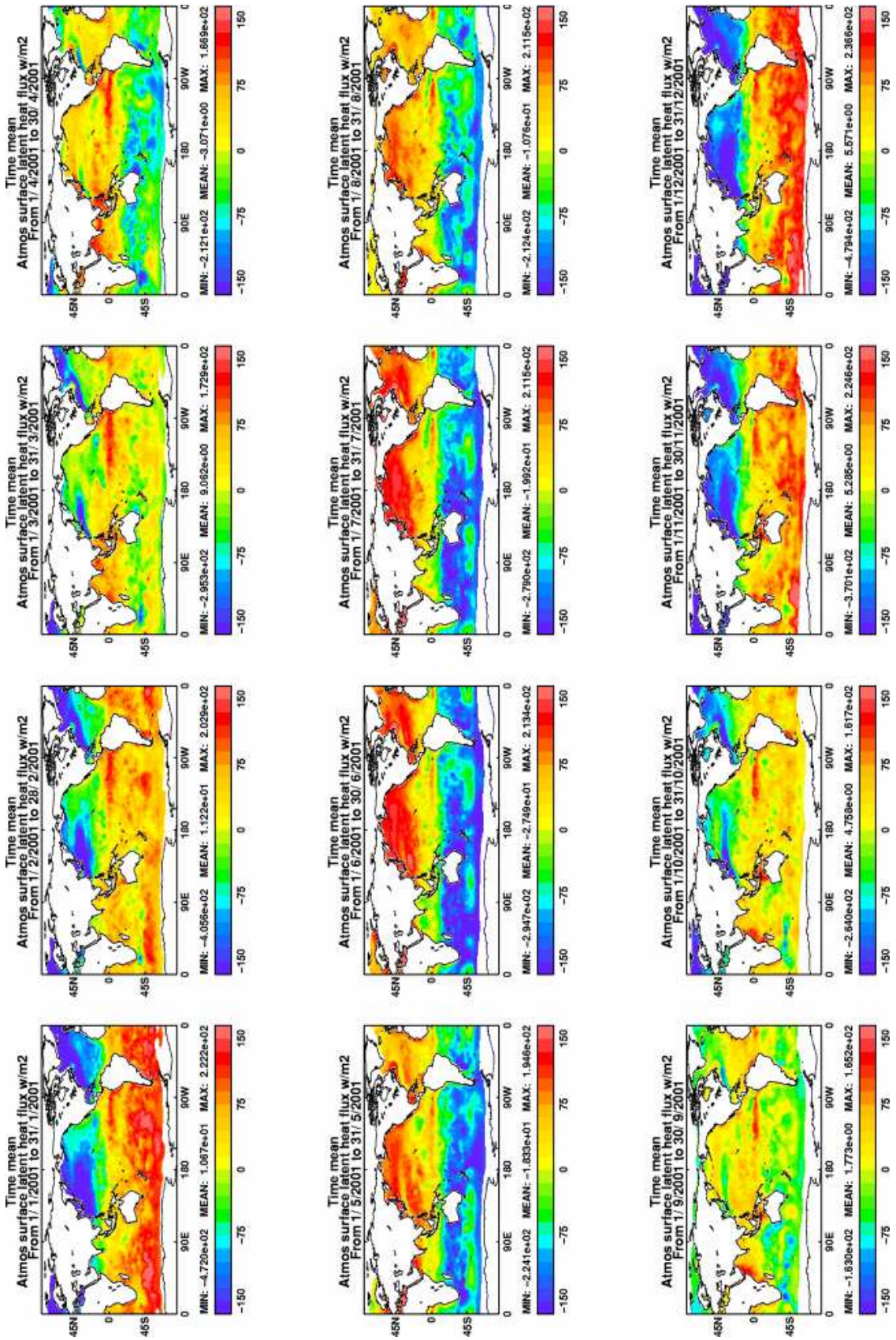

Fig C.1e: As Fig C.1a but for total (LH+SH+SW+LW) heating.

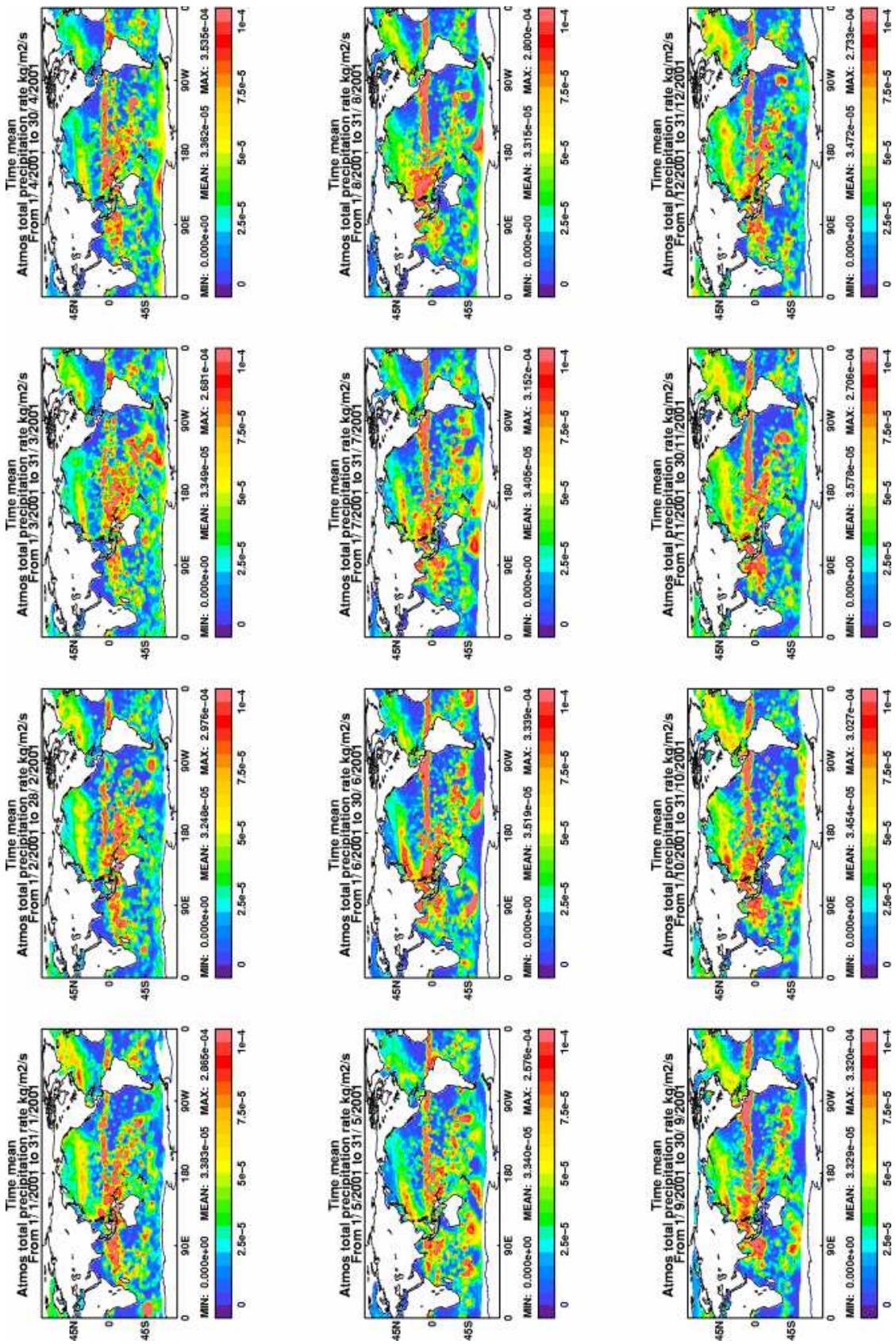

Fig C.1f: As Fig C.1a but for precipitation rate.

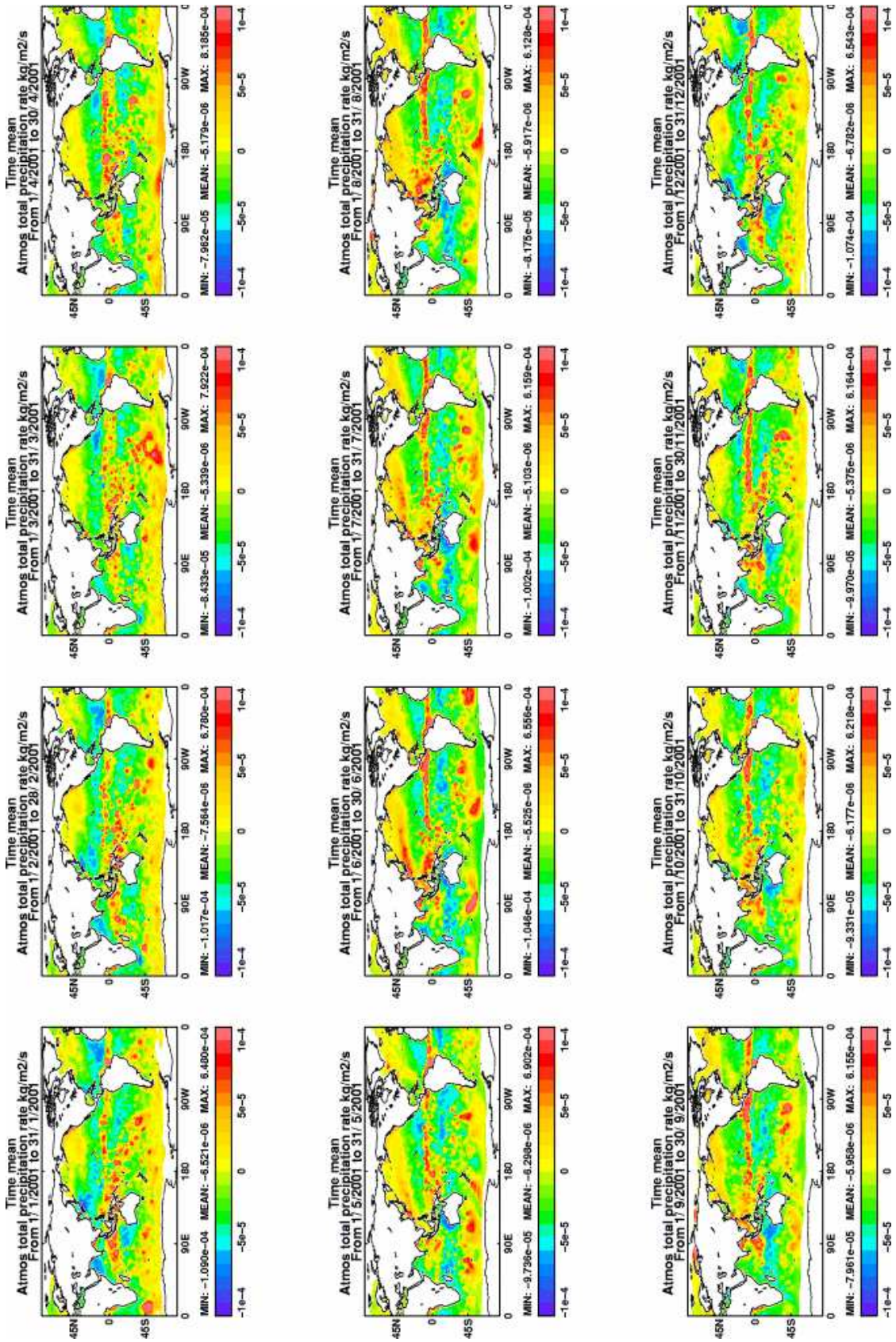

Fig C.1g: As Fig C.1a but for total freshwater (P-E+R) rate.

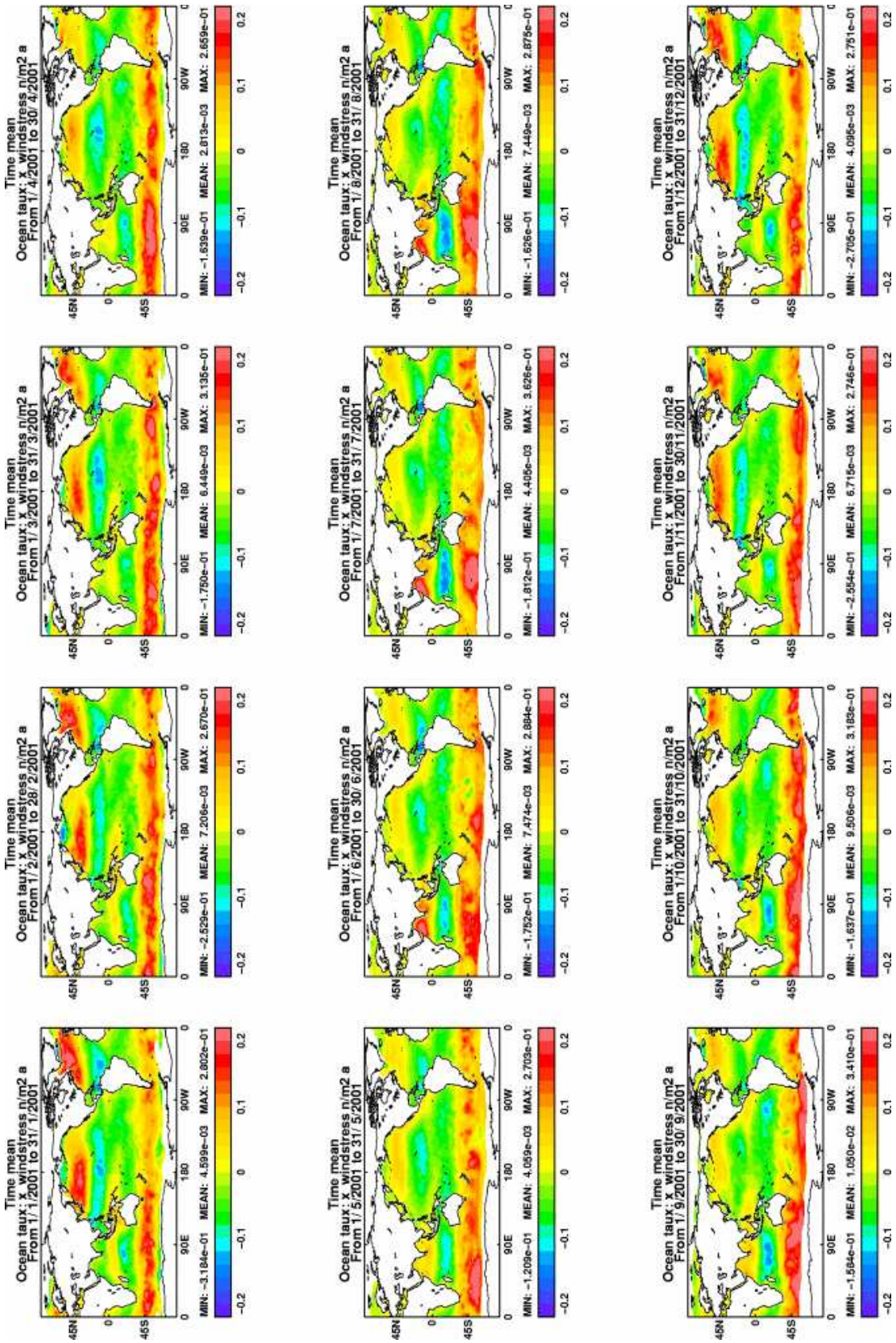

Fig C.1h: As Fig C.1a but for zonal windstress.

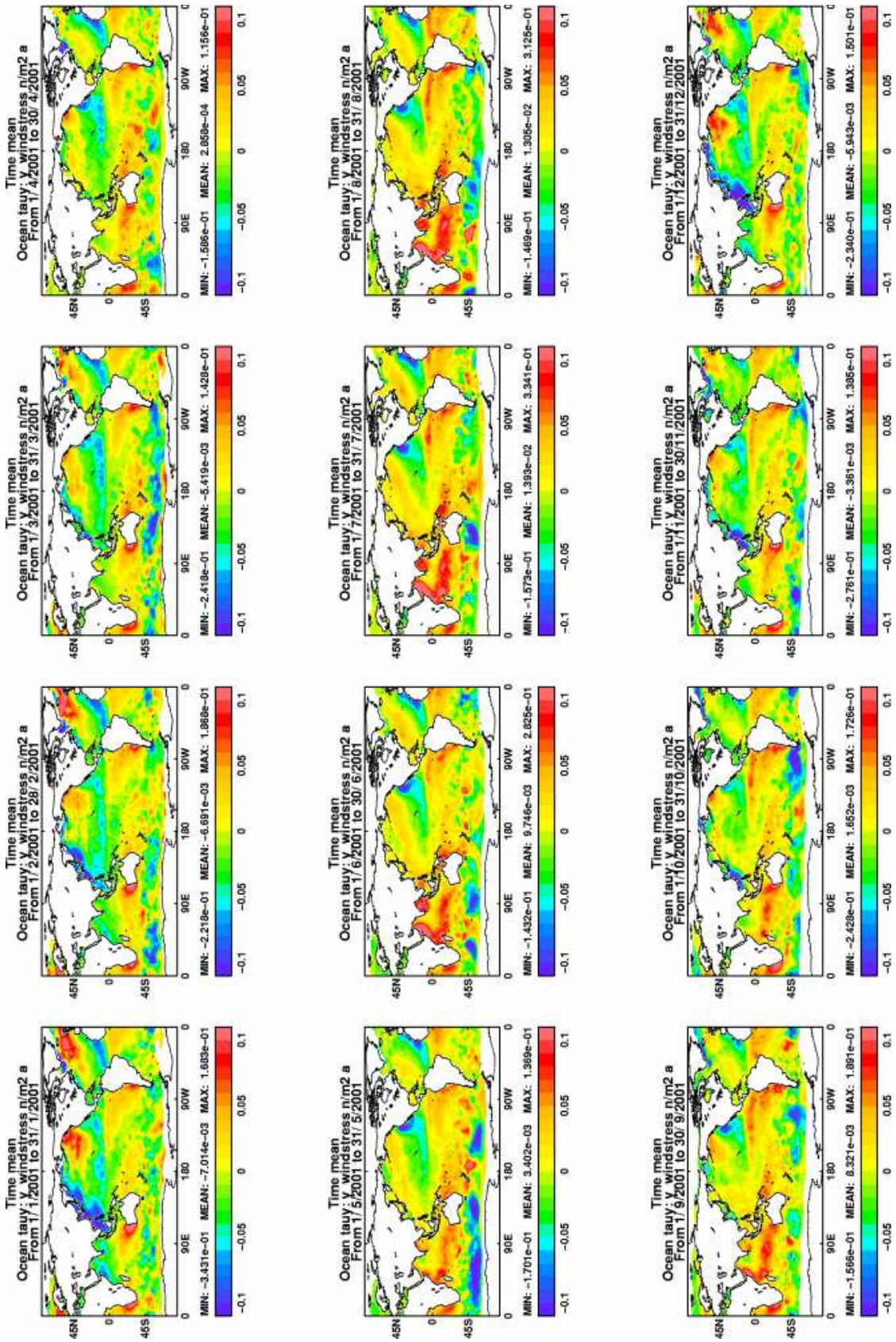

Fig C.1i: As Fig C.1a but for meridional windstress.

This page is intentionally left blank.

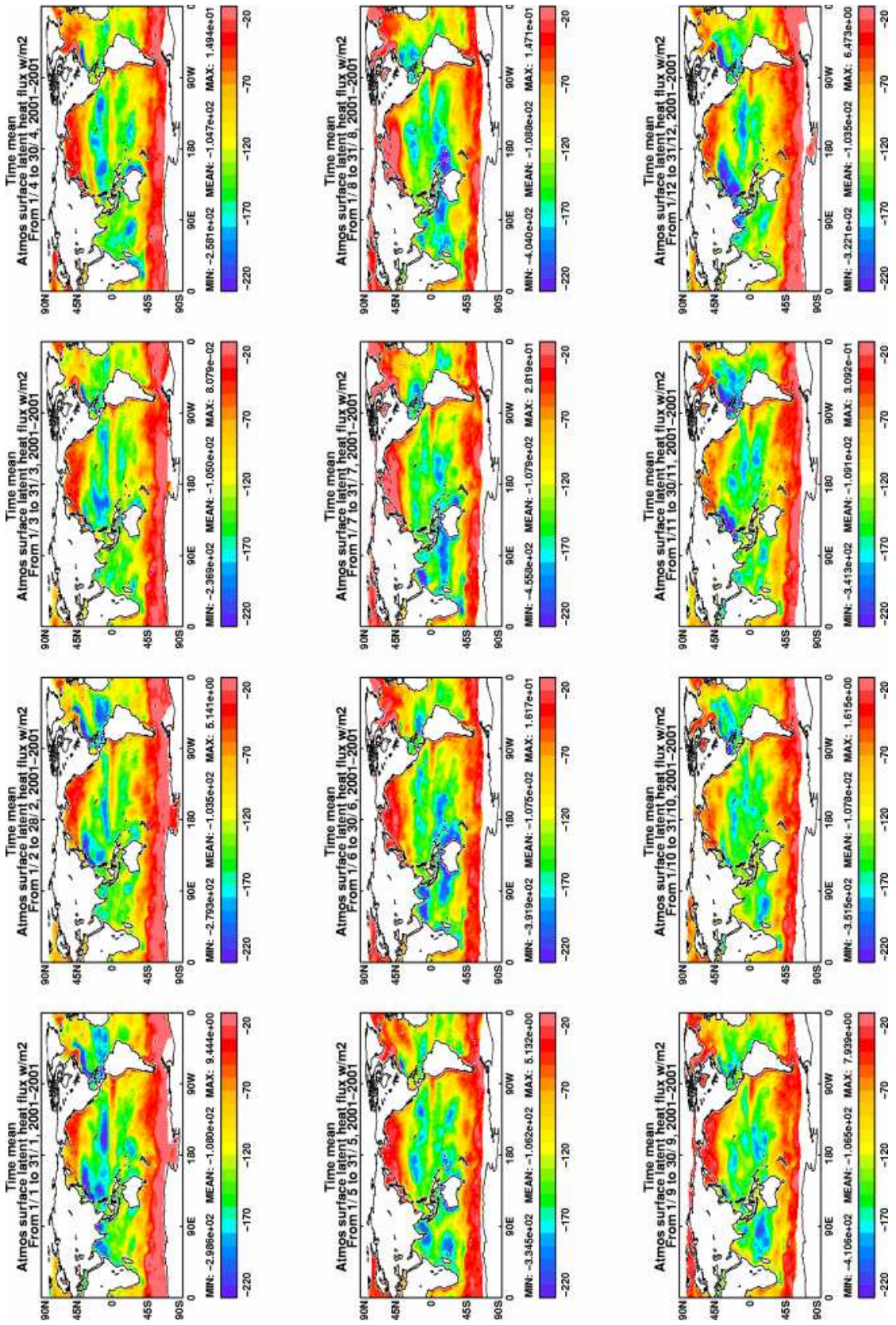

Fig C.2a: Monthly mean latent heating for corrected GFDL flux dataset.

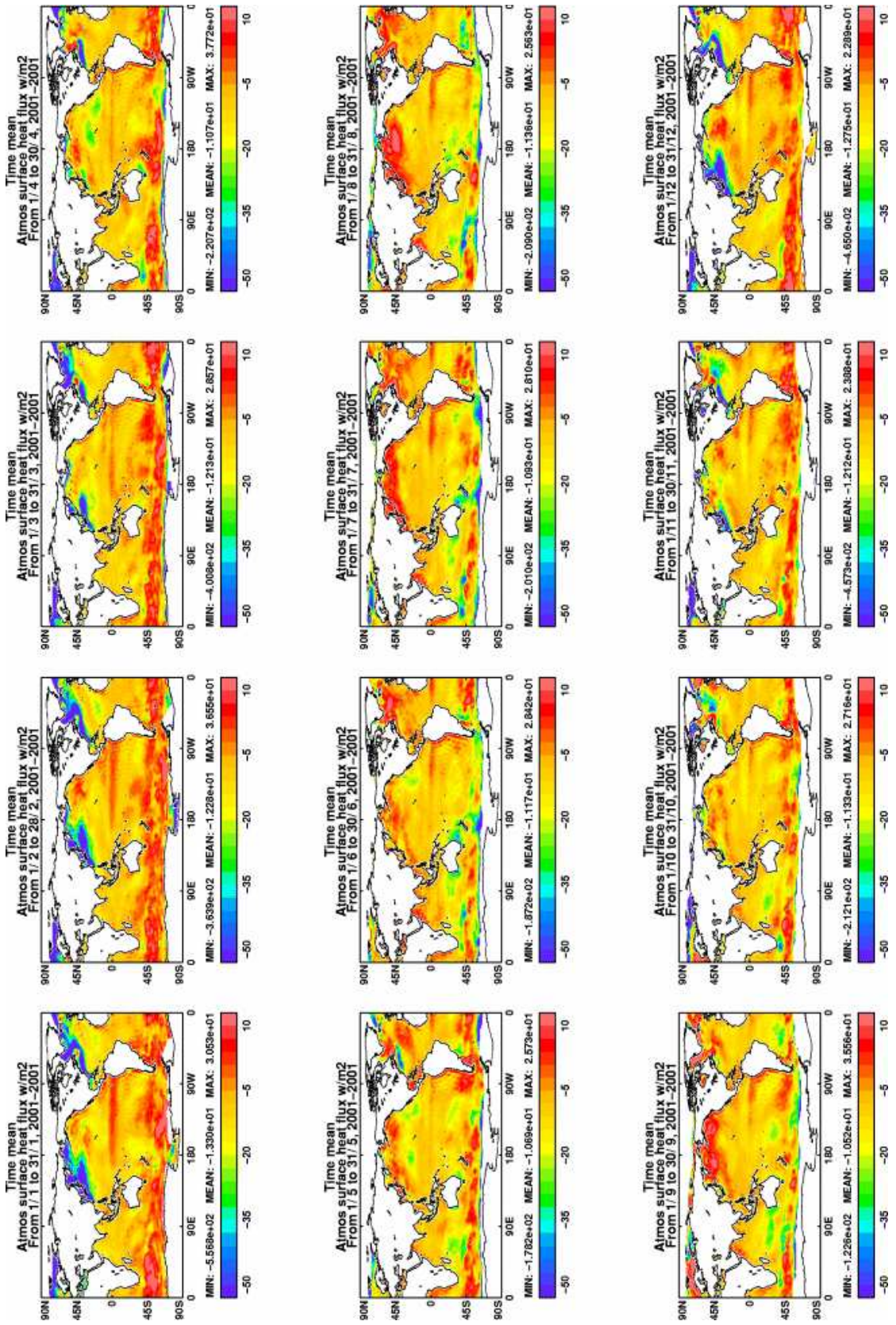

Fig C.2b: As Fig C.2a but for sensible heating.

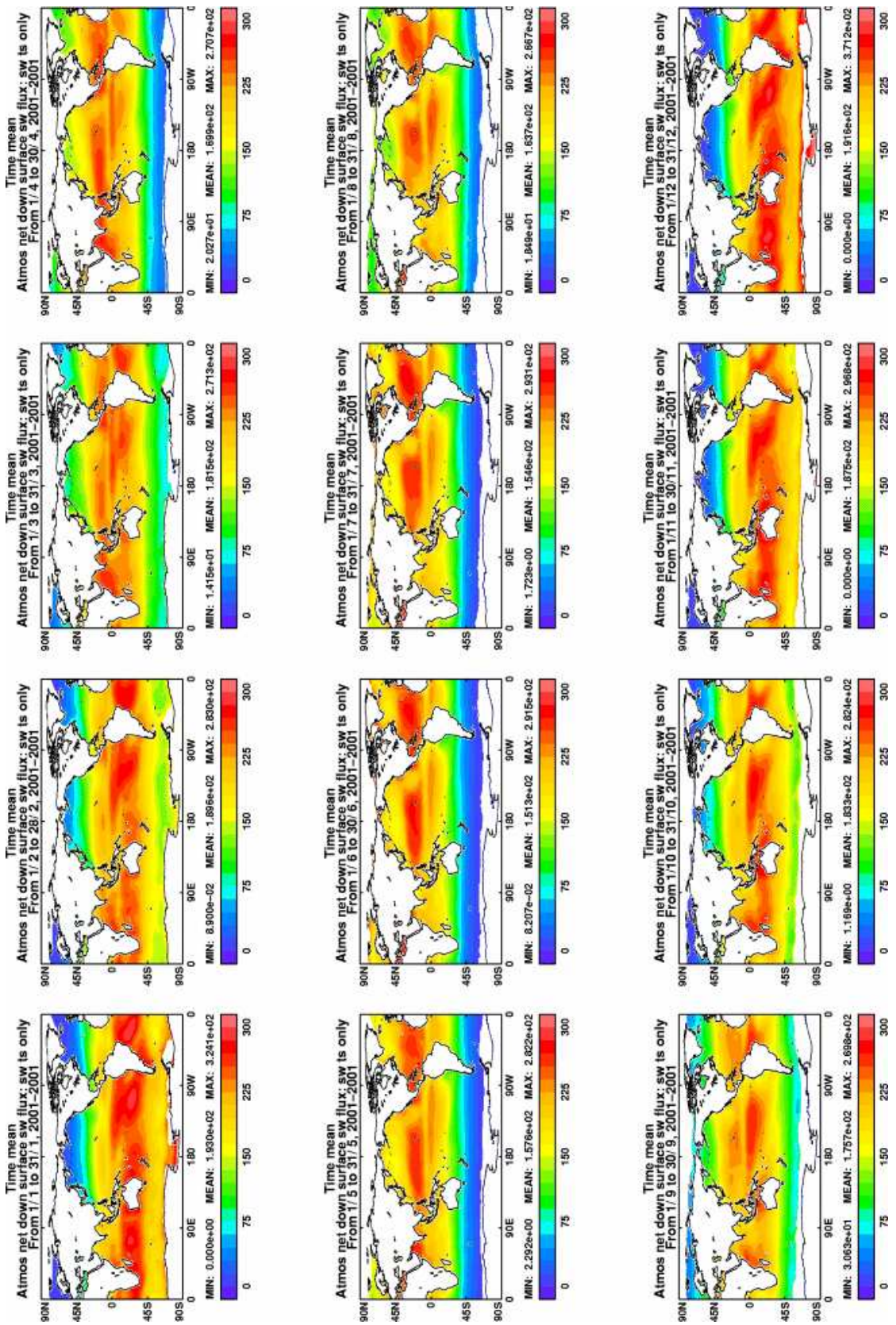

Fig C.2c: As Fig C.2a but for shortwave heating.

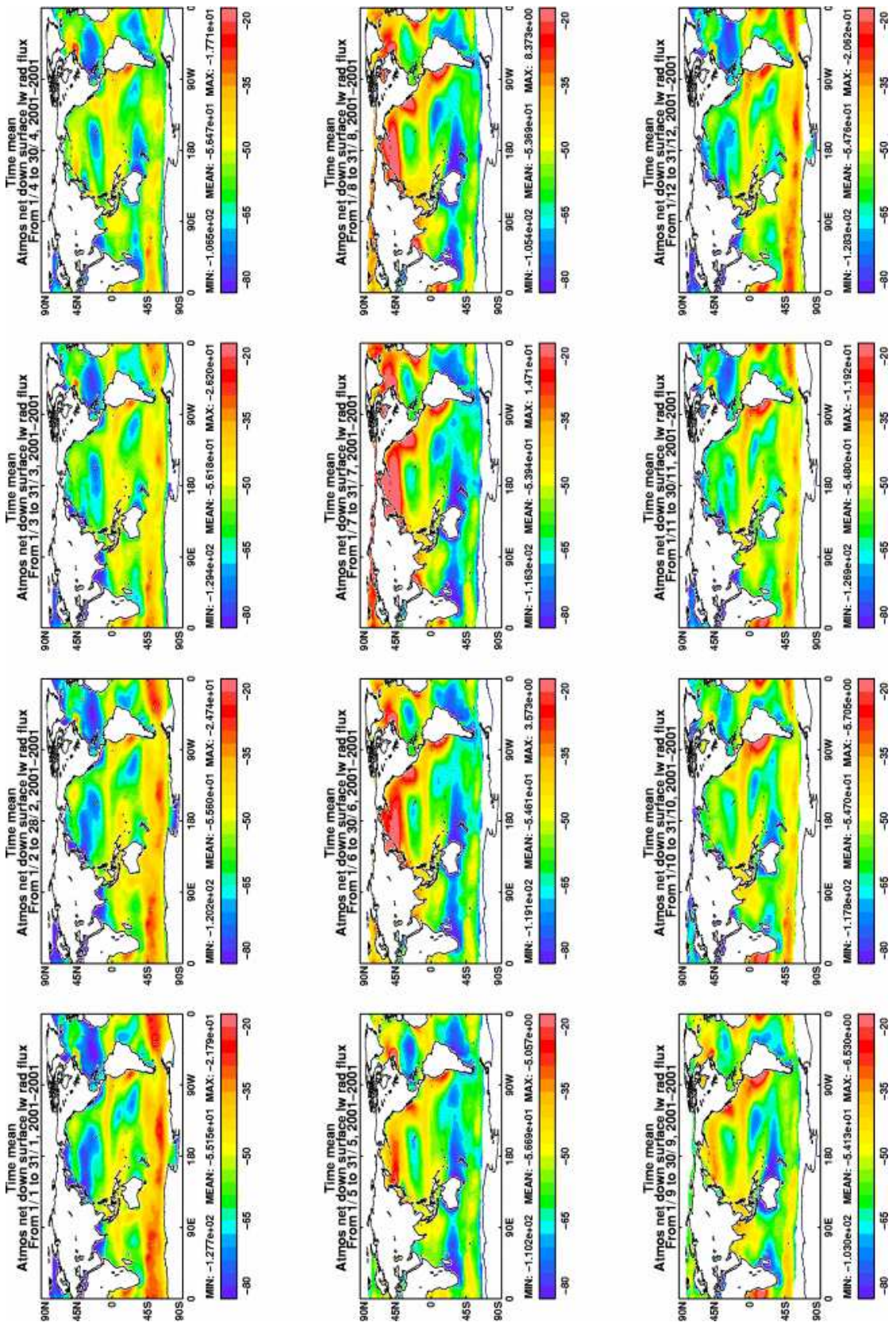

Fig C.2d: As Fig C.2a but for longwave heating.

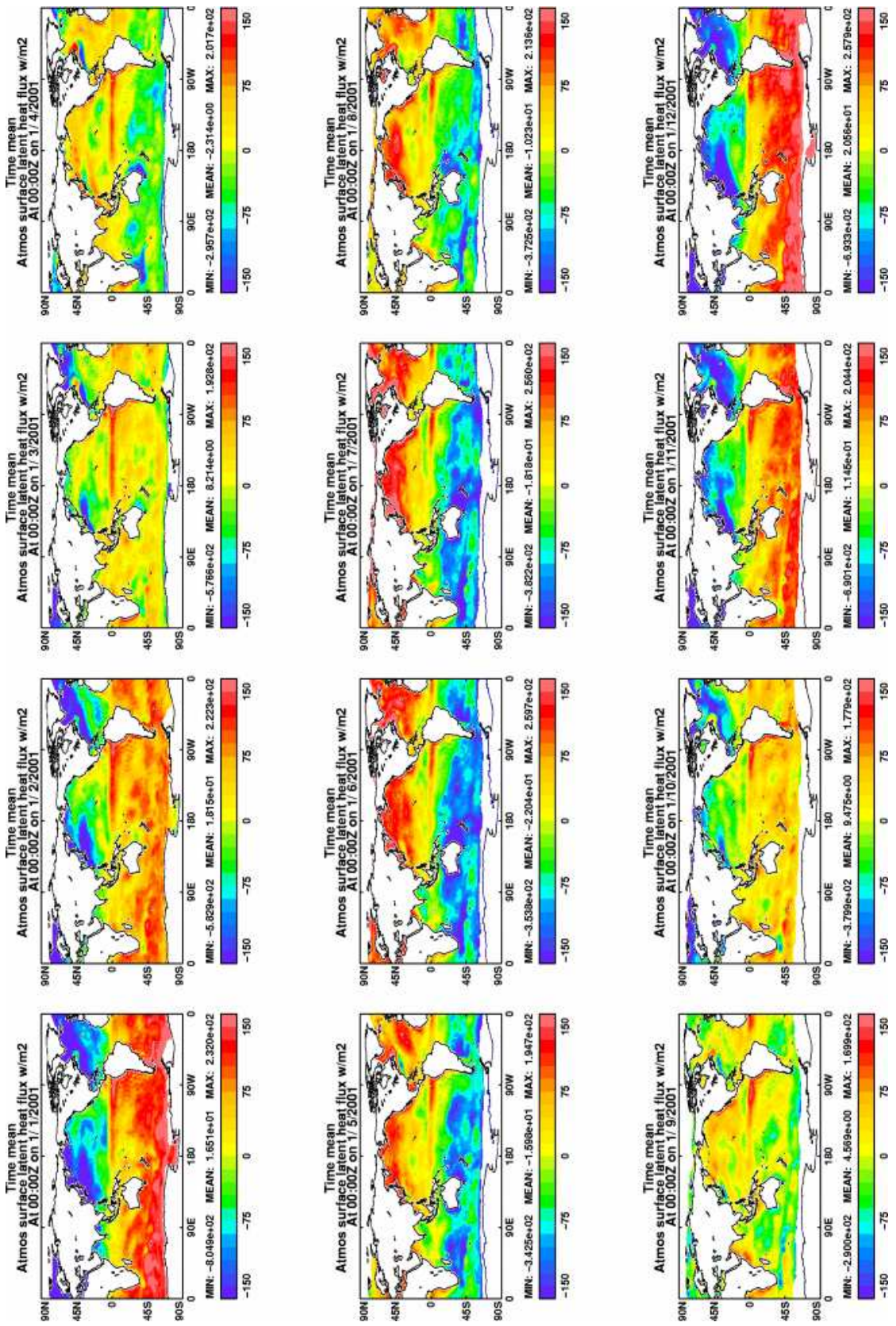

Fig C.2e: As Fig C.2a but for total (LH+SH+SW+LW) heating.

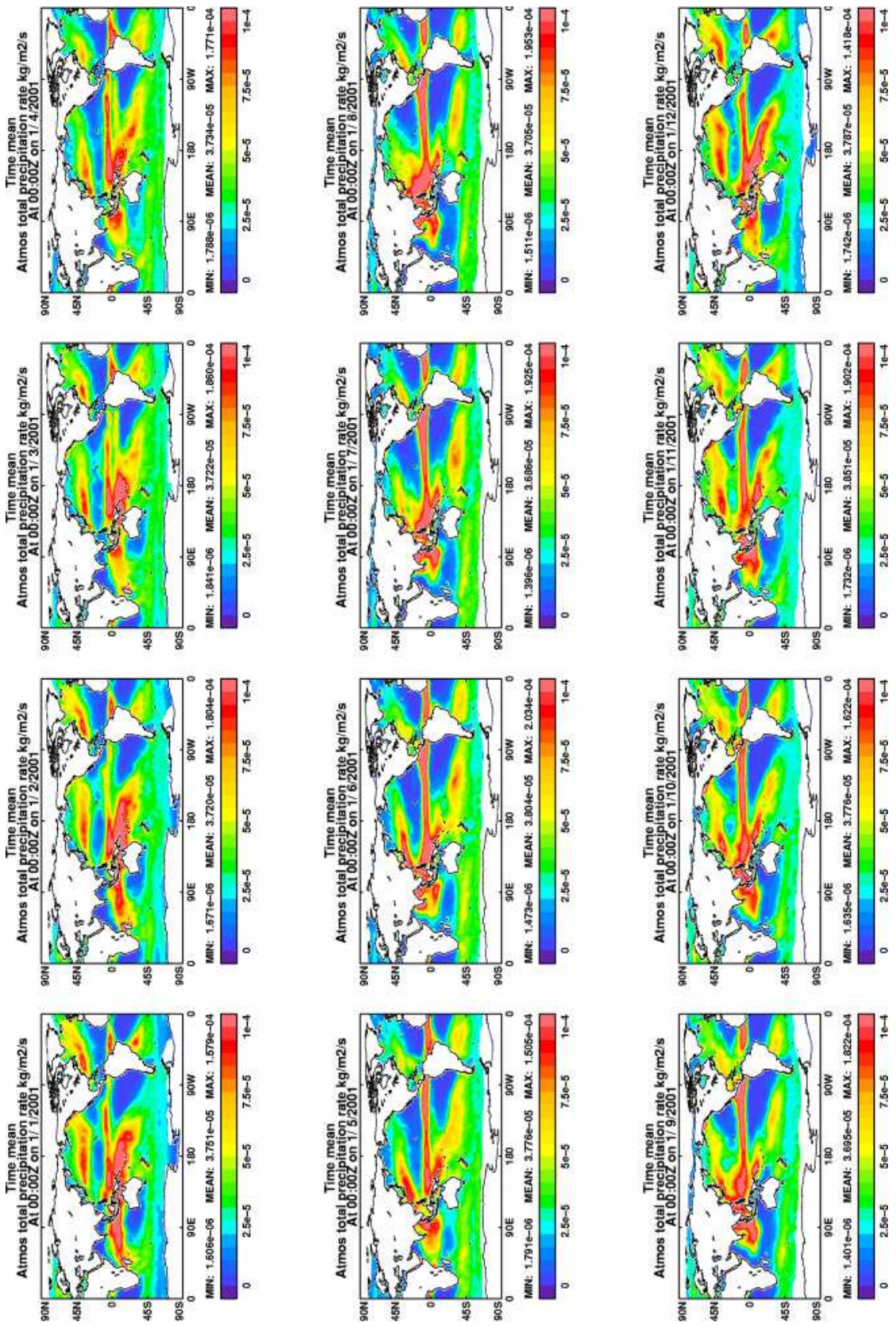

Fig C.2f: As Fig C.2a but for precipitation rate.

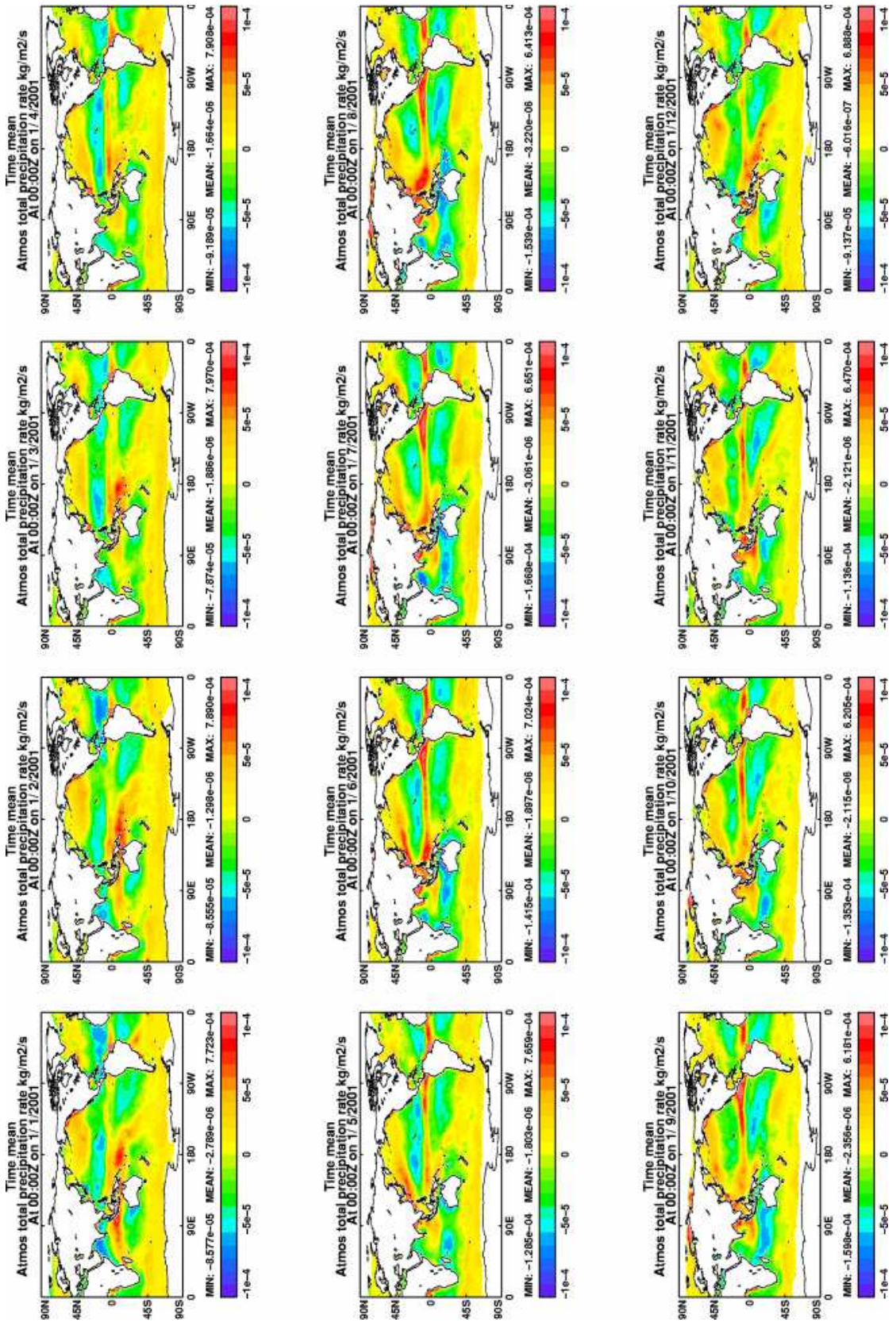

Fig C.2g: As Fig C.2a but for total freshwater (P-E+R) rate.

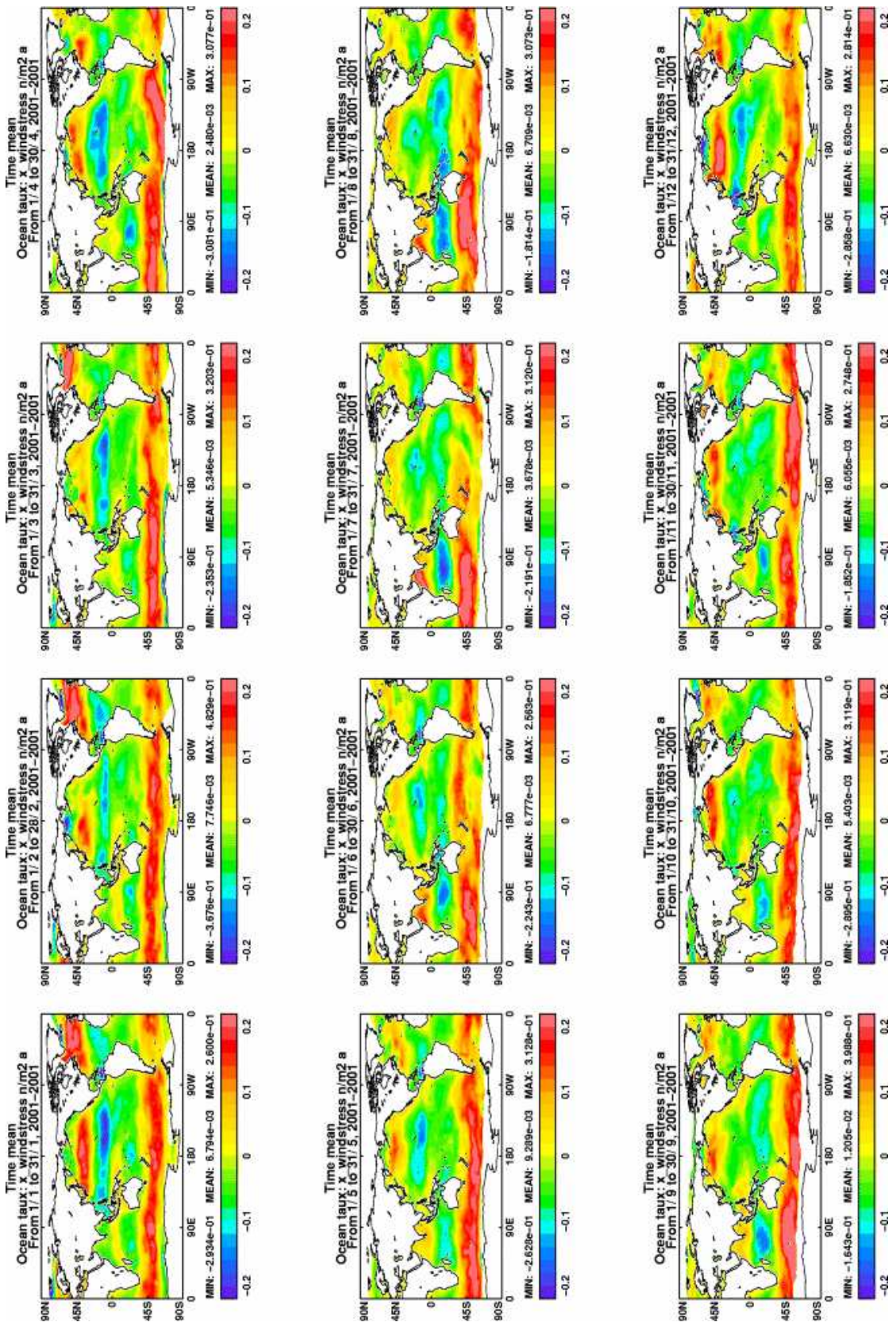

Fig C.2h: As Fig C.2a but for zonal windstress.

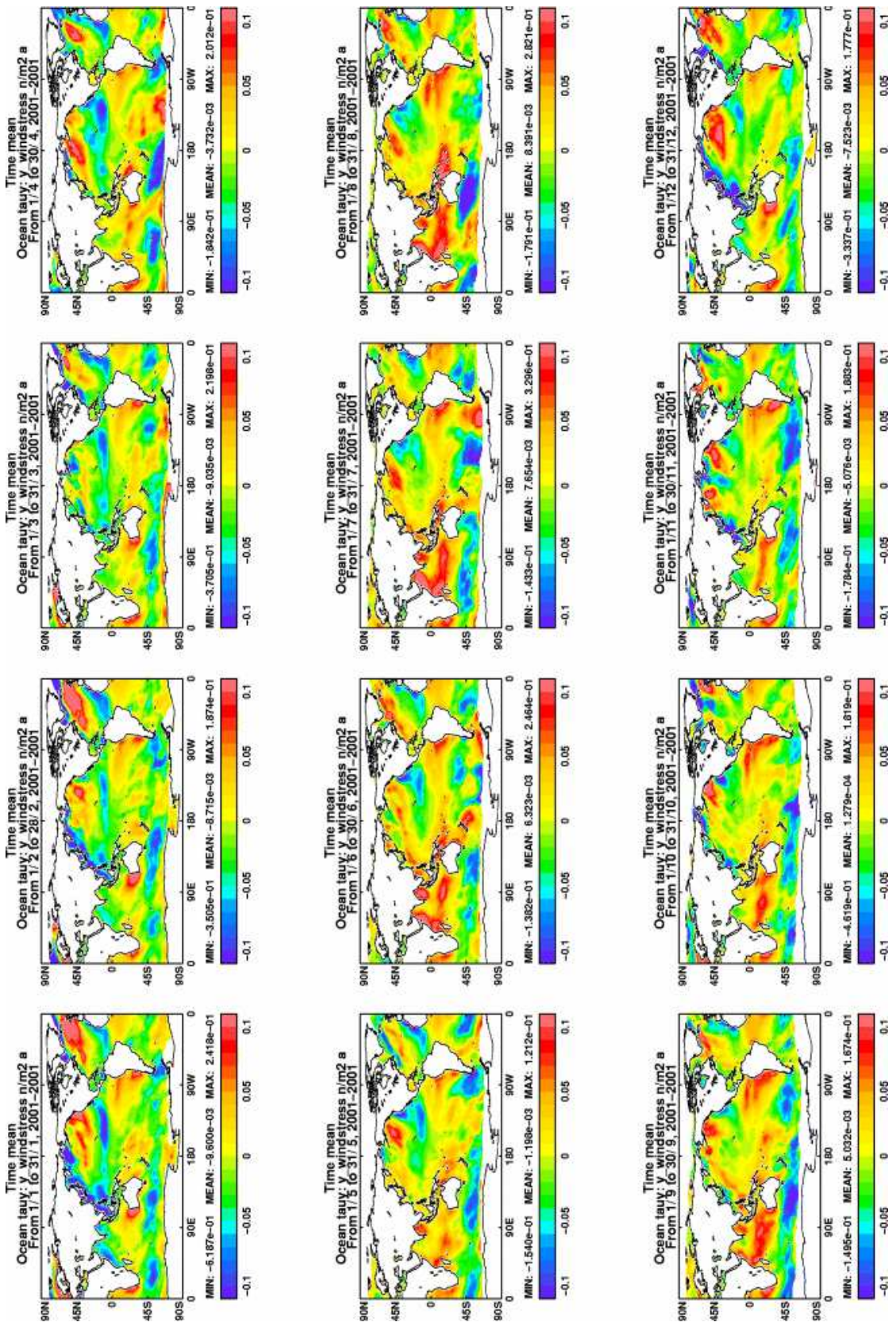

Fig C.2i: As Fig C.2a but for meridional windstress.

This page is intentionally left blank.

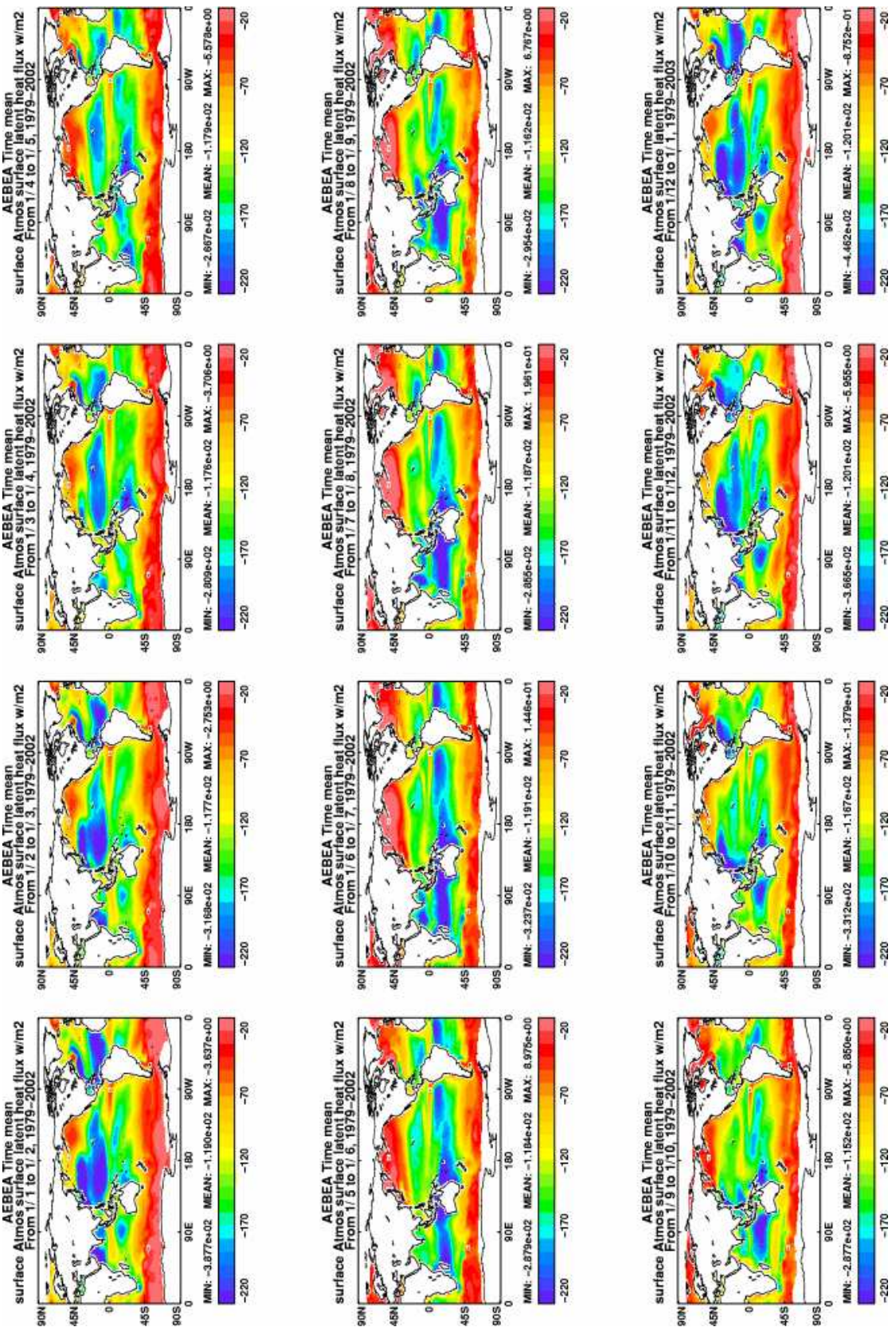

Fig C.3a: Monthly mean latent heating for HadGAM1 flux dataset.

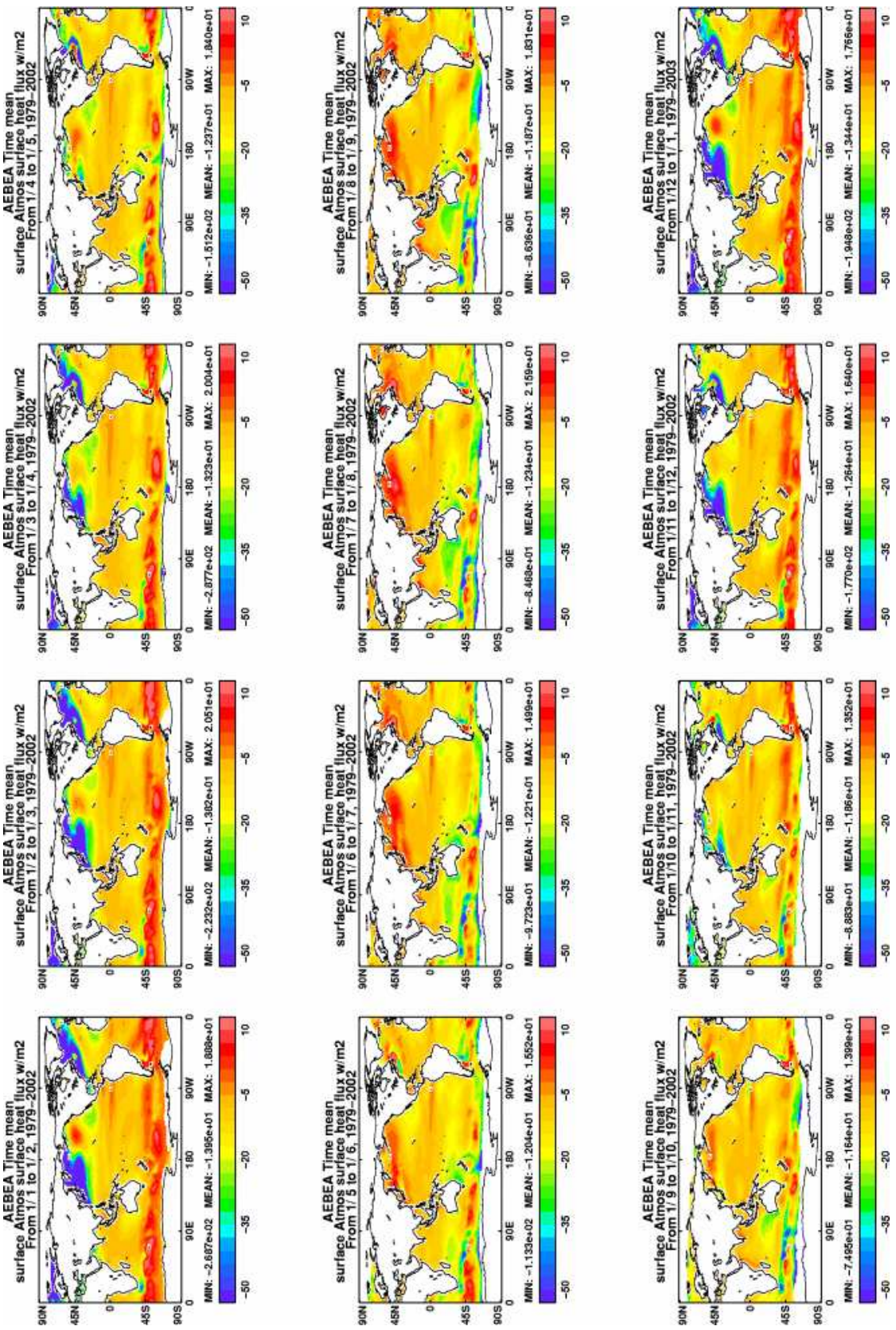

Fig C.3b: As Fig C.3a but for sensible heating.

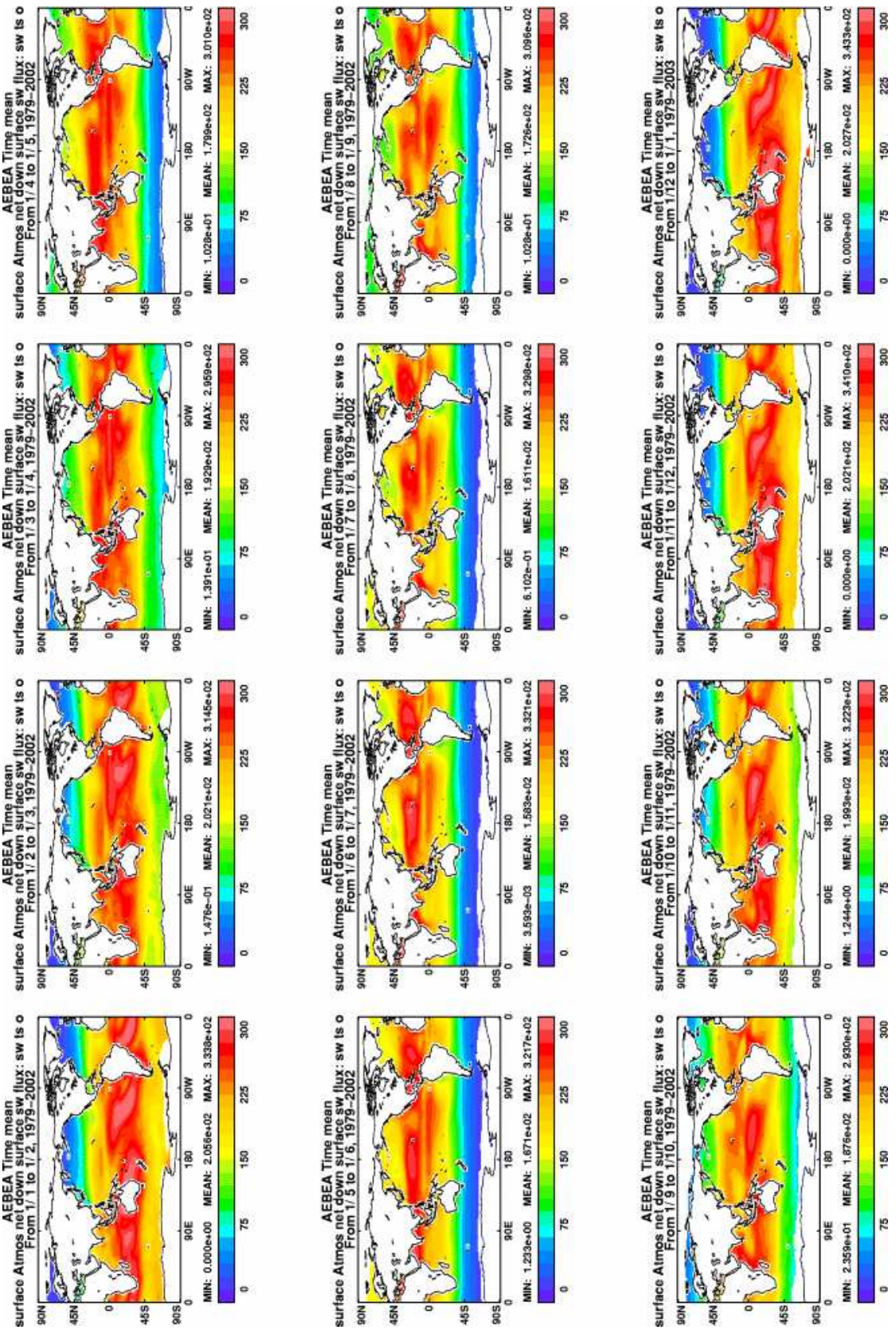

Fig C.3c: As Fig C.3a but for shortwave heating.

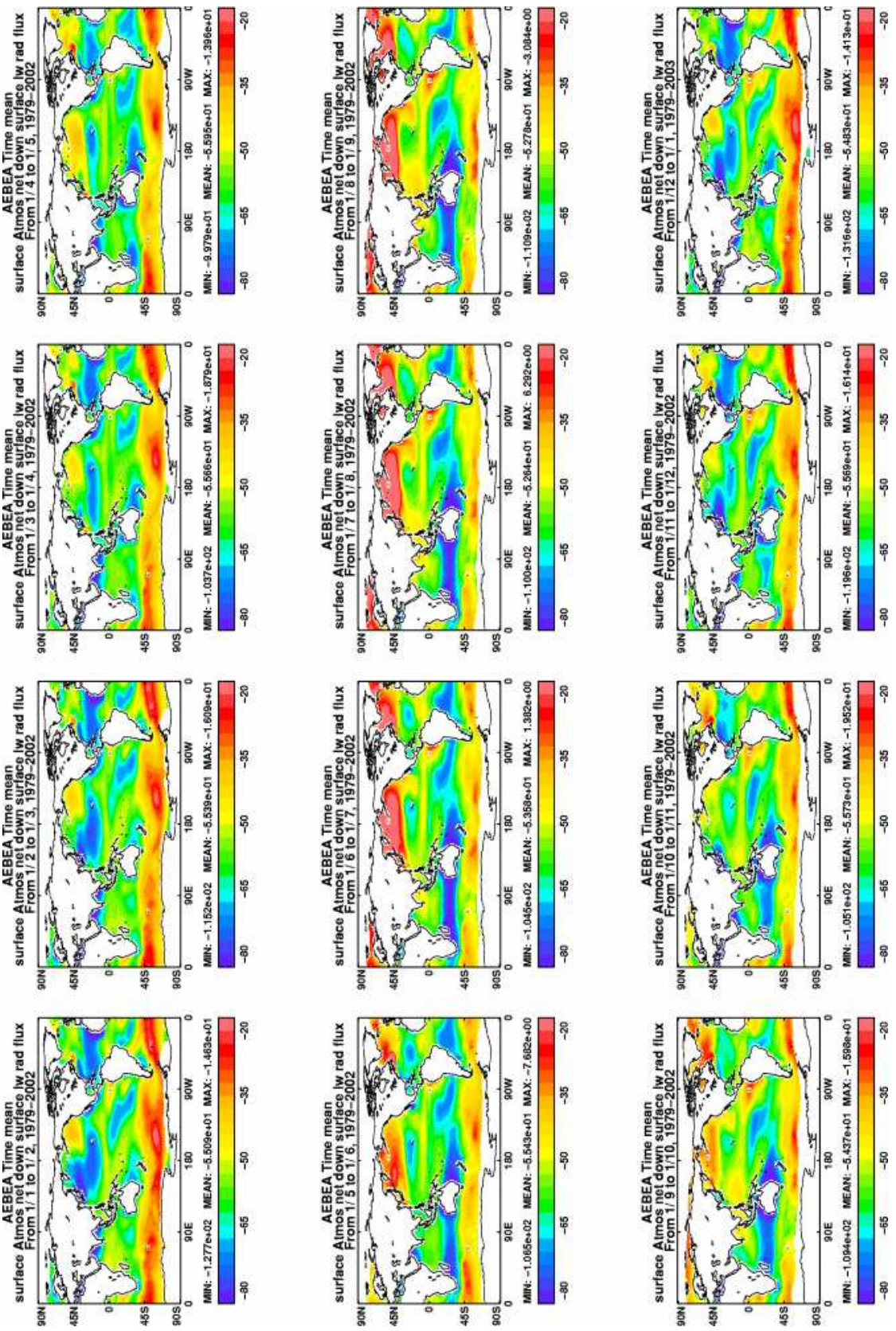

Fig C.3d: As Fig C.3a but for longwave heating.

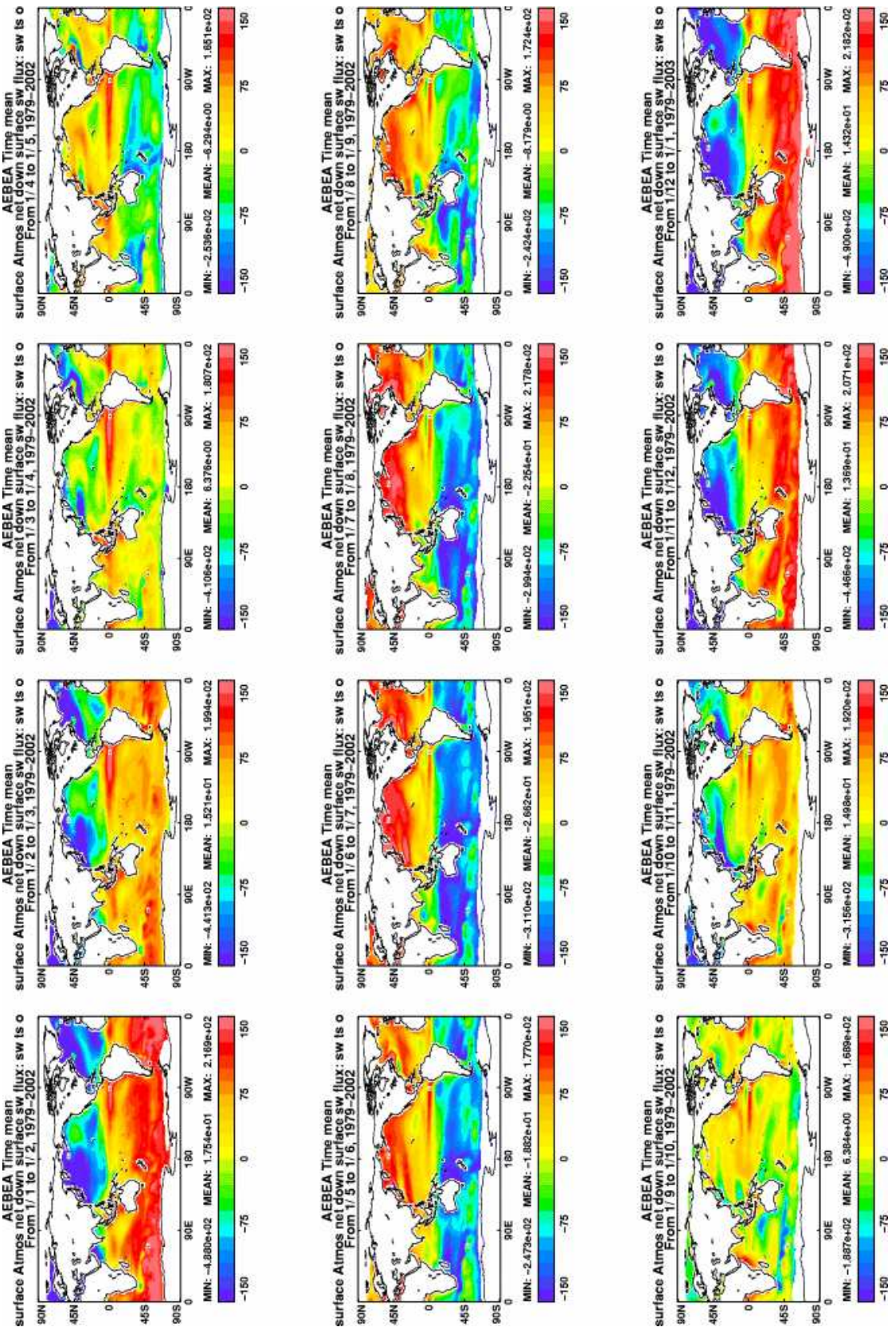

Fig C.3e: As Fig C.3a but for total (LH+SH+SW+LW) heating.

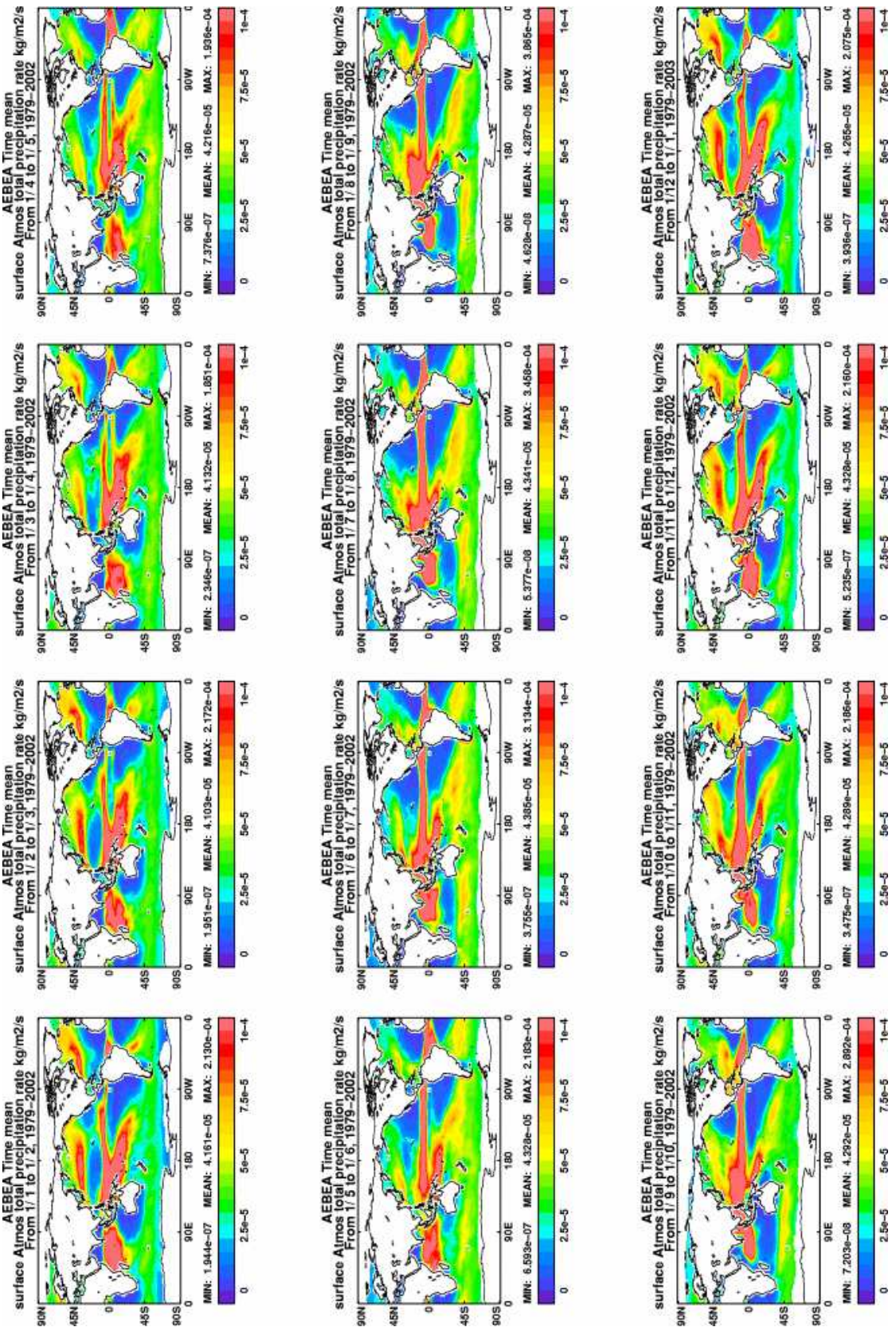

Fig C.3f: As for Fig C.3a but for precipitation rate.

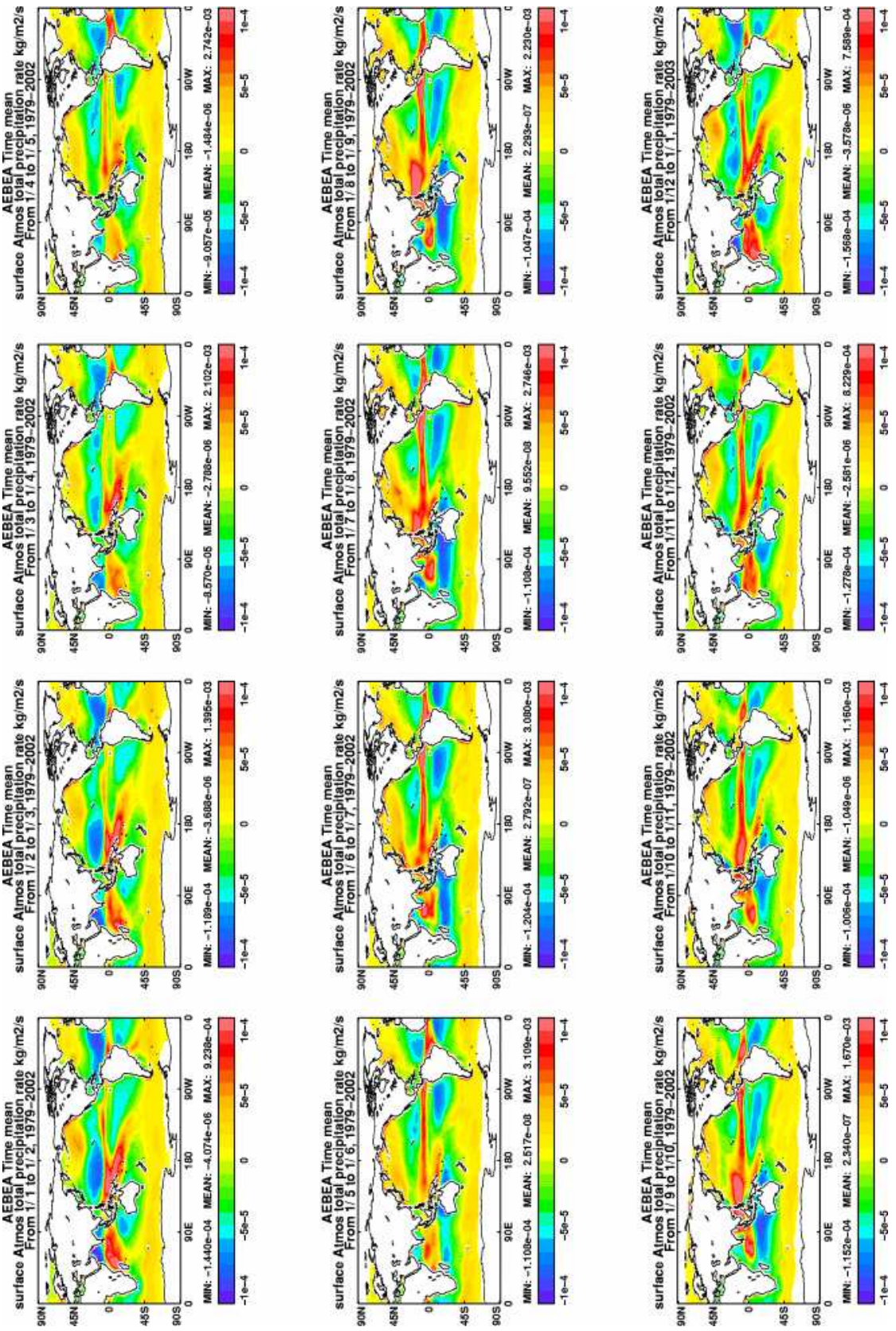

Fig C.3g: As Fig C.3a but for total freshwater (P-E+R) rate.

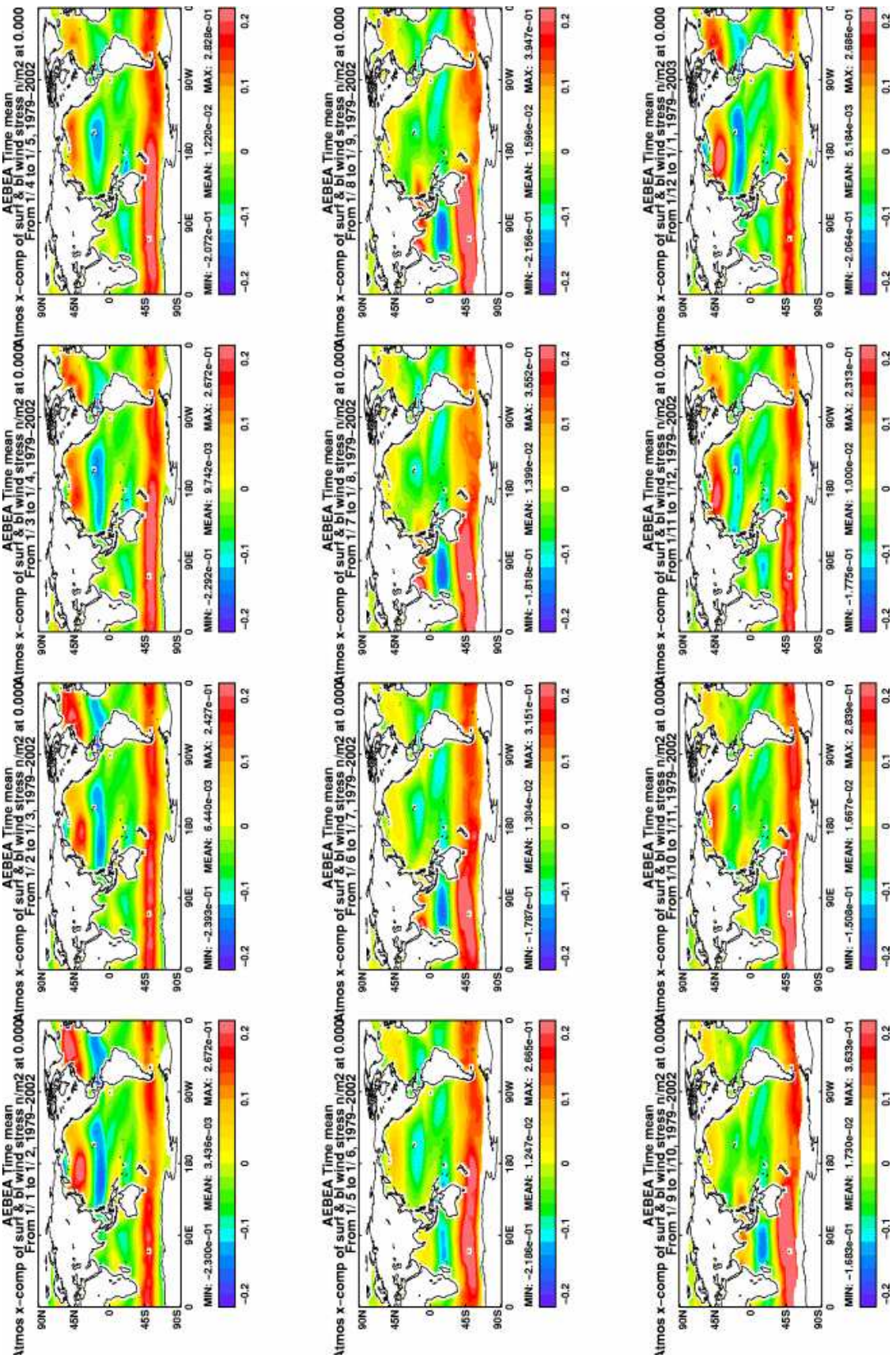

Fig C.3h: As Fig C.3a but for zonal windstress.

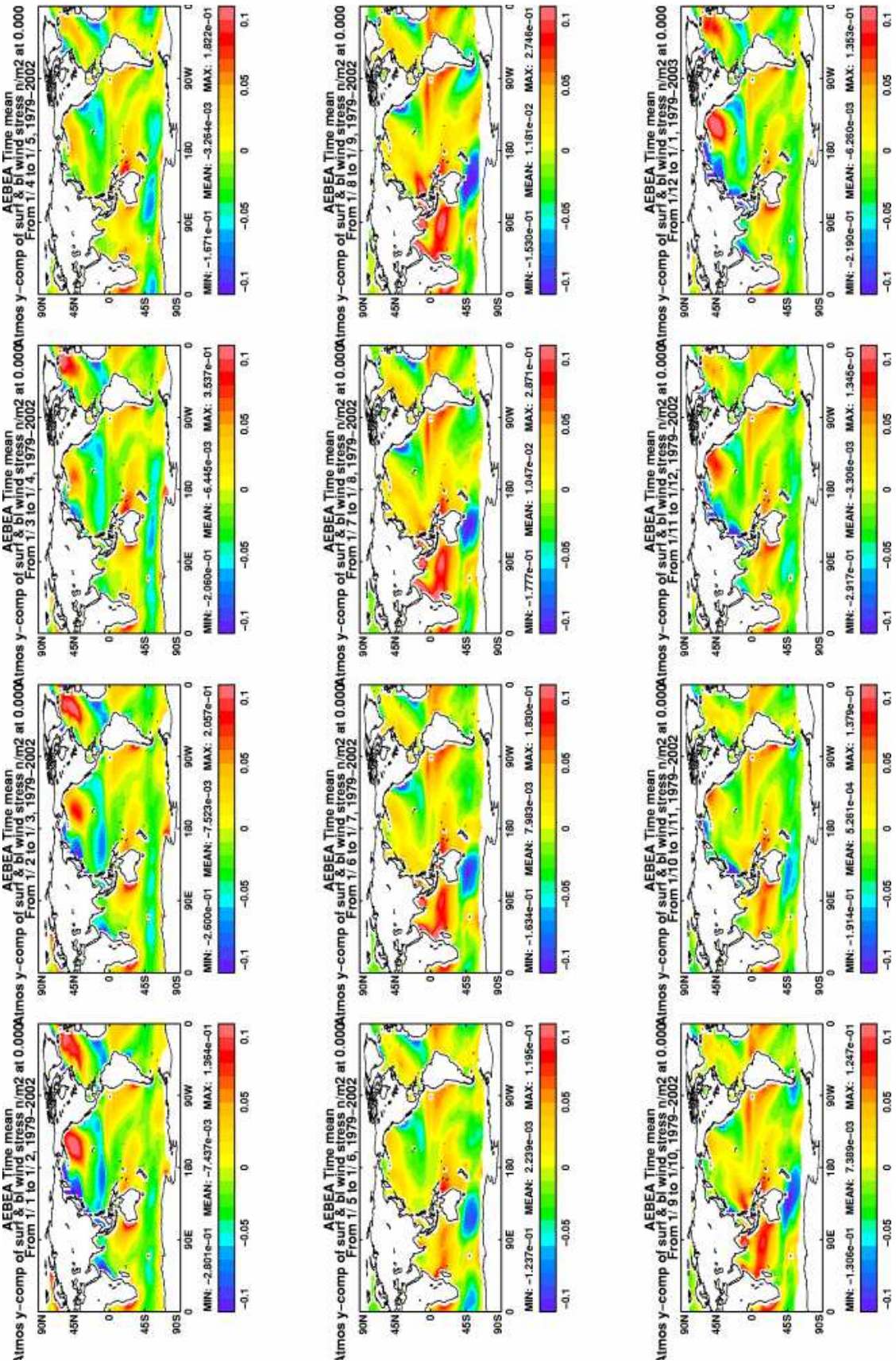

Fig C.3i: As Fig C.3a but for meridional windstress.